2018

ATTITUDE CONTROL ON SO(3) WITH PIECEWISE SINUSOIDS

Shaoqian Wang
University of Kentucky, shaoqian.wang@gmail.com
Digital Object Identifier: https://doi.org/10.13023/etd.2018.431

STUDENT AGREEMENT:

I represent that my thesis or dissertation and abstract are my original work. Proper attribution has been given to all outside sources. I understand that I am solely responsible for obtaining any needed copyright permissions. I have obtained needed written permission statement(s) from the owner(s) of each third-party copyrighted matter to be included in my work, allowing electronic distribution (if such use is not permitted by the fair use doctrine) which will be submitted to UKnowledge as Additional File.

I hereby grant to The University of Kentucky and its agents the irrevocable, non-exclusive, and royalty-free license to archive and make accessible my work in whole or in part in all forms of media, now or hereafter known. I agree that the document mentioned above may be made available immediately for worldwide access unless an embargo applies.

I retain all other ownership rights to the copyright of my work. I also retain the right to use in future works (such as articles or books) all or part of my work. I understand that I am free to register the copyright to my work.

REVIEW, APPROVAL AND ACCEPTANCE

The document mentioned above has been reviewed and accepted by the student's advisor, on behalf of the advisory committee, and by the Director of Graduate Studies (DGS), on behalf of the program; we verify that this is the final, approved version of the student's thesis including all changes required by the advisory committee. The undersigned agree to abide by the statements above.

Shaoqian Wang, Student

Dr. T. Michael Seigler, Major Professor

Dr. Alexandre Martin, Director of Graduate Studies

ATTITUDE CONTROL ON SO(3) WITH PIECEWISE SINUSOIDS

DISSERTATION

A dissertation submitted in partial
fulfillment of the requirements for
the degree of Doctor of Philosophy
in the College of Engineering at the
University of Kentucky

By
Shaoqian Wang
Lexington, Kentucky

Advisor: Dr. T. Michael Seigler, Professor of Mechanical Engineering
Lexington, Kentucky

2018

ABSTRACT OF DISSERTATION

ATTITUDE CONTROL ON SO(3) WITH PIECEWISE SINUSOIDS

This dissertation addresses rigid body attitude control with piecewise sinusoidal signals. We consider rigid-body attitude kinematics on SO(3) with a class of sinusoidal inputs. We present a new closed-form solution of the rotation matrix kinematics. The solution is analyzed and used to prove controllability. We then present kinematic-level orientation-feedback controllers for setpoint tracking and command following.

Next, we extend the sinusoidal kinematic-level control to the dynamic level. As a representative dynamic system, we consider a CubeSat with vibrating momentum actuators that are driven by small ϵ-amplitude piecewise sinusoidal internal torques. The CubeSat kinetics are derived using Newton-Euler's equations of motion. We assume there is no external forcing and the system conserves zero angular momentum. A second-order approximation of the CubeSat rotational motion on SO(3) is derived and used to derive a setpoint tracking controller that yields order $O(\epsilon^2)$ closed-loop error. Numerical simulations are presented to demonstrate the performance of the controls. We also examine the effect of the external damping on the CubeSat kinetics.

In addition, we investigate the feasibility of the piecewise sinusoidal control techniques using an experimental CubeSat system. We present the design of the CubeSat mechanical system, the control system hardware, and the attitude control software. Then, we present and discuss the experiment results of yaw motion control. Furthermore, we experimentally validate the analysis of the external damping effect on the CubeSat kinetics.

KEYWORDS: attitude control, SO(3), sinusoidal control, CubeSat, vibrating momentum wheels

Author's signature: Shaoqian Wang

Date: October 25, 2018

ATTITUDE CONTROL ON SO(3) WITH PIECEWISE SINUSOIDS

By
Shaoqian Wang

Director of Dissertation: T. Michael Seigler

Director of Graduate Studies: Alexandre Martin

Date: October 25, 2018

In loving memory of my grandpa and grandma

ACKNOWLEDGMENTS

First of all, I would like to thank my advisor Dr. T. Michael Seigler for his tremendous patience and full support, and for providing me with opportunities to explore my interests. I also want to thank my co-advisor Dr. Jesse B. Hoagg for his guidance and encouragement.

I am indebted to a lot of people who have helped me at some point in the CubeSat attitude control project. I would like to thank my former colleague Joshua Evans for helping me debug the CubeSat control circuit board and review the final PCB design; Floyd Taylor and Herb Mefford from the machine shop, for helping with the CubeSat prototype mechanical design and machining; Richard Anderson from EE Department, for printing the test circuit board for the piezo driver and for showing me how to use the reflow oven; Bradley Engel from Physik Instrumente (PI), for discussing the air bearing issues; my colleague Roshan Chavan and undergraduate assistant Katie Grimes for helping assembling the piezo actuators and conducting some of the experiments; Todd Hastings and Brian Wajdyk from the Center for Nanoscale Science and Engineering, for helping me set up the experiment platform in the clean room; and Cynthia Lane for ordering the electronics without any fuss. And there are many others.

I would also like to thank my colleagues/former colleagues, notably Amirhossein Ghasemi, Brandon J. Wellman, Xingye Zhang, Daniel Poston, Thomas Kirven, Zahra Abbasi, Roshan Chavan, Alireza Moosavi, Mohammadreza Kamaldar, Zack Lippay, Chris Heinz, and Ajin Sunny. I have benefitted a lot from conversations with them, and they have made the underground lab a nice place to study and work in. I also want to thank my friends for keeping me outside of the lab, especially, Yulong Yao, Xu Zhang, Yunqing Han, and Bo Tan. I would also like to thank Emma Xu for keeping me company for a journey.

Furthermore, I would like to thank my parents and siblings for their love, care, and support. Finally and most importantly, I would like to thank my grandpa and my grandma. They built a place I call home. I dedicate this work to them.

CONTENTS

LIST OF FIGURES

LIST OF TABLES

NOTATION

$\mathbb{R}$	set of real numbers
$\mathbb{R}^{3\times 3}$	set of 3 by 3 real matrices
$\mathbb{C}$	set of complex numbers
I	identity matrix in $\mathbb{R}^{3\times 3}$
SO(3)	3 dimensional special orthogonal group
so(3)	set of 3 dimensional skew symmetric matrices
tr	trace of a matrix
exp	(matrix) exponential
log	(matrix) principal logarithm
Ω	angular velocity vector
$\Omega_1, \Omega_2, \Omega_3$	components of angular velocity vector Ω
ω	angular frequency of sinusoids
$A_{(ij)}$	element in the ith row and jth column of matrix A
e_1, e_2, e_3	natural bases of $\mathbb{R}^3$
E_1, E_2, E_3	skew-symmetric matrix form of e_1, e_2, e_3
$\|\cdot\|_{\mathrm{F}}$	Frobenius norm of a vector or a matrix
$\|\cdot\|_2$	2-norm of a vector or a matrix
$\times$	cross product of two vectors
$\hat{\cdot}$	map from $\mathbb{R}^3$ to so(3)
$\mathbf{i}_{\mathrm{i}}$, $\mathbf{j}_{\mathrm{i}}$, $\mathbf{k}_{\mathrm{i}}$	unit vectors corresponding to the coordinate axes of the inertial frame
$\mathbf{i}_{\mathrm{b}}$, $\mathbf{j}_{\mathrm{b}}$, $\mathbf{k}_{\mathrm{b}}$	unit vectors corresponding to the coordinate axes of a body-fixed frame
$\mathcal{I}_k$	$[t_k, t_{k+1})$

Chapter 1 Introduction

Rigid-body attitude control problem has a long and rich history, and it remains an active research topic due to important applications in aircraft, spacecraft, and underwater vehicles [1–11]. The problem of interest in this dissertation is attitude control of a free rigid body with applications to spacecraft systems. In this introduction, we first review the attitude control problem and conventional attitude control techniques. Next, we introduce an attitude control approach that uses piecewise sinusoid controls. This nonconventional approach takes advantage of the noncommutative property of rigid-body rotation and has some advantages for small-scale systems such as small satellites. Finally, we provide an overview of this dissertation.

1.1 The attitude control problem

The attitude of a rigid body can be uniquely quantified by a 3×3 rotation matrix R, which relates a body-fixed coordinate frame to an inertial coordinate frame. The attitude kinematics of a rigid body are

$$\dot{R}(t) = R(t)\hat{\Omega}(t), \tag{1.1}$$

where Ω is the rigid body's angular velocity and $\hat{\Omega}$ is the skew-symmetric representation of Ω. The attitude kinetics of a rigid body can be derived from Newton-Euler's laws of motion, and are typically of the form

$$\dot{\Omega}(t) = f(\Omega, u), \tag{1.2}$$

where f is a function of Ω and the control u. The attitude control problem is to design u for the system (1.1) and (1.2), potentially using feedback of R and/or Ω,

such that the attitude R achieves a desired behavior.

In this dissertation, we distinguish between kinematic-level control and dynamic-level control. Kinematic-level control considers only the attitude kinematics (1.1) and treats Ω as the control input. Kinematic controllers can be used as inner-loop steering controls and are also applicable for dynamic systems with high-bandwidth actuation and negligible transient response. Conversely, dynamic-level control considers both (1.1) and (1.2). We refer to the system (1.1) and (1.2) as the *rigid-body system*.

Rotation matrices form the special orthogonal group SO(3), which is a three-dimensional manifold. Since SO(3) is not a Euclidean space, attitude control is frequently approached using various parameterizations of SO(3), such as Euler angles, rotation vectors, unit quaternions, Rodrigues parameters, and modified Rodrigues parameters. Since the dimension of SO(3) is three, at least three parameters are needed to quantify attitude. A parameterization that uses three parameters is called a minimum parameterization. Examples of minimum parameterization include Euler angles, rotation vectors, and Rodrigues parameters.

In addition to the simpler treatment in a Euclidean space, attitude control using parameterizations of SO(3) can have other advantages. For example, global asymptotically stabilization can be achieved with unit quaternions using continuous time-invariant feedback control laws [4]. On the contrary, the best possible result for attitude stabilization of the SO(3) kinematics using continuous time-invariant feedback is *almost* global stabilization [10, 12, 13]. This limitation occurs because such control laws necessarily yield more than one equilibrium [10], regardless of the form of the attitude kinetics (1.2).

However, it is well known that no parameterization of SO(3) is both unique and global [10, 14]. Control laws based on a non-unique parameterization, such as unit quaternions, can yield undesired behavior such as unwinding [6, 10]. In addition, control laws based on a local parameterization cannot have global properties, such as

global asymptotic stability of the closed loop.

The rigid-body attitude kinematic equation (1.1) is a drift-free system on SO(3), which is also a matrix Lie group. The controllability of (1.1) can be analyzed with the Lie algebra rank condition [15]. The attitude kinetic equation (1.2) includes drift in general. The controllability of the rigid-body system can be analyzed using the geometric control theory. In particular, [3] establishes sufficient and necessary conditions for controllability of the rigid-body system in case of one, two and three independent control torques.

Since the early 1970s, numerous attitude stabilization and tracking control laws for fully actuated systems have been reported [4,10,16–19]. In particular, [4] presents a range of control laws including model independent, model dependent, and adaptive control laws to address the attitude tracking problem. Attitude control for rigid spacecraft with model uncertainty (e.g., unknown inertia, unknown momentum wheel alignment) and external disturbance has also been addressed [20–22].

Attitude control for underactuated systems, that is, systems with fewer independent controls than the dimensions of the system's configuration space, has also been studied extensively [3,5,23–28]. As indicated by [3], under some conditions, the rigid-body system is controllable with only one control torque. However, this case yields substantial theoretical and practical difficulties. As such, most of the underactuated systems considered in the literature have two independent torque inputs. It is proved in [23] that a rigid body with only two controls cannot be locally asymptotically stabilized with smooth time-invariant feedback controls since Brockett's necessary condition [29] for smooth feedback stabilization is not satisfied. Moreover, for underactuated systems, the time-invariant feedback controls that asymptotically stabilize the rigid-body system to any equilibrium cannot even be continuous [24]. Piecewise continuous time-invariant feedback control laws and time-varying control laws are proposed in [5,26,27,30]. In particular, [27] presents nonsmooth bounded kinematic-level

stabilizing and tracking control laws for an axisymmetric spacecraft. A time-varying feedback control law is constructed in [5] that locally asymptotically stabilizes an equilibrium of the rigid spacecraft with two control torques.

More recent attitude-control research is focused on the distributed cooperative attitude synchronization and tracking problem for multiple rigid bodies, which form a communication network [9, 11, 31]. Distributed cooperative attitude control finds its applications in cooperative sensing and actuation for multi-agent systems, such as satellite swarms and multiple robotic manipulators.

1.2 Conventional attitude control approaches

Attitude control is a nonlinear control problem, which has been addressed using various nonlinear control approaches, for example, linearization and feedback linearization [4, 10, 32–34], backstepping [8, 35], adaptive control [20–22], sliding mode control [34, 36, 37], and optimal control [38, 39]. In this section, we review some of these control approaches.

Linearization and feedback linearization are often used to design and analyze control laws for attitude stabilization [4, 10, 32–34]. These approaches consider the rigid-body attitude kinetics together with the attitude kinematics based on a minimum parameterization of SO(3). Linearization near an equilibrium point is then applied to obtain a linear system in $\mathbb{R}^6$. Linearization can also be carried out with rotation matrices using the Lie-group properties of SO(3) [10]. For example, in [10], a proportional-derivative (PD) feedback control law is designed for attitude stabilization, and then the closed-loop system is linearized near the equilibria. The local structure of the closed-loop system is then analyzed by calculating the eigenvalues of the linearized system. In [33], two non-standard projective plane coordinates are chosen as outputs. Then input-out linearization is carried out yielding a second-order linear system, which gives rise to a control law that spin-stabilizes a satellite. Note

that for underactuated systems, linearization fails because the linearized system is not controllable [3, 10]; center manifold theory [40] is often used together with feedback linearization to analyze the zero dynamics [33].

Another common control approach uses PD state feedback [4, 17, 20, 41]. For example, [4] addresses the attitude tracking problem. By using the vector part of the error quaternion and the relative angular velocity as feedback, the control law globally asymptotically stabilizes the error attitude. A control Lyapunov function motivated by the consideration of the total energy of the system is used to prove global stability. In addition, by exploiting the geometric structure of SO(3), [17] presents a PD control law for almost global attitude stabilization.

Attitude control laws can also be designed using passivity based approach. The rigid-body rotational kinematics, in unit quaternion coordinates, are passive with angular velocity as input and with the vector part of the unit quaternion as output [18]. Moreover, the attitude kinetics are passive with torque as input and angular velocity as output [18]. By exploiting the passivity of the rigid-body system, [18] presents control laws that address the setpoint tracking problem without the requirement of angular velocity measurement.

It is also common to view the rigid-body system as a multi-loop structure, treating the attitude dynamics as the outer-loop system and the attitude kinematics as the inner-loop system. The kinematic-level control law is first designed by assuming the angular velocity as the control input, and then the dynamic-level control law is derived using backstepping or singular perturbation theory [8, 35, 42]. In particular, [42] first addresses the kinematic-level attitude control problem for an underactuated axisymmetric spacecraft. By using a nonstandard attitude parameterization, [42] provides small and bounded angular velocity controls for stabilization and tracking of the spacecraft. Then, a dynamic-level control law is derived using singular perturbation theory such that the actual angular velocity trace the desired angular velocity profile.

Another important control design approach is based on the exact or approximate solution of the rigid-body system. Analytic solutions provide a detailed picture of the transient and asymptotic behavior of a system. In particular, an exact (or approximate) solution of a closed-loop system can be used to establish asymptotic stability of an equilibrium point and to determine the rate of convergence. In addition, if a solution for an open-loop control is available, then a priori knowledge of the system can be exploited to yield improved performance with reduced control effort. Intermittent feedback corrections can also be implemented to reduce sensitivity to disturbance.

No general closed-form solutions exist for the rigid-body system (see [43–45] and the reference therein). However, some specific solutions do exist and have proved to be useful.

Closed-loop solutions can be obtained in the control design process, for example, using exact linearization [46]. Some special feedback control laws also yield exact solution of the rigid body system. For example, [19] presents some classes of kinematic-level feedback control laws that admit a closed-loop solution. One interesting example is the following. Consider the attitude kinematics (1.1) with control $\hat{\Omega}(t) = R(t)^{\mathrm{T}}P - PR(t)$, where $P \in \mathbb{R}^{n\times n}$ is a positive semidefinite matrix with rank $n-1$ or n. Then, the solution of the system is

$$R(t) = (\sinh(Pt) + \cosh(Pt)R(0))\,(\cosh(Pt) + \sinh(Pt)R(0))^{-1}\,,$$

which can be used to determine the region of convergence as well as the convergence rate of $R(t)$. As another example, if for all $t > 0$,

$$\hat{\Omega}(t)\exp\left(\int_0^t \hat{\Omega}(\tau)\mathrm{d}\tau\right) = \exp\left(\int_0^t \hat{\Omega}(\tau)\mathrm{d}\tau\right)\hat{\Omega}(t),$$

then the solution of the attitude kinematics (1.1) is

$$R(t) = R(0) \exp\left(\int_0^t \hat{\Omega}(\tau) \mathrm{d}\tau \right).$$

The solution of the rigid-body system is also available if the control torque is piecewise constant such that at any time only one components of $\Omega(t)$ is nonzero. The solutions of the rigid-body system with piecewise constant control have been used to specify attitude maneuver strategies for underactuated spacecraft in [24, 33]. Recall that for underactuated systems, time-invariant feedback control laws that yield a global asymptotically stable equilibrium are necessarily discontinuous.

An approximate solution of the rigid-body system with time-varying controls can be obtained using averaging. For example, [47] studies the motion control (including attitude control) for underactuated systems evolving on matrix Lie groups using periodic forcing. By exploiting the Lie group structure, [47] derives an averaging formula for the system response. A pth-order averaging formula is then used to explicitly specify piecewise sinusoidal open-loop control to solve the motion planning problem with $O(\epsilon^p)$ accuracy.

1.3 Attitude control with piecewise sinusoids

Rigid-body rotations are noncommutative. That is, the final orientation of a rigid body that undergoes a sequence of angular displacements depends on the order of that sequence. In contrast, rigid-body translation is commutative, since a rigid body's final position is independent of the order of the sequence of translations.

The noncommutative property of rigid-body rotation has interesting consequences for attitude control. For example, Fig. 1.1 shows a book and a reference frame that is attached to the book. The book first rotates about its body x_b axis by 90 degrees, then rotates about its body y_b axis by 90 degrees, and finally rotates about its body

x_b axis by -90 degrees. After this sequence of three rotations, the book is rotated 90 degrees about its body z_b axis. Note that no rotations in this sequence are about the body z_b axis.

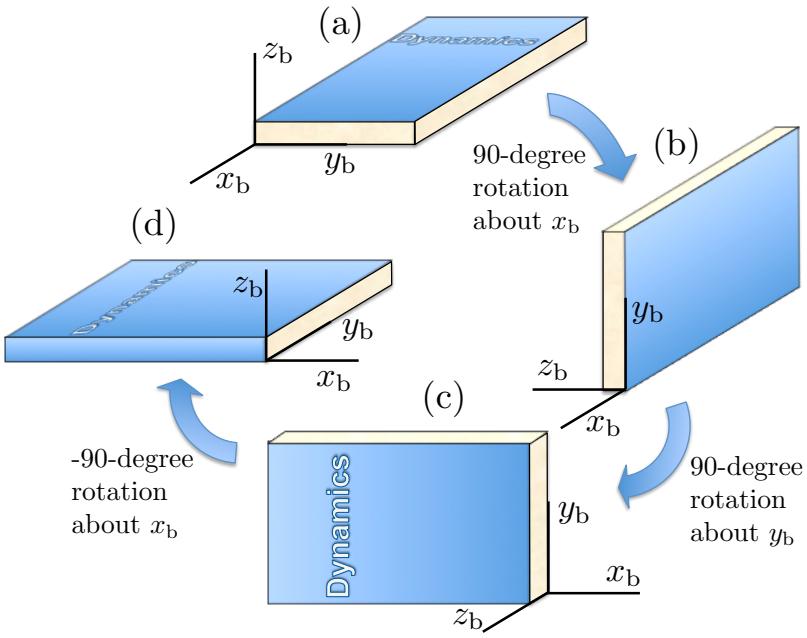

Figure 1.1: Rigid-body rotations are noncommutative.

Attitude control using piecewise sinusoidal signal can be viewed as attitude actuation with a sequence of infinitesimal rotations. Attitude control using sinusoids finds one application in the shape-change actuation system, which can be used to control the orientation of a system by altering the internal mass distribution (shape). Examples of shape-change actuation systems include moving masses, vibrating beams, and oscillating flywheels [48–55]. For example, [48] uses a pair of internal vibrating masses to change the orientation of an air spindle testbed; [49] uses electro-thermal actuators to control the attitude of a micro-satellite.

This approach of attitude control with sinusoids is closely related to the control strategies used for nonholonomic system motion planning. A nonholonomic system is a system that has nonholonomic constraints, that is, constraint equations that cannot be written as time derivatives of some function of the generalized coordinates.

Time-varying feedback controls, including the form of piecewise constant [56, 57], polynomial [56], and sinusoids [31, 33, 47, 58, 59], have been studied extensively in the context of underactuated spacecraft attitude control and nonholonomic motion planning, see [58, 60] and the references therein. In particular, sinusoidal controls are commonly used in applications including wheeled vehicles [58], underactuated satellites [33, 47], and underwater vehicles [47, 61]. Optimality of sinusoidal controls for a class of nonholonomic systems is addressed in [62].

Vibrational actuation systems that rely on this control approach may be applicable for many small systems for which conventional actuation techniques are infeasible. For example, a vibrational actuation system may be ideally suitable for small satellites.

1.4 Dissertation overview

In this dissertation, we address the attitude control problem using piecewise sinusoids. We consider a CubeSat system, which consists of a rigid body and oscillatory momentum wheels, as a representative example of the attitude kinetics. We first design the kinematic-level piecewise sinusoidal control by following the solution-based approach, and then we extend the control to the dynamic level. Note that the piecewise sinusoidal control laws proposed in this dissertation are not restricted to the CubeSat system. Our control strategies may also apply to the attitude control for other applications, such as underwater vehicles and micro-robots.

Here we note that attitude control is typically studied in the dynamic level, that is, the control variable is a force, torque, or voltage, etc. However, we emphasize that kinematic-level attitude control is of great value in its own right. Kinematic controllers are used as inner-loop steering controls in various applications, such as spacecraft, underwater vehicles, and wheeled robots [19, 27, 47, 63].

Kinematic controls are applicable to dynamic systems with high-bandwidth actuation and negligible transient response [42, 64]. For example, for a spacecraft with

"fast-enough" actuators, i.e., actuators with large bandwidth, a singular perturbation approach can be used to implement the kinematic-level angular velocity command [42]. For underwater vehicle at low Reynolds number, the velocity of the vehicle is able to track the force inputs without time delay [64].

Kinematic control can also be used for cases that dynamic effects are not negligible. For example, kinematic controllers are used as subsystem controllers in nonlinear control techniques such as backstepping, sliding mode control, and passivity-based control [8,18,34,36,46,65]. Dynamic-level control can also be designed in a backward manner. For example, [64] extends the kinematic-level control in [47] to the dynamic level by deriving an approximate solution of the system response with sinusoidal forcing. In addition, there is a large volume of literature on kinematic level control, especially in the area of motion planning of nonholonomic systems.

The remaining of this dissertation is organized as follows. In Chapter 2, we first present the definition and properties of the rotation matrices. Then we derive the attitude kinematics on SO(3). Various parameterizations of SO(3) are briefly reviewed and compared. The fact that there is no unique and global parameterization of the SO(3) manifold motivates our consideration of attitude kinematics on SO(3). Then, we derive the equations of motion of the CubeSat system. Finally, we formulate the problems that are addressed in this dissertation.

In Chapter 3, we derive the exact closed-form solution of the attitude kinematics $\dot{R} = R\hat{\Omega}$ with a class of sinusoidal angular velocity inputs. By comparing this solution with two pure rotations, we show that this class of sinusoidal inputs yield an average net rotation like a spin. Then, we analyze the solution through averaging and through motion decomposition. The controllability of the attitude kinematics is also discussed in this chapter. Finally, we present kinematic-level attitude feedback controllers for setpoint tracking and command following. In particular, we propose algorithms with constant and nonconstant actuation frequency, constant and nonconstant update rate.

Simulations are also performed to demonstrate the effectiveness of the controls.

In Chapter 4, we focus on the CubeSat system that is not subject to external damping or gravity. Thus, the system conserves total angular momentum. First we motivate the use of sinusoidal kinematic control on the dynamic level through an example. Then, by exploring the properties of the CubeSat angular velocity induced by the internal torques, we develop a second order approximation of the rotation matrix trajectory. Based on this approximation, small (ϵ) amplitude piecewise sinusoidal internal torques are designed to steer R on SO(3) with $O(\epsilon^2)$ error. Additionally, we numerically investigate the effect of the external damping on the CubeSat kinetics, and propose a heuristic setpoint tracking control algorithm for the case where the CubeSat is subject to external damping.

In Chapter 5, we investigate the feasibility of the piecewise sinusoidal control techniques using an experimental CubeSat system. We first present the design of the CubeSat mechanical system, the control system hardware, and the attitude control software. Then, we describe the experiment setup, present and discuss the experiment results. Additionally, we experimentally validate the analysis of the external damping effect on the CubeSat kinetics.

In Chapter 6, we summarize the contributions of this dissertation and discuss the future work.

Chapter 2 Problem Description

In this chapter, we define the attitude control problem that is addressed in this dissertation. The configuration space of rigid-body attitude is the special orthogonal group SO(3). We first review some important properties of SO(3). We also provide a brief discussion of other attitude representations. Next, we present a dynamic model for a CubeSat system, which consists of a rigid body and three pairs of oscillatory momentum wheels. This CubeSat system serves as a representative example of attitude kinetics. Finally, we formulate the problems that are addressed in this dissertation.

We use the following notations. Let $\mathbb{R}$ be the set of real numbers, $\mathbb{Z}$ the set of integers. Let $R_{(ij)}$ be the element in the ith row and jth column of matrix R. Let tr denote the trace of a square matrix. Let $\|\cdot\|_2$ be the 2 norm. If $x \in \mathbb{R}^3$ and $\|x\|_2 = 1$, then we call x a unit vector in $\mathbb{R}^3$.

2.1 Rotation matrix and rotation vector

The attitude of a rigid body is quantified by the orientation of a body-fixed coordinate frame relative to an inertial coordinate frame. Let $\mathbf{i}_\mathrm{b}$, $\mathbf{j}_\mathrm{b}$, and $\mathbf{k}_\mathrm{b}$ be mutually orthogonal unit vectors of the body-fixed frame, and $\mathbf{i}_\mathrm{i}$, $\mathbf{j}_\mathrm{i}$, and $\mathbf{k}_\mathrm{i}$ be mutually orthogonal unit vectors of the inertial frame, see Fig. 2.1. All coordinate frames in this dissertation are right-handed. Let $x = [x_1\ x_2\ x_3]^\mathrm{T} \in \mathbb{R}^3$, $y = [y_1\ y_2\ y_3]^\mathrm{T} \in \mathbb{R}^3$, $z = [z_1\ z_2\ z_3]^\mathrm{T} \in \mathbb{R}^3$ be such that

$$\mathbf{i}_\mathrm{b} = x_1\mathbf{i}_\mathrm{i} + x_2\mathbf{j}_\mathrm{i} + x_3\mathbf{k}_\mathrm{i}, \tag{2.1}$$

$$\mathbf{j}_\mathrm{b} = y_1\mathbf{i}_\mathrm{i} + y_2\mathbf{j}_\mathrm{i} + y_3\mathbf{k}_\mathrm{i}, \tag{2.2}$$

$$\mathbf{k}_\mathrm{b} = z_1\mathbf{i}_\mathrm{i} + z_2\mathbf{j}_\mathrm{i} + z_3\mathbf{k}_\mathrm{i}. \tag{2.3}$$

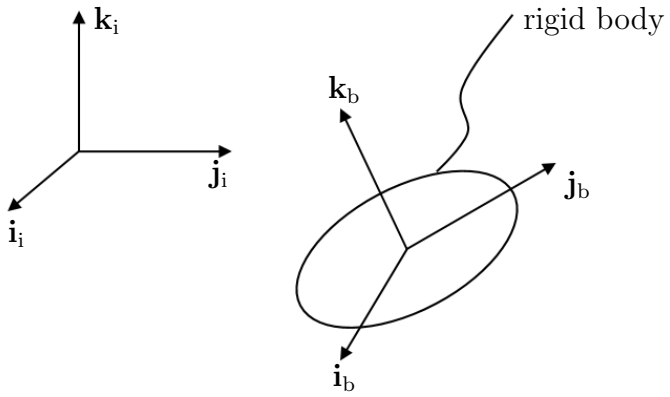

Figure 2.1: Inertial coordinate frame and body-fixed coordinate frame.

Informally, (2.1)–(2.3) can be written as

$$\begin{bmatrix} \mathbf{i}_\mathrm{b} & \mathbf{j}_\mathrm{b} & \mathbf{k}_\mathrm{b} \end{bmatrix} = \begin{bmatrix} \mathbf{i}_\mathrm{i} & \mathbf{j}_\mathrm{i} & \mathbf{k}_\mathrm{i} \end{bmatrix} \begin{bmatrix} x_1 & y_1 & z_1 \\ x_2 & y_2 & z_2 \\ x_3 & y_3 & z_3 \end{bmatrix}. \tag{2.4}$$

We define the rotation matrix

$$R \triangleq \begin{bmatrix} x_1 & y_1 & z_1 \\ x_2 & y_2 & z_2 \\ x_3 & y_3 & z_3 \end{bmatrix} \in \mathbb{R}^{3\times 3}.$$

Since the coordinate frame unit vectors are mutually orthogonal, it follows that

$$R^\mathrm{T} R = \begin{bmatrix} x^\mathrm{T} \\ y^\mathrm{T} \\ z^\mathrm{T} \end{bmatrix} \begin{bmatrix} x & y & z \end{bmatrix} = I, \tag{2.5}$$

where I is the 3×3 identity matrix. It follows from (2.5) that R is nonsingular, and $R^{-1} = R^\mathrm{T}$. Furthermore, since the coordinate frames are right-handed, $\det R = x^\mathrm{T}(y \times z) = x^\mathrm{T} x = 1$, where $\times$ denotes the vector cross product. Therefore, R belongs

to the set

$$\mathrm{SO}(3) \triangleq \{R \in \mathbb{R}^{3\times 3} : RR^{\mathrm{T}} = R^{\mathrm{T}}R = I, \det R = +1\}.$$

Conversely, it can be shown that every element of SO(3) is a rotation matrix. Thus, rotation matrices form the set SO(3).

It can be verified that SO(3) forms a group, called the three-dimensional special orthogonal group, with the matrix multiplication as the group operation [66]. Note that rotation matrices are not commutative, that is, for $R_1, R_2 \in \mathrm{SO}(3)$, $R_1R_2 \neq R_2R_1$.

The geodesic *distance* between $R_1 \in \mathrm{SO}(3)$ and $R_2 \in \mathrm{SO}(3)$ is

$$d(R_1, R_2) \triangleq \arccos \frac{\mathrm{tr}\ R_1^{\mathrm{T}}R_2 - 1}{2} \in [0, \pi]. \tag{2.6}$$

We later show that $d(\cdot, \cdot)$ is a metric on SO(3).

The set of skew-symmetric matrices in $\mathbb{R}^{3\times 3}$ is $\mathrm{so}(3) \triangleq \{S \in \mathbb{R}^{3\times 3} : S = -S^{\mathrm{T}}\}$. For $x = [x_1\ x_2\ x_3]^{\mathrm{T}} \in \mathbb{R}^3$, define the map $\hat{\cdot} : \mathbb{R}^3 \to \mathrm{so}(3)$ by

$$\hat{x} = \begin{bmatrix} 0 & -x_3 & x_2 \\ x_3 & 0 & -x_1 \\ -x_2 & x_1 & 0 \end{bmatrix}.$$

Note that the map $\hat{\cdot}$ is one-to-one and onto, and $\hat{x}y = x \times y$ for all $x, y \in \mathbb{R}^3$. We also use the notation $(x)^\wedge$ as a replacement for $\hat{x}$. Define the map $(\cdot)^\vee : \mathrm{so}(3) \to \mathbb{R}^3$ to be the inverse of $(\cdot)^\wedge$. An important property of $(\cdot)^\wedge$ is given in the following proposition.

Proposition 2.1 ([67] Lemma 2.1)**.** If $R \in \mathrm{SO}(3)$ and $x \in \mathbb{R}^3$, then

$$(Rx)^\wedge = R\hat{x}R^{\mathrm{T}}. \tag{2.7}$$

The set so(3) forms a vector space. A basis of so(3) is $\hat{e}_1$, $\hat{e}_2$, and $\hat{e}_3$, where $e_1 \triangleq [1\ 0\ 0]^{\mathrm{T}}$, $e_2 \triangleq [0\ 1\ 0]^{\mathrm{T}}$, and $e_3 \triangleq [0\ 0\ 1]^{\mathrm{T}}$. Define $E_1 \triangleq \hat{e}_1$, $E_2 \triangleq \hat{e}_2$, and $E_3 \triangleq \hat{e}_3$. The Lie bracket $[\cdot,\cdot] : \mathrm{so}(3) \times \mathrm{so}(3) \to \mathrm{so}(3)$ on so(3) is defined by $[A, B] = AB - BA$.

The *matrix exponential* of $B \in \mathrm{so}(3)$ is

$$e^B = \sum_{k=0}^{\infty} \frac{1}{k!} B^k. \tag{2.8}$$

For all $B \in \mathrm{so}(3)$ the sequence (2.8) converges (absolutely) and thus the matrix exponential is well defined. Let $A \in \mathrm{SO}(3)$, then $B \in \mathrm{so}(3)$ is a *logarithm* of A if $e^B = A$. Note that the logarithm of $A \in \mathrm{SO}(3)$ exists ([68, Proposition 11.4.2]) but it is not unique.

Let $A \in \mathrm{SO}(3)$, and assume that A has no real eigenvalues in $(-\infty, 0]$. Then, there exists a unique $B \in \mathrm{so}(3)$ such that its eigenvalues are elements of $\{z \in \mathbb{C} : -\pi < \operatorname{Im} z < \pi\}$ and $e^B = A$. We call $\log A = B$ the *principal logarithm* of A.

The following result is known as Rodrigues' formula, which provides an efficient way to compute the matrix exponential of matrices in so(3).

Proposition 2.2. Let w be a unit vector in $\mathbb{R}^3$, and let $\eta \in \mathbb{R}$. Then

$$e^{\eta\hat{w}} = I + (\sin\eta)\hat{w} + (1 - \cos\eta)\hat{w}^2. \tag{2.9}$$

Exponentials of skew symmetric matrices are orthogonal ([67, Proposition 2.4]), and the exponential map $\exp : \mathrm{so}(3) \to \mathrm{SO}(3)$ is surjective ([67, Proposition 2.5]).

Let $R = \exp(\eta\hat{w})$, where $\eta \in \mathbb{R}$, and w is a unit vector in $\mathbb{R}^3$. Then $\eta w \in \mathbb{R}^3$ is the *rotation vector* of R, where w is the axis of rotation and η is the rotation angle.

This method of representing a rotation using a rotation vector is called the equivalent axis representation. The rotation vector for a rotation matrix can be found using the following proposition.

Proposition 2.3. Let $R \in \mathrm{SO}(3)$ and $\mathcal{A} \triangleq \{A \in \mathrm{so}(3) : e^A = R\}$.

(i) If $d(R, I) = 0$, then

$$\mathcal{A} = \{2k\pi\hat{w} : k \in \mathbb{Z}, w \in \mathbb{R}^3 \text{ and } \|w\|_2 = 1\}.$$

(ii) If $0 < d(R, I) < \pi$, then

$$\begin{aligned}\mathcal{A} =&\{(2k\pi + \eta)\hat{w},\ (2k\pi - \eta)\hat{w}^{\mathrm{T}} : k \in \mathbb{Z},\\ &\eta = \arccos\frac{\mathrm{tr}R - 1}{2}, \quad w = \frac{1}{2\sin\eta}\begin{bmatrix} R_{(32)} - R_{(23)} \\ R_{(13)} - R_{(31)} \\ R_{(21)} - R_{(12)} \end{bmatrix}\Bigg\}. \end{aligned} \tag{2.10}$$

(iii) If $d(R, I) = \pi$, then

$$\mathcal{A} = \left\{(2k+1)\pi\hat{w},\ (2k+1)\pi\hat{w}^{\mathrm{T}} : k \in \mathbb{Z}, \quad w = \begin{bmatrix} \sqrt{\frac{R_{(11)}+1}{2}} \\ \frac{R_{(12)}}{\sqrt{2(R_{(11)}+1)}} \\ \frac{R_{(13)}}{\sqrt{2(R_{(11)}+1)}} \end{bmatrix}\right\}.$$

The proof of Proposition 2.3 follows from [67, Proposition 2.5]. Let $R \in \mathrm{SO}(3)$ and $d(R, I) < \pi$. Proposition 2.3 implies that

$$\log R = \begin{cases} 0, & \text{if } d(R, I) = 0, \\ \eta\hat{w}, & \text{if } 0 < d(R, I) < \pi, \end{cases} \tag{2.11}$$

where η and w are given by (2.10). Note that $\log R$ is not defined if $d(R, I) = \pi$, because if $d(R, I) = \pi$, then -1 is an eigenvalue of R.

Next we show that $d(\cdot, \cdot)$ is a metric on SO(3).

Definition 2.4. A *metric* on a set X is a function

$$d : X \times X \to \mathbb{R}$$

having the following properties:

(i) $d(x, y) \geq 0$ for all $x, y \in X$; equality holds if and only if $x = y$.

(ii) $d(x, y) = d(y, x)$ for all $x, y \in X$.

(iii) $d(x, y) + d(y, z) \geq d(x, z)$, for all $x, y, z \in X$.

Lemma 2.5. Let $R = e^{\eta \hat{w}}$, where $\eta \in [0, \pi]$ and $w \in \mathbb{R}^3$ is a unit vector. Then,

$$d(R, I) = \eta. \tag{2.12}$$

Proof. First, note that tr $I = 3$, tr $\hat{w} = 0$, and tr $\hat{w}^2 = -2$. It follows from Proposition 2.2 that

$$\text{tr } e^{\eta \hat{w}} = \text{tr } \big(I + \sin \eta \hat{w} + (1 - \cos \eta)\hat{w}^2\big) = 3 - 2(1 - \cos \eta) = 1 + 2 \cos \eta. \tag{2.13}$$

It follows from (2.13) that

$$d(R, I) = d(e^{\eta \hat{w}}, I) = \arccos \frac{\text{tr } (e^{\eta \hat{w}})^{\mathrm{T}} - 1}{2} = \arccos \frac{\text{tr } e^{\eta \hat{w}} - 1}{2} = \eta,$$

which confirms (2.12). □

Proposition 2.6. The geodesic distance $d(\cdot, \cdot)$ defined by (2.6) is a metric on SO(3).

Proof. We show $d(\cdot,\cdot)$ satisfies (i)-(iii) of Definition 2.4. Let $R_1, R_2, R_3 \in \mathrm{SO}(3)$. First, the range of arccos implies that $d(R_1, R_2) \geq 0$. Also, $d(R_1, R_2) = 0$ if and only if tr $R_1^{\mathrm{T}} R_2 = 3$, which holds if and only if $R_1^{\mathrm{T}} R_2 = I$, that is, $R_1 = R_2$. Thus, (i) is confirmed.

Next, it follows from (2.6) that

$$d(R_1, R_2) = \arccos \frac{\mathrm{tr} R_1^{\mathrm{T}} R_2 - 1}{2} = \arccos \frac{\mathrm{tr} R_2^{\mathrm{T}} R_1 - 1}{2} = d(R_2, R_1),$$

which confirms (ii).

We now show that d satisfies (iii). Assume $A, B \in \mathrm{SO}(3)$. It follows from the surjectivity of the exp map, we can write

$$A = e^{\theta_1 \hat{\xi}_1}, \quad B = e^{\theta_2 \hat{\xi}_2}, \tag{2.14}$$

where $\theta_1, \theta_2 \in [0, \pi]$ and ξ_1, ξ_2 are unit vectors in $\mathbb{R}^3$. We first need to show that

$$\theta_1 + \theta_2 \geq \arccos \frac{\mathrm{tr} e^{\theta_1 \hat{\xi}_1} e^{\theta_2 \hat{\xi}_2} - 1}{2}. \tag{2.15}$$

It follows from Lemma 2.5 that (2.15) holds in the case that $\theta_1 = 0$, or $\theta_2 = 0$. Also note that (2.15) holds trivially in the case that $\theta_1 + \theta_2 \geq \pi$.

We now assume $\theta_1 > 0$, $\theta_2 > 0$, and $\theta_1 + \theta_2 < \pi$. By applying Rodrigues' formula,

$$e^{\theta_1 \hat{\xi}_1} = I + \sin\theta_1 \hat{\xi}_1 + (1 - \cos\theta_1)\hat{\xi}_1^2,$$
$$e^{\theta_2 \hat{\xi}_2} = I + \sin\theta_2 \hat{\xi}_2 + (1 - \cos\theta_2)\hat{\xi}_2^2.$$

By direct calculation it follows that

$$\begin{aligned}\text{tr } e^{\theta_1\hat{\xi}_1}e^{\theta_2\hat{\xi}_2} = &(1-\cos\theta_1)(1-\cos\theta_2)(\xi_1^{\mathrm{T}}\xi_2)^2 - 2\sin\theta_1\sin\theta_2(\xi_1^{\mathrm{T}}\xi_2)\\ &+ (\cos\theta_1+\cos\theta_2+\cos\theta_1\cos\theta_2).\end{aligned}$$

Note that the quadratic function $f:[-1,1]\to\mathbb{R}$

$$f(x) =(1-\cos\theta_1)(1-\cos\theta_2)x^2 - 2\sin\theta_1\sin\theta_2 x + \cos\theta_1+\cos\theta_2+\cos\theta_1\cos\theta_2,$$

is minimized at $x=1$. For the parabola opens upwards and the x-coordinate of the vertex

$$\frac{\sin\theta_1\sin\theta_2}{(1-\cos\theta_1)(1-\cos\theta_2)} = \frac{\cos\frac{\theta_1+\theta_2}{2}}{\sin\frac{\theta_1}{2}\sin\frac{\theta_2}{2}} + 1 \geq 1.$$

Therefore,

$$\begin{aligned}\text{tr } e^{\theta_1\hat{\xi}_1}e^{\theta_2\hat{\xi}_2} &\geq (1-\cos\theta_1)(1-\cos\theta_2) - 2\sin\theta_1\sin\theta_2 + \cos\theta_1+\cos\theta_2+\cos\theta_1\cos\theta_2\\ &= 2\cos(\theta_1+\theta_2)+1,\end{aligned}$$

which implies (2.15) since $0<\theta_1+\theta_2<\pi$.

Next, it follows from (2.15) and Lemma 2.5 that for all $A, B\in \mathrm{SO}(3)$,

$$d(A,I)+d(B,I)\geq d(I,AB),$$

which implies that

$$d(A,I)+d(B,I)\geq d(AB,I), \tag{2.16}$$

since $d(I, AB) = d(AB, I)$. Therefore, for all $R_1, R_2, R_3 \in \mathrm{SO}(3)$,

$$\begin{aligned} d(R_1, R_2) + d(R_2, R_3) &= d(R_1 R_2^{\mathrm{T}}, I) + d(R_2 R_3^{\mathrm{T}}, I) \\ &= d(R_1 R_2^{\mathrm{T}} R_2 R_3^{\mathrm{T}}, I) \\ &= d(R_1 R_3^{\mathrm{T}}, I) \\ &= d(R_1, R_3), \end{aligned}$$

which confirms (iii). Note that the first equality and the fourth equality follow from $d(A, B) = d(AB^{\mathrm{T}}, I)$ for all $A, B \in \mathrm{SO}(3)$, and the second equality follows from (2.16). □

2.2 Rigid body attitude kinematics on SO(3)

Let $\mathbf{r}_{\mathrm{e}}$ be a unit vector attached to the rigid body. The time derivative of $\mathbf{r}_{\mathrm{e}}$ with respect to the inertial frame is [69, Eq. (3.3.16)]

$$\dot{\mathbf{r}}_{\mathrm{e}} = \boldsymbol{\omega} \times \mathbf{r}_{\mathrm{e}}, \tag{2.17}$$

where $\boldsymbol{\omega}$ is the angular velocity of the rigid body. Vector derivatives in this dissertation are always taken with respect to an inertial frame, unless noted otherwise. It follows from (2.17) that

$$\dot{\mathbf{i}}_{\mathrm{b}} = \boldsymbol{\omega} \times \mathbf{i}_{\mathrm{b}}, \quad \dot{\mathbf{j}}_{\mathrm{b}} = \boldsymbol{\omega} \times \mathbf{j}_{\mathrm{b}}, \quad \dot{\mathbf{k}}_{\mathrm{b}} = \boldsymbol{\omega} \times \mathbf{k}_{\mathrm{b}}. \tag{2.18}$$

The time derivatives of the inertial frame unit vectors are zero, that is,

$$\dot{\mathbf{i}}_{\mathrm{i}} = 0, \quad \dot{\mathbf{j}}_{\mathrm{i}} = 0, \quad \dot{\mathbf{k}}_{\mathrm{i}} = 0. \tag{2.19}$$

Differentiating (2.4) yields

$$\begin{bmatrix} \dot{\mathbf{i}}_\mathrm{b} & \dot{\mathbf{j}}_\mathrm{b} & \dot{\mathbf{k}}_\mathrm{b} \end{bmatrix} = \begin{bmatrix} \dot{\mathbf{i}}_\mathrm{i} & \dot{\mathbf{j}}_\mathrm{i} & \dot{\mathbf{k}}_\mathrm{i} \end{bmatrix} R + \begin{bmatrix} \mathbf{i}_\mathrm{i} & \mathbf{j}_\mathrm{i} & \mathbf{k}_\mathrm{i} \end{bmatrix} \dot{R}. \tag{2.20}$$

Combining (2.18), (2.19), and (2.20) yields

$$\boldsymbol{\omega} \times \begin{bmatrix} \mathbf{i}_\mathrm{b} & \mathbf{j}_\mathrm{b} & \mathbf{k}_\mathrm{b} \end{bmatrix} = \begin{bmatrix} \mathbf{i}_\mathrm{i} & \mathbf{j}_\mathrm{i} & \mathbf{k}_\mathrm{i} \end{bmatrix} \dot{R}. \tag{2.21}$$

Let the coordinates of $\boldsymbol{\omega}$ in the body frame be the components of Ω, that is,

$$\boldsymbol{\omega} = \begin{bmatrix} \mathbf{i}_\mathrm{b} & \mathbf{j}_\mathrm{b} & \mathbf{k}_\mathrm{b} \end{bmatrix} \Omega. \tag{2.22}$$

Substituting (2.22) and $\begin{bmatrix} \mathbf{i}_\mathrm{i} & \mathbf{j}_\mathrm{i} & \mathbf{k}_\mathrm{i} \end{bmatrix} = \begin{bmatrix} \mathbf{i}_\mathrm{b} & \mathbf{j}_\mathrm{b} & \mathbf{k}_\mathrm{b} \end{bmatrix} R^\mathrm{T}$ into (2.21) yields

$$\hat{\Omega} = R^\mathrm{T} \dot{R}. \tag{2.23}$$

Left multiplying both sides of (2.23) by R yields

$$\dot{R} = R\hat{\Omega}. \tag{2.24}$$

The kinematic system (2.24) is a left-invariant system on SO(3). See [15, Chapter 8] for the definition of left-invariant systems. One important feature of left-invariance is that the relative motion is invariant with respect to the initial condition. Suppose that $R_\mathrm{i}(t)$ is the solution to (2.24) with initial condition $R(0) = I$. Then for arbitrary initial condition $R(0) \in \mathrm{SO}(3)$, the solution $R(t)$ satisfies $R(0)^\mathrm{T} R(t) = R_\mathrm{i}(t)$, that is, the motion relative to $R(0)$ is $R_\mathrm{i}(t)$.

2.3 Other attitude representations

The set of all possible attitudes of a rigid body is SO(3), which is not a Euclidean space. Attitude control problems are commonly studied using parameterizations of the SO(3) manifold. These parameterizations can be embedded in the standard $\mathbb{R}^n$ vector space, thus enabling the use of conventional analysis tools in linear systems theory. Commonly used parameterizations, in addition to rotation vectors, include Euler angles, unit quaternions, Rodrigues parameters (Gibbs vector), and modified Rodrigues parameters (MRP). We briefly review some of the parameterizations.

Euler angles. The attitude of the rigid body with respect to an inertial frame can be described using a sequence of three rotations about the coordinate axes of the body-fixed frame. Specifically, if $R \in \mathrm{SO}(3)$, then there exist $\psi, \theta, \phi \in [-\pi, \pi]$ such that

$$R = e^{\psi E_3} e^{\theta E_2} e^{\phi E_1}. \tag{2.25}$$

The angles (ψ, θ, ϕ) are called the 3-2-1 Euler angles, and they are commonly referred to as yaw, pitch, and roll. There are other Euler angles representations, such as 1-2-3, 3-2-3, 2-1-3 Euler angles, which use different body-fixed rotation sequences [1].

Unit quaternions. Consider $R \in \mathrm{SO}(3)$, which can be expressed as $R = \exp(\eta \hat{w})$, where $w \in \mathbb{R}^3$ is a unit vector along the axis of rotation and $\eta \in \mathbb{R}$ is the rotation angle. The associated unit quaternion is defined as

$$q = q_0 + q_1 \mathbf{i} + q_2 \mathbf{j} + q_3 \mathbf{k},$$

or in vector form

$$q = \begin{bmatrix} q_0 & q_1 & q_2 & q_3 \end{bmatrix}^{\mathrm{T}},$$

where $q_0 = \cos(\eta/2)$, and $\begin{bmatrix} q_1 & q_2 & q_3 \end{bmatrix}^{\mathrm{T}} = w \sin(\eta/2)$. Unit quaternions form the set $S^3 \triangleq \{x \in \mathbb{R}^4 : \|x\|_2 = 1\}$.

Rodrigues parameters. Consider again $R = \exp(\eta\hat{w})$, where $\omega \in \mathbb{R}^3$ is a unit vector and $\eta \in \mathbb{R}$. The Rodrigues parameters are the components of the vector (Gibbs vector)

$$g = w \tan \frac{\eta}{2} \in \mathbb{R}^3.$$

The modified Rodrigues parameters are the components of

$$p = w \tan \frac{\eta}{4} \in \mathbb{R}^3.$$

A rigid body has three rotational degrees of freedom, thus requiring at minimum three parameters to represent the orientation. Rotation vectors, Euler angles, Rodrigues parameters, and MRP use three parameters; therefore, they are referred to as minimal representations. On the contrary, rotation matrices and unit quaternions use nine and four parameters, respectively; therefore, they are not minimal representations.

It is a topological fact that singularities exist in any three-dimensional parameterization of SO(3) [67]. The singularities refer to the points where the parameterization that maps SO(3) to $\mathbb{R}^3$ is undefined or not smooth. For example, for the rotation vector representation, $R = I$ is a singularity. For the 3-2-1 Euler angle representation, any R corresponding to $\theta = \pm\pi/2$ is a singularity.

No attitude parameterization is unique. For example, any $R \in \mathrm{SO}(3)$ is represented by a pair of antipodal unit quaternions, that is, for $R = \exp(\eta\hat{w})$ both of the unit quaternions $q = \pm \begin{bmatrix} \cos(\eta/2) & w^{\mathrm{T}} \sin(\eta/2) \end{bmatrix}^{\mathrm{T}}$ are valid representations. Nevertheless, the range of parameterization can be restricted to get a unique parameterization. For example, it is possible to restrain the amplitude of the rotation vector to be no

greater than π to get a unique parameterization provided that $d(R, I) < \pi$. As another example, for MRP, $\|p\|_2 \leq 1$ can be enforced to get a unique parameterization provided that $d(R, I) < \pi$.

Not all parameterizations are global, and thus any kinematic level feedback control that uses local representation does not have a globally asymptotically stable equilibrium. A global representation is one in which the associated rigid body kinematic (differential) equation is defined at all possible attitude points. For example, unit quaternions provide a global parameterization. The unit quaternion kinematic equation is

$$\dot{q} = \frac{1}{2} M q, \tag{2.26}$$

where

$$M = \begin{bmatrix} 0 & -\Omega_1 & -\Omega_2 & -\Omega_3 \\ \Omega_1 & 0 & \Omega_3 & -\Omega_2 \\ \Omega_2 & -\Omega_3 & 0 & \Omega_1 \\ \Omega_3 & \Omega_2 & -\Omega_1 & 0 \end{bmatrix},$$

and $\Omega = [\Omega_1 \quad \Omega_2 \quad \Omega_3]^{\mathrm{T}} \in \mathbb{R}^3$ is the angular velocity of the rigid body. As another example, the kinematic equation using 3-2-1 Euler angles (ψ, θ, ϕ) is

$$\begin{bmatrix} \dot{\psi} \\ \dot{\theta} \\ \dot{\phi} \end{bmatrix} = \begin{bmatrix} 0 & \sin\phi \sec\theta & \cos\phi \sec\theta \\ 0 & \cos\phi & -\sin\phi \\ 1 & \sin\phi \tan\theta & \cos\phi \tan\theta \end{bmatrix} \Omega. \tag{2.27}$$

The kinematic equation (2.27) is not defined at $\theta = \pm\pi/2$, rendering the 3-2-1 Euler angles a local representation. Rotation vectors are a global representation, although

there is a singularity at $R = I$. In fact, the rotation vector kinematic equation is

$$\dot{\xi} = \left(I + \frac{1}{2}\hat{\xi} + \frac{1 - \alpha(\|\xi\|_2)}{\|\xi\|_2^2}\hat{\xi}^2 \right) \Omega, \tag{2.28}$$

where ξ is the rotation vector, and $\alpha(x) \triangleq (x/2)\cot(x/2)$. It can be shown that at $\xi = 0$ (the corresponding rotation matrix $R = I$), (2.28) is well-defined.

Table 2.1 summarizes the key properties of the attitude representations covered in this section. It shows that none of the attitude parameterizations are global, unique, and singularity free. Therefore, in this dissertation, we mainly use rotation matrices to represent the attitude of a rigid body. Since unit quaternions are more compact than rotation matrices, and calculating unit quaternions is computationally efficient (due to the absence of trigonometric functions), we use quaternions primarily in simulations.

Table 2.1: Properties of attitude representations

Attitude representation	No. of params.	Singularities	Unique	Global
Euler angles	3	Exist	No	No
Rodrigues parameters	3	Exist	No	No
MRP	3	Exist	No	No
Unit quaternions	4	None	No	Yes
Rotation vector	3	Exist	No	Yes
Rotation matrix	9	None	Yes	Yes

2.4 The CubeSat system

The attitude dynamics of a mechanical system consist of kinematic and kinetic equations of motion. The attitude kinetics vary with the system's inertial properties, the actuation system, and external forcing. In this dissertation, we use a representative dynamic system to study the attitude control problem using piecewise-sinusoidal controls. This representative system is a CubeSat, which is cube-shaped miniaturized satellite with edge length 10 cm, that is equipped with a vibrational actuation

system. As discussed in Chapter 1, vibrational actuation systems have advantages over conventional flywheel actuation systems.

As shown in Fig. 2.2, the CubeSat system consists of a cubic rigid body and three pairs of vibrating momentum wheels. Each of the three momentum-wheel pairs is a rigid body and their rotational axes coincide with the principal axes of the cube. We use a pair of momentum wheels instead of a single momentum wheel for two reasons: first, a momentum-wheel pair provides larger interactive torque between the wheels and the cube when the wheels are actuated; second, the momentum-wheel pair is mass balanced about the center of mass of the cube, thus simplifying the dynamics. We label these three pairs of momentum wheels as momentum-wheel pair 1, 2, and 3, as shown in Fig. 2.2. Note that this actuation system is not meant to be a practical design with regards to the size, quantity, and location of the momentum wheels.

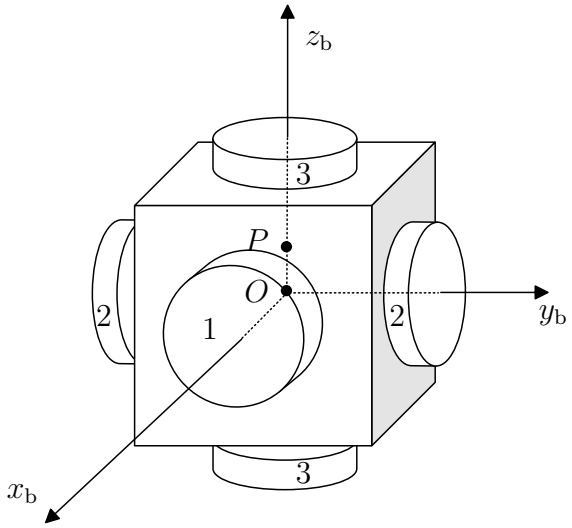

Figure 2.2: The CubeSat system consists of a cubic rigid body and three pairs of vibrating momentum wheels.

Let O be the center of mass of the cube, whose mass denoted m_c is uniformly distributed. The coordinate axes $\mathbf{i}_\mathrm{b}$, $\mathbf{j}_\mathrm{b}$, and $\mathbf{k}_\mathrm{b}$ of the body-fixed frame coincide with the principal axes of the cube. The moment of inertia tensor of the cube about O is

$\mathbf{I}_o = I_1\mathbf{i}_\mathrm{b}\mathbf{i}_\mathrm{b} + I_2\mathbf{j}_\mathrm{b}\mathbf{j}_\mathrm{b} + I_3\mathbf{k}_\mathrm{b}\mathbf{k}_\mathrm{b}$, and the angular velocity of the cube is

$$\boldsymbol{\omega} = \Omega_1\mathbf{i}_\mathrm{b} + \Omega_2\mathbf{j}_\mathrm{b} + \Omega_3\mathbf{k}_\mathrm{b}. \tag{2.29}$$

Let ψ, θ, and ϕ be the 3-2-1 Euler angles of the cube. Note that a rigid body has three rotational degrees of freedom and three translational degree of freedom, and the rotational motion is decoupled with the translational motion. Therefore, in the attitude control problem, we can ignore the translational degrees of freedom and assume the CubeSat rotates about its center of mass O. However, in this section, we derive the equations of motion for a more general case and assume the CubeSat rotates about a fixed point P, which is located by the vector $\mathbf{r}_{P/O} = h\mathbf{k}_\mathrm{b}$. This generalization is motivated by the experimental CubeSat system described in Chapter 5. Note that if $h = 0$, then point P coincides with point O. We discuss more about this generalization later in this section.

The total mass of each and every pair of wheels is m_w, and the centers of mass of the wheel-pairs are all at point O. The moment of inertia of any wheel-pair is I_a about the rotational axis and I_t about the other two perpendicular axes that go through O. Let the relative rotation angles of the moment wheels with respect to the cube be β_1, β_2, and β_3. Each of the momentum-wheel pairs is connected with the cube by a torsional spring and dashpot. The spring constant is K and the damping coefficient is C. Note that the interaction forces between a satellite and the momentum-wheel actuators do not typically include the stiffness term $K\beta$. However, the stiffness term is an important component of the vibrating momentum wheel actuator dynamics.

The CubeSat system is in a gravity field with gravity constant g. The momentum wheels are actuated by internal time-varying torques $-u_1(t)\mathbf{i}_\mathrm{b}$, $-u_2(t)\mathbf{j}_\mathrm{b}$, and $-u_3(t)\mathbf{k}_\mathrm{b}$. Equal and opposite colocated torques $u_1(t)\mathbf{i}_\mathrm{b}$, $u_2(t)\mathbf{j}_\mathrm{b}$, and $u_3(t)\mathbf{k}_\mathrm{b}$ are

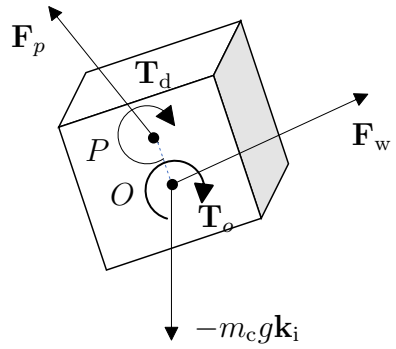

Figure 2.3: Free body diagram of the cube.

applied to the cube. We assume the external damping torque applied to the cube is

$$\mathbf{T}_\mathrm{d} = -\mu\Omega_1\mathbf{i}_\mathrm{b} - \mu\Omega_2\mathbf{j}_\mathrm{b} - \mu\Omega_3\mathbf{k}_\mathrm{b}, \tag{2.30}$$

where μ is the damping coefficient.

The constraint force and torque acting on the momentum-wheel pair 1 are denoted $-\mathbf{F}_{\mathrm{w},1}$ and $-T_{1,\mathrm{y}}\mathbf{j}_\mathrm{b}-T_{1,\mathrm{z}}\mathbf{k}_\mathrm{b}$. The constraint force and torque acting on the momentum-wheel pair 2 are denoted $-\mathbf{F}_{\mathrm{w},2}$ and $-T_{2,\mathrm{x}}\mathbf{i}_\mathrm{b} - T_{2,z}\mathbf{k}_\mathrm{b}$. The constraint force and torque acting on the momentum-wheel pair 3 are denoted $-\mathbf{F}_{\mathrm{w},3}$ and $-T_{3,\mathrm{x}}\mathbf{i}_\mathrm{b}-T_{3,\mathrm{y}}\mathbf{j}_\mathrm{b}$. Therefore, the constraint force and torque acting on the cube are $\mathbf{F}_\mathrm{w} = \mathbf{F}_{\mathrm{w},1}+\mathbf{F}_{\mathrm{w},2}+\mathbf{F}_{\mathrm{w},3}$ and $\mathbf{T}_\mathrm{w} = (T_{2,\mathrm{x}}+T_{3,\mathrm{x}})\mathbf{i}_\mathrm{b} + (T_{1,\mathrm{y}}+T_{3,\mathrm{y}})\mathbf{j}_\mathrm{b} + (T_{1,\mathrm{z}}+T_{2,\mathrm{z}})\mathbf{k}_\mathrm{b}$. The constraint force acting on the cube from point P is $\mathbf{F}_p$. Therefore, the total torque acting on the cube, excluding $\mathbf{T}_\mathrm{d}$, is

$$\begin{aligned}\mathbf{T}_o =&(u_1 + K\beta_1 + C\dot{\beta}_1 + T_{2,\mathrm{x}} + T_{3,\mathrm{x}})\mathbf{i}_\mathrm{b} + (u_2 + K\beta_2 + C\dot{\beta}_2 + T_{1,\mathrm{y}} + T_{3,\mathrm{y}})\mathbf{j}_\mathrm{b}\\ &+ (u_3 + K\beta_3 + C\dot{\beta}_3 + T_{1,\mathrm{z}} + T_{2,\mathrm{z}})\mathbf{k}_\mathrm{b}.\end{aligned} \tag{2.31}$$

We draw the free body diagram of the cube in Fig. 2.3. Note that $\mathbf{k}_\mathrm{i}$ is the unit

vector pointing upwards in the inertial frame, and it can be shown that

$$\mathbf{k}_{\mathrm{i}} = (-\sin\theta)\mathbf{i}_{\mathrm{b}} + (\sin\phi\cos\theta)\mathbf{j}_{\mathrm{b}} + (\cos\phi\cos\theta)\mathbf{k}_{\mathrm{b}}. \tag{2.32}$$

It follows from Newton-Euler's equations of motion that

$$\mathbf{M}_p + \mathbf{T}_o + \mathbf{T}_{\mathrm{d}} = \mathbf{I}_p\dot{\boldsymbol{\omega}} + \boldsymbol{\omega} \times (\mathbf{I}_p\boldsymbol{\omega}), \tag{2.33}$$

where

$$\mathbf{M}_p = (-h\mathbf{k}_{\mathrm{b}}) \times (\mathbf{F}_{\mathrm{w}} - m_{\mathrm{c}}g\mathbf{k}_{\mathrm{i}}) \tag{2.34}$$

is the total moment acting on the cube about P,

$$\mathbf{I}_p = (I_1 + m_{\mathrm{c}}h^2)\mathbf{i}_{\mathrm{b}}\mathbf{i}_{\mathrm{b}} + (I_2 + m_{\mathrm{c}}h^2)\mathbf{j}_{\mathrm{b}}\mathbf{j}_{\mathrm{b}} + I_3\mathbf{k}_{\mathrm{b}}\mathbf{k}_{\mathrm{b}} \tag{2.35}$$

is the moment of inertia of the cube about P, and

$$\dot{\boldsymbol{\omega}} = \dot{\Omega}_1\mathbf{i}_{\mathrm{b}} + \dot{\Omega}_2\mathbf{j}_{\mathrm{b}} + \dot{\Omega}_3\mathbf{k}_{\mathrm{b}}. \tag{2.36}$$

Substituting (2.29)–(2.31) and (2.34)–(2.36) into (2.33) yields

$$\begin{aligned}
&(u_1 + K\beta_1 + C\dot{\beta}_1 + T_{2,\mathrm{x}} + T_{3,\mathrm{x}} - \mu\Omega_1)\mathbf{i}_{\mathrm{b}} + (u_2 + K\beta_2 + C\dot{\beta}_2 + T_{1,\mathrm{y}} + T_{3,\mathrm{y}} - \mu\Omega_2)\mathbf{j}_{\mathrm{b}} \\
&\quad + (u_3 + K\beta_3 + C\dot{\beta}_3 + T_{1,\mathrm{z}} + T_{2,\mathrm{z}} - \mu\Omega_3)\mathbf{k}_{\mathrm{b}} - h\mathbf{k}_{\mathrm{b}} \times (\mathbf{F}_{\mathrm{w},1} + \mathbf{F}_{\mathrm{w},2} + \mathbf{F}_{\mathrm{w},3} - m_{\mathrm{c}}g\mathbf{k}_{\mathrm{i}}) \\
&= \left((I_1 + m_{\mathrm{c}}h^2)\dot{\Omega}_1 + (I_3 - I_2 - m_{\mathrm{c}}h^2)\Omega_2\Omega_3\right)\mathbf{i}_b \\
&\quad + \left((I_2 + m_{\mathrm{c}}h^2)\dot{\Omega}_2 + (I_1 - I_3 + m_{\mathrm{c}}h^2)\Omega_1\Omega_3\right)\mathbf{j}_b + \left(I_3\dot{\Omega}_3 + (I_2 - I_1)\Omega_1\Omega_2\right)\mathbf{k}_b.
\end{aligned} \tag{2.37}$$

Next, we examine the momentum-wheel pair 1. The free body diagram is shown

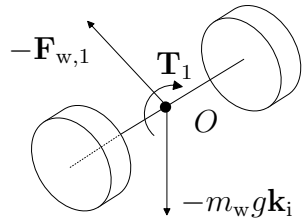

Figure 2.4: Free body diagram of momentum wheels about the x_{b} axis.

in Fig. 2.4, where the resultant torque

$$\mathbf{T}_1 = -(u_1 + K\beta_1 + C\dot{\beta}_1)\mathbf{i}_{\mathrm{b}} - T_{1,\mathrm{y}}\mathbf{j}_{\mathrm{b}} - T_{1,\mathrm{z}}\mathbf{k}_{\mathrm{b}}. \tag{2.38}$$

Note that the center of mass of the momentum-wheel pair 1 is O, which is a fixed point on the cube. The velocity of point O is

$$\mathbf{v} = \frac{\mathrm{d}}{\mathrm{d}t}(-h\mathbf{k}_{\mathrm{b}}) = -h\boldsymbol{\omega} \times \mathbf{k}_{\mathrm{b}},$$

and the acceleration of point O is

$$\mathbf{a} = \dot{\mathbf{v}} = -h[\dot{\boldsymbol{\omega}} \times \mathbf{k}_{\mathrm{b}} + \boldsymbol{\omega} \times (\boldsymbol{\omega} \times \mathbf{k}_{\mathrm{b}})]. \tag{2.39}$$

Substituting (2.29) and (2.36) into (2.39) yields

$$\mathbf{a} = (-h\Omega_1\Omega_3 - h\dot{\Omega}_2)\mathbf{i}_{\mathrm{b}} + (-h\Omega_2\Omega_3 + h\dot{\Omega}_1)\mathbf{j}_{\mathrm{b}} + (h\Omega_1^2 + h\Omega_2^2)\mathbf{k}_{\mathrm{b}}. \tag{2.40}$$

The angular velocity of momentum-wheel pair 1 is

$$\boldsymbol{\omega}_1 = \boldsymbol{\omega} + \dot{\beta}_1\mathbf{i}_{\mathrm{b}}, \tag{2.41}$$

and its angular acceleration is

$$\boldsymbol{\alpha}_1 = \dot{\boldsymbol{\omega}} + \ddot{\beta}_1 \mathbf{i}_\mathrm{b} + \dot{\beta}_1 \boldsymbol{\omega} \times \mathbf{i}_\mathrm{b}. \tag{2.42}$$

Let $\mathbf{I}_1 \triangleq I_\mathrm{a}\mathbf{i}_\mathrm{b}\mathbf{i}_\mathrm{b} + I_\mathrm{t}\mathbf{j}_\mathrm{b}\mathbf{j}_\mathrm{b} + I_\mathrm{t}\mathbf{k}_\mathrm{b}\mathbf{k}_\mathrm{b}$ be the momentum of inertia tensor of momentum-wheel pair 1. It follows from Newton-Euler equations of motion that

$$-\mathbf{F}_{\mathrm{w},1} - m_\mathrm{w} g \mathbf{k}_\mathrm{i} = m_\mathrm{w}\mathbf{a}, \tag{2.43}$$

$$\mathbf{T}_1 = \mathbf{I}_1\boldsymbol{\alpha}_1 + \boldsymbol{\omega}_1 \times (\mathbf{I}_1\boldsymbol{\omega}_1). \tag{2.44}$$

Following the same procedure for the momentum-wheel pairs about the y_b and z_b axes, we have

$$-\mathbf{F}_{\mathrm{w},2} - m_\mathrm{w} g \mathbf{k}_\mathrm{i} = m_\mathrm{w}\mathbf{a}, \tag{2.45}$$

$$\mathbf{T}_2 = \mathbf{I}_2\boldsymbol{\alpha}_2 + \boldsymbol{\omega}_2 \times (\mathbf{I}_2\boldsymbol{\omega}_2), \tag{2.46}$$

$$-\mathbf{F}_{\mathrm{w},3} - m_\mathrm{w} g \mathbf{k}_\mathrm{i} = m_\mathrm{w}\mathbf{a}, \tag{2.47}$$

$$\mathbf{T}_3 = \mathbf{I}_3\boldsymbol{\alpha}_3 + \boldsymbol{\omega}_3 \times (\mathbf{I}_3\boldsymbol{\omega}_3), \tag{2.48}$$

where $\mathbf{I}_2 \triangleq I_\mathrm{t}\mathbf{i}_\mathrm{b}\mathbf{i}_\mathrm{b} + I_\mathrm{a}\mathbf{j}_\mathrm{b}\mathbf{j}_\mathrm{b} + I_\mathrm{t}\mathbf{k}_\mathrm{b}\mathbf{k}_\mathrm{b}$, $\mathbf{I}_3 \triangleq I_\mathrm{t}\mathbf{i}_\mathrm{b}\mathbf{i}_\mathrm{b} + I_\mathrm{t}\mathbf{j}_\mathrm{b}\mathbf{j}_\mathrm{b} + I_\mathrm{a}\mathbf{k}_\mathrm{b}\mathbf{k}_\mathrm{b}$, and

$$\boldsymbol{\omega}_2 = \boldsymbol{\omega} + \dot{\beta}_2 \mathbf{j}_\mathrm{b}, \tag{2.49}$$

$$\boldsymbol{\omega}_3 = \boldsymbol{\omega} + \dot{\beta}_3 \mathbf{k}_\mathrm{b}, \tag{2.50}$$

$$\boldsymbol{\alpha}_2 = \dot{\boldsymbol{\omega}} + \ddot{\beta}_2 \mathbf{j}_\mathrm{b} + \dot{\beta}_2 \boldsymbol{\omega} \times \mathbf{j}_\mathrm{b}, \tag{2.51}$$

$$\boldsymbol{\alpha}_3 = \dot{\boldsymbol{\omega}} + \ddot{\beta}_3 \mathbf{k}_\mathrm{b} + \dot{\beta}_3 \boldsymbol{\omega} \times \mathbf{k}_\mathrm{b}, \tag{2.52}$$

$$\mathbf{T}_2 = -T_{2,\mathrm{x}}\mathbf{i}_\mathrm{b} - (u_2 + K\beta_2 + C\dot{\beta}_2)\mathbf{j}_\mathrm{b} - T_{2,\mathrm{z}}\mathbf{k}_\mathrm{b}, \tag{2.53}$$

$$\mathbf{T}_3 = -T_{3,\mathrm{x}}\mathbf{i}_\mathrm{b} - T_{3,\mathrm{y}}\mathbf{j}_\mathrm{b} - (u_3 + K\beta_3 + C\dot{\beta}_3)\mathbf{k}_\mathrm{b}. \tag{2.54}$$

It follows from (2.40), (2.43), (2.45), and (2.47) that

$$
\begin{aligned}
&-\mathbf{F}_{\mathrm{w},1}-\mathbf{F}_{\mathrm{w},2}-\mathbf{F}_{\mathrm{w},3}-3m_{\mathrm{w}}g\mathbf{k}_{\mathrm{i}}\\
&\quad=3m_{\mathrm{w}}\left((-h\Omega_1\Omega_3-h\dot{\Omega}_2)\mathbf{i}_{\mathrm{b}}+(-h\Omega_2\Omega_3+h\dot{\Omega}_1)\mathbf{j}_{\mathrm{b}}+(h\Omega_1^2+h\Omega_2^2)\mathbf{k}_{\mathrm{b}}\right). \qquad (2.55)
\end{aligned}
$$

Combining (2.29), (2.36), (2.41), (2.42), (2.44), (2.46), (2.48)–(2.54) yields

$$
\begin{aligned}
&-(u_1+K\beta_1+C\dot{\beta}_1)\mathbf{i}_{\mathrm{b}}-T_{1,\mathrm{y}}\mathbf{j}_{\mathrm{b}}-T_{1,\mathrm{z}}\mathbf{k}_{\mathrm{b}}=(I_{\mathrm{a}}\dot{\Omega}_1+I_{\mathrm{a}}\ddot{\beta}_1)\mathbf{i}_{\mathrm{b}}\\
&\quad+\left((I_{\mathrm{a}}-I_{\mathrm{t}})\Omega_1\Omega_3+I_{\mathrm{a}}\dot{\beta}_1\Omega_3+I_{\mathrm{t}}\dot{\Omega}_2\right)\mathbf{j}_{\mathrm{b}}+\left((I_{\mathrm{t}}-I_{\mathrm{a}})\Omega_1\Omega_2-I_{\mathrm{a}}\dot{\beta}_1\Omega_2+I_{\mathrm{t}}\dot{\Omega}_3\right)\mathbf{k}_{\mathrm{b}}, \qquad (2.56)\\
&-T_{2,\mathrm{x}}\mathbf{i}_{\mathrm{b}}-(u_2+K\beta_2+C\dot{\beta}_2)\mathbf{j}_{\mathrm{b}}-T_{2,\mathrm{z}}\mathbf{k}_{\mathrm{b}}=\left((I_{\mathrm{t}}-I_{\mathrm{a}})\Omega_2\Omega_3-I_{\mathrm{a}}\dot{\beta}_2\Omega_3+I_{\mathrm{t}}\dot{\Omega}_1\right)\mathbf{i}_{\mathrm{b}}\\
&\quad+(I_{\mathrm{a}}\dot{\Omega}_2+I_{\mathrm{a}}\ddot{\beta}_2)\mathbf{j}_{\mathrm{b}}+\left((I_{\mathrm{a}}-I_{\mathrm{t}})\Omega_1\Omega_2+I_{\mathrm{a}}\dot{\beta}_2\Omega_1+I_{\mathrm{t}}\dot{\Omega}_3\right)\mathbf{k}_{\mathrm{b}}, \qquad (2.57)\\
&-T_{3,\mathrm{x}}\mathbf{i}_{\mathrm{b}}-T_{3,\mathrm{y}}\mathbf{y}_{\mathrm{b}}-(u_3+K\beta_3+C\dot{\beta}_3)\mathbf{k}_{\mathrm{b}}=\left((I_{\mathrm{a}}-I_{\mathrm{t}})\Omega_2\Omega_3+I_{\mathrm{a}}\dot{\beta}_3\Omega_2+I_{\mathrm{t}}\dot{\Omega}_1\right)\mathbf{i}_{\mathrm{b}}\\
&\quad+\left((I_{\mathrm{t}}-I_{\mathrm{a}})\Omega_1\Omega_3-I_{\mathrm{a}}\dot{\beta}_3\Omega_1+I_{\mathrm{t}}\dot{\Omega}_2\right)\mathbf{j}_{\mathrm{b}}+(I_{\mathrm{a}}\dot{\Omega}_3+I_{\mathrm{a}}\ddot{\beta}_3)\mathbf{k}_{\mathrm{b}}. \qquad (2.58)
\end{aligned}
$$

Now, it follows from (2.32), (2.37), (2.55)–(2.58) that the equations of motion of the CubeSat system are

$$
\begin{aligned}
&(I_1+I_{\mathrm{a}}+2I_{\mathrm{t}}+mh^2)\dot{\Omega}_1+I_{\mathrm{a}}\ddot{\beta}_1-I_{\mathrm{a}}\Omega_3\dot{\beta}_2+I_{\mathrm{a}}\Omega_2\dot{\beta}_3=(I_2-I_3+mh^2)\Omega_2\Omega_3\\
&\qquad\qquad-\mu\Omega_1-mgh\sin\phi\cos\theta, \qquad (2.59)\\
&(I_2+I_{\mathrm{a}}+2I_{\mathrm{t}}+mh^2)\dot{\Omega}_2+I_{\mathrm{a}}\ddot{\beta}_2+I_{\mathrm{a}}\Omega_3\dot{\beta}_1-I_{\mathrm{a}}\Omega_1\dot{\beta}_3=(I_3-I_1-mh^2)\Omega_1\Omega_3\\
&\qquad\qquad-\mu\Omega_2-mgh\sin\theta, \qquad (2.60)\\
&(I_3+I_{\mathrm{a}}+2I_{\mathrm{t}})\dot{\Omega}_3+I_{\mathrm{a}}\ddot{\beta}_3-I_{\mathrm{a}}\Omega_2\dot{\beta}_1+I_{\mathrm{a}}\Omega_1\dot{\beta}_2=(I_1-I_2)\Omega_1\Omega_2-\mu\Omega_3, \qquad (2.61)\\
&I_{\mathrm{a}}\dot{\Omega}_1+I_{\mathrm{a}}\ddot{\beta}_1+C\dot{\beta}_1=-u_1-K\beta_1, \qquad (2.62)\\
&I_{\mathrm{a}}\dot{\Omega}_2+I_{\mathrm{a}}\ddot{\beta}_2+C\dot{\beta}_2=-u_2-K\beta_2, \qquad (2.63)\\
&I_{\mathrm{a}}\dot{\Omega}_3+I_{\mathrm{a}}\ddot{\beta}_3+C\dot{\beta}_3=-u_3-K\beta_3, \qquad (2.64)
\end{aligned}
$$

where $m = m_c + 3m_{\rm w}$. Define

$$\Omega \triangleq \begin{bmatrix} \Omega_1 \\ \Omega_2 \\ \Omega_3 \end{bmatrix}, \quad \beta \triangleq \begin{bmatrix} \beta_1 \\ \beta_2 \\ \beta_3 \end{bmatrix}, \quad u \triangleq \begin{bmatrix} u_1 \\ u_2 \\ u_3 \end{bmatrix},$$

$$J \triangleq \begin{bmatrix} I_1 + I_{\rm a} + 2I_{\rm t} + mh^2 & 0 & 0 \\ 0 & I_2 + I_{\rm a} + 2I_{\rm t} + mh^2 & 0 \\ 0 & 0 & I_3 + I_{\rm a} + 2I_{\rm t} \end{bmatrix}. \tag{2.65}$$

Then, the equations of motion of the CubeSat system can be written into the matrix form,

$$J\dot{\Omega} + I_{\rm a}\ddot{\beta} - J\Omega \times \Omega + I_{\rm a}\Omega \times \dot{\beta} = -\mu\Omega + mghb, \tag{2.66}$$

$$I_{\rm a}(\dot{\Omega} + \ddot{\beta}) + C\dot{\beta} + K\beta = -u, \tag{2.67}$$

where $b = [-\sin\phi\cos\theta \quad -\sin\theta \quad 0]^{\rm T}$. Note that equations (2.66)(2.67) combined with the rigid body rotation kinematics (2.27) form the complete set of system equations.

The dynamics (2.66) and (2.67) are rather general in that they cover various cases of CubeSat systems:

(i) $g > 0$ corresponds to the case that the CubeSat is in a gravity field. We let $g = 0$ if the CubeSat is in the deep space.

(ii) $\mu > 0$ corresponds to the case that the CubeSat is subject to external viscous damping. If we let $\mu = 0$ and $g = 0$, then there is no external damping and no gravitational force, and the angular momentum of the system is conserved.

(iii) $h > 0$ corresponds to the case that the rotational center doesn't coincide with the center of mass of the CubeSat system. This case accommodates experimen-

tal testing that is described in Chapter 5.

We now let $g = \mu = h = 0$, and consider a special case. In this case, there are no external torques and no gravitational forces, and the total angular momentum is conserved. Additionally, we assume the total angular momentum is zero, that is,

$$\mathbf{I}_o\boldsymbol{\omega} + \mathbf{I}_1\boldsymbol{\omega}_1 + \mathbf{I}_2\boldsymbol{\omega}_2 + \mathbf{I}_3\boldsymbol{\omega}_3 = 0. \tag{2.68}$$

Substituting (2.29), (2.41), (2.49), and (2.50) into (2.68) yields that

$$J\Omega + I_{\mathrm{a}}\dot{\beta} = 0, \tag{2.69}$$

where $h = 0$ in the definition of J.

To simplify the kinetics further, we consider (2.69), and assume all the diagonal components of the momentum of inertia matrix (2.65) are equal to J_{d}. Define $J_{\mathrm{s}} \triangleq I_{\mathrm{a}}(1 - I_{\mathrm{a}}/J_{\mathrm{d}})$, where $I_{\mathrm{a}} > 0$ is mass moment of inertia of a pair of momentum wheels about the rotational axis.

Next, we use the characteristic time and characteristic frequency [70] that (2.67) and (2.69) demonstrate to derive equations of motion in dimensionless form. It follows from (2.24) (2.67) and (2.69) that the complete set of equations of motion of the CubeSat system is

$$\dot{R}(t^*) = R(t^*)\hat{\Omega}^*(t^*), \tag{2.70}$$

$$J_{\mathrm{d}}\Omega^* + I_{\mathrm{a}}\dot{\beta}^* = 0, \tag{2.71}$$

$$J_{\mathrm{s}}\ddot{\beta}^* + C\dot{\beta}^* + K\beta^* = -u^*, \tag{2.72}$$

where we have intentionally used variables with star to denote that the variables are with dimensions. To express (2.70)–(2.72) in dimensionless form, we define the characteristic frequency $\Omega_0 \triangleq \sqrt{K/J_{\mathrm{s}}}$, the characteristic angle $\beta_0 \triangleq 1$ rad, and the

characteristic torque $u_0 \triangleq J_{\mathrm{d}} K \beta_0 / I_{\mathrm{a}}$. Let

$$t \triangleq \Omega_0 t^*, \quad \Omega \triangleq \frac{\Omega^*}{\Omega_0}, \quad \beta \triangleq \frac{\beta^*}{\beta_0}, \quad u \triangleq \frac{u^*}{u_0}. \tag{2.73}$$

Then, it follows that (2.70)–(2.72) can be expressed as

$$\dot{R}(t) = R(t)\hat{\Omega}(t), \tag{2.74}$$

$$\kappa \Omega(t) + \dot{\beta}(t) = 0, \tag{2.75}$$

$$\ddot{\beta}(t) + 2\zeta \dot{\beta}(t) + \beta(t) = -\kappa u(t), \tag{2.76}$$

where $\zeta = C/(2\sqrt{J_{\mathrm{s}} K})$, and $\kappa = J_{\mathrm{d}}/(I_{\mathrm{a}} \beta_0)$. Note that in (2.70)–(2.72) the derivatives are taken with respect to t^*, and in (2.74)–(2.76) the derivatives are taken with respect to the dimensionless time t. This is the attitude dynamics model we focus on in this dissertation.

2.5 Problem statement

In this dissertation, we consider the attitude control problem using piecewise sinusoids. Specifically, we consider the CubeSat kinetics (2.75) and (2.76), and study the setpoint tracking and command following problems. In addition, we consider the CubeSat kinetics (2.66) and (2.66), and study the external damping effect on the CubeSat kinetics through numerical simulation.

This dissertation considers controls in the form of piecewise sinusoids. To facilitate the presentation, we use the following notations. Let all references to k in this dissertation be for all $k \in \mathbb{N} \triangleq \{0, 1, 2, \cdots\}$, unless otherwise stated. Let $\Delta t_k > 0$ be a time increment, and define the time $t_{k+1} \triangleq t_k + \Delta t_k$, where $t_0 \triangleq 0$. We also define the interval $\mathcal{I}_k \triangleq [t_k, t_{k+1})$. Finally, if f is a function of time $t \geq 0$, then we let $f_k \triangleq f(t_k)$.

Furthermore, let $\omega_{\max} > 0$. We call Ω an *admissible kinematic control* if for all $t \in \mathcal{I}_k$,

$$\Omega(t) = S_k \left[c_k(\cos \omega_k t)e_1 + c_k(\sin \omega_k t)e_2 + \omega_{\mathrm{d}k} e_3 \right], \tag{2.77}$$

where $S_k \in \mathrm{SO}(3)$, $\omega_k \in (0, \omega_{\max}]$, and $c_k, \omega_{\mathrm{d}k} \in \mathbb{R}$. The control parameters in (2.77) are S_k, ω_k, c_k, $\omega_{\mathrm{d}k}$ and Δt_k. For all $t \in \mathcal{I}_k$, Ω can be expressed as

$$\Omega(t) = \Omega_1(t)e_1 + \Omega_2(t)e_2 + \Omega_3(t)e_3,$$

where $\Omega_1, \Omega_2, \Omega_3 : [0, \infty) \to \mathbb{R}$ are piecewise sinusoids.

We call u an *admissible dynamic control* if for all $t \in \mathcal{I}_k$,

$$u(t) = \sum_{i=1}^{3} A_{ik} \sin(\omega t + \varphi_k)e_i, \tag{2.78}$$

where $A_{ik} \in \mathbb{R}$, $\omega \in (0, \omega_{\max}]$, and $\varphi_k \in \mathbb{R}$. We note that the angular frequency ω of $u(t)$ is constant. This is motivated by the actuator dynamics of the CubeSat system. In particular, if the oscillatory moment wheels are driven at a frequency close to the system's natural frequency, then the cube would get bigger angular velocities, yielding a higher control authority.

Next, consider the reference model

$$\dot{R}_{\mathrm{d}}(t) = R_{\mathrm{d}}(t)\hat{\Omega}_{\mathrm{d}}(t), \tag{2.79}$$

where $t \geq 0$, $R_{\mathrm{d}}(t) \in \mathrm{SO}(3)$ is the command, $R_{\mathrm{d}}(0) = R_{\mathrm{d}0} \in \mathrm{SO}(3)$ is the initial condition, and $\Omega_{\mathrm{d}} : [0, \infty) \to \mathbb{R}^3$ is the reference-model input. Define the command-

following error

$$Z(t) \triangleq R_{\mathrm{d}}^{\mathrm{T}}(t)R(t), \tag{2.80}$$

and the scalar performance

$$z(t) \triangleq d(R(t), R_{\mathrm{d}}(t)) = d(Z(t), I). \tag{2.81}$$

Next, we formulate the kinematic-level and dynamic-level attitude control problems.

Kinematic-level attitude control. Consider (2.79) and (2.74), where $t \geq 0$, $R(t) \in \mathrm{SO}(3)$, $R(0) = R_0 \in \mathrm{SO}(3)$ is the initial condition, and $\Omega(t) \in \mathbb{R}^3$ is the kinematic control. The objective is to design an admissible kinematic control Ω that uses Z feedback and makes the performance z small in some sense.

Chapter 3 considers kinematic-level attitude control. We first analyze the solution of (2.74) and (2.77), and note that in the case of $\omega_{\mathrm{d}} \neq 0$, the control design is trivial. This is because we can always let $c_k = 0$ and choose S_k and $\omega_{\mathrm{d}k}$ properly to achieve the control objective. We focus on the case that $\omega_{\mathrm{d}} = 0$. In particular, section 3.3 considers the setpoint tracking problem where $\Omega_{\mathrm{d}}(t) \equiv 0$. In this case, the objective is to make z converge to zero. For the general command-following problem, the restriction (2.77) prohibits perfect command following, and thus our objective is approximate command following. This problem is considered in Section 3.4.

Note that the dimensionless attitude kinematic equation (2.74) is identical with (2.24). Therefore, in Chapter 3 we don't differentiate dimensionless t from t with dimension.

Dynamic-level attitude control. Consider (2.74)–(2.76), where $t \geq 0$, $R(t) \in \mathrm{SO}(3)$, $\kappa > 0$, $\zeta \in (0, 1)$, $R(0) = R_0 \in \mathrm{SO}(3)$, $\beta(0) = \beta_0 \in \mathbb{R}^3$, and $\dot{\beta}(0) = p \in \mathbb{R}^3$ are the initial conditions, and $u(t) \in \mathbb{R}^3$ is the dynamic control. The objective is to design an admissible dynamic control u that uses Z feedback and yields $\lim_{t\to\infty} R(t) = R_{\mathrm{d}}$,

where $R_{\mathrm{d}} \in \mathrm{SO}(3)$ is the desired attitude.

The dynamic-level attitude control problem is covered in Chapter 4. Additionally, we study the external damping effect on the CubeSat kinetics through numerical simulations.

Chapter 3 Kinematic-Level Attitude Control

In this chapter, we derive the exact analytic solution of the attitude kinematic system $\dot{R} = R\hat{\Omega}$ with a class of sinusoidal angular velocity inputs. We show that this class of sinusoidal inputs yield an average net rotation like a spin. We then comment on the controllability of the system. Finally, we present kinematic-level orientation feedback controllers for setpoint tracking and command following.

In this chapter, and especially the next chapter, we make use of the big O notation, which is defined as the following.

Definition 3.1. Big O notation. Let V be a set. Let $\epsilon \in \mathbb{R}$, and δ_1, δ_2 be functions mapping $\mathbb{R}$ to V. Let $\|\cdot\|_{\mathrm{V}}$, $\|\cdot\|_{\mathrm{R}}$ be norms on V and $\mathbb{R}$ respectively. If there exist positive constant k_1 and k_2 such that

$$\|\delta_1(\epsilon)\|_{\mathrm{V}} \leq k_1 \|\delta_2(\epsilon)\|_{\mathrm{V}}, \quad \forall \|\epsilon\|_{\mathrm{R}} < k_2,$$

then, we write $\delta_1(\epsilon) = O(\delta_2(\epsilon))$.

3.1 Exact solutions of the attitude kinematic system

Consider the three-dimensional rotation system

$$\dot{R}(t) = R(t)\hat{\Omega}(t), \tag{3.1}$$

and the admissible control

$$\Omega(t) = S[c(\cos \omega t)e_1 + c(\sin \omega t)e_2 + \omega_{\mathrm{d}} e_3], \tag{3.2}$$

where $t \geq 0$, $c \geq 0$, $\omega > 0$, $\omega_{\mathrm{d}} \in \mathbb{R}$, and $R(0) = R_0 \in \mathrm{SO}(3)$ is the initial condition. We now provide a solution to (3.1) and (3.2).

Let $R' \triangleq S^{\mathrm{T}} R S$, and it follows from (3.1) that

$$\dot{R}'(t) = R'(t) S^{\mathrm{T}} \hat{\Omega}(t) S = R'(t) (S^{\mathrm{T}} \Omega(t))^{\wedge}. \tag{3.3}$$

Substituting (3.2) into (3.3) yields for $i \in \{1, 2, 3\}$,

$$\dot{R}'_{(i1)} = \omega_{\mathrm{d}} R'_{(i2)} - c(\sin \omega t) R'_{(i3)}, \tag{3.4}$$

$$\dot{R}'_{(i2)} = -\omega_{\mathrm{d}} R'_{(i1)} + c(\cos \omega t) R'_{(i3)}, \tag{3.5}$$

$$\dot{R}'_{(i3)} = c(\sin \omega t) R'_{(i1)} - c(\cos \omega t) R'_{(i2)}. \tag{3.6}$$

Differentiating (3.6) twice and using (3.4) and (3.5) yields

$$\dddot{R}'_{(i3)} = -\left(c^2 + (\omega + \omega_{\mathrm{d}})^2\right) \dot{R}'_{(i3)}. \tag{3.7}$$

Solving (3.7) for $\dot{R}'_{(i3)}$ and using (3.4)–(3.6) yields the solution to (3.1) and (3.2), which is

$$R(t) = R_0 S \Phi(t) S^{\mathrm{T}}, \tag{3.8}$$

where

$$\Phi_{(11)}(t) = \frac{(\omega + \omega_{\mathrm{d}})^2}{\omega_{\mathrm{n}}^2} (\cos \omega_{\mathrm{n}} t)(\cos \omega t) + \frac{\omega + \omega_{\mathrm{d}}}{\omega_{\mathrm{n}}} (\sin \omega_{\mathrm{n}} t)(\sin \omega t) + \frac{c^2}{\omega_{\mathrm{n}}^2} \cos \omega t,$$

$$\Phi_{(12)}(t) = \frac{(\omega + \omega_{\mathrm{d}})^2}{\omega_{\mathrm{n}}^2} (\cos \omega_{\mathrm{n}} t)(\sin \omega t) - \frac{\omega + \omega_{\mathrm{d}}}{\omega_{\mathrm{n}}} (\sin \omega_{\mathrm{n}} t)(\cos \omega t) + \frac{c^2}{\omega_{\mathrm{n}}^2} \sin \omega t,$$

$$\Phi_{(13)}(t) = \frac{c(\omega + \omega_{\mathrm{d}})}{\omega_{\mathrm{n}}^2} - \frac{c(\omega + \omega_{\mathrm{d}})}{\omega_{\mathrm{n}}^2} \cos \omega_{\mathrm{n}} t,$$

$$\Phi_{(21)}(t) = \frac{\omega+\omega_{\mathrm{d}}}{\omega_{\mathrm{n}}}(\sin\omega_{\mathrm{n}}t)(\cos\omega t) - (\cos\omega_{\mathrm{n}}t)(\sin\omega t),$$
$$\Phi_{(22)}(t) = (\cos\omega_{\mathrm{n}}t)(\cos\omega t) + \frac{\omega+\omega_{\mathrm{d}}}{\omega_{\mathrm{n}}}(\sin\omega_{\mathrm{n}}t)(\sin\omega t),$$
$$\Phi_{(23)}(t) = -\frac{c}{\omega_{\mathrm{n}}}\sin\omega_{\mathrm{n}}t,$$
$$\Phi_{(31)}(t) = -\frac{c(\omega+\omega_{\mathrm{d}})}{\omega_{\mathrm{n}}^2}(\cos\omega_{\mathrm{n}}t)(\cos\omega t) - \frac{c}{\omega_{\mathrm{n}}}(\sin\omega_{\mathrm{n}}t)(\sin\omega t) + \frac{c(\omega+\omega_{\mathrm{d}})}{\omega_{\mathrm{n}}^2}\cos\omega t,$$
$$\Phi_{(32)}(t) = \frac{c}{\omega_{\mathrm{n}}}(\sin\omega_{\mathrm{n}}t)(\cos\omega t) - \frac{c(\omega+\omega_{\mathrm{d}})}{\omega_{\mathrm{n}}^2}(\cos\omega_{\mathrm{n}}t)(\sin\omega t) + \frac{c(\omega+\omega_{\mathrm{d}})}{\omega_{\mathrm{n}}^2}\sin\omega t,$$
$$\Phi_{(33)}(t) = \frac{(\omega+\omega_{\mathrm{d}})^2}{\omega_{\mathrm{n}}^2} + \frac{c^2}{\omega_{\mathrm{n}}^2}\cos\omega_{\mathrm{n}}t,$$

where

$$\omega_{\mathrm{n}} \triangleq \sqrt{(\omega+\omega_{\mathrm{d}})^2+c^2}. \tag{3.9}$$

Next, define the pure rotation $\tilde{R} : [0,\infty) \to \mathrm{SO}(3)$ by

$$\tilde{R}(t) \triangleq R_0 S \exp\left(\left(\sqrt{(\omega+\omega_{\mathrm{d}})^2+c^2}-\omega\right)tE_3\right)S^{\mathrm{T}}. \tag{3.10}$$

Note that (3.10) is the solution of (3.1) with $\Omega(t) = \left(\sqrt{(\omega+\omega_{\mathrm{d}})^2+c^2}-\omega\right)Se_3$, which is an constant control. The following result compares (3.8) and (3.10).

Proposition 3.2. Consider (3.8) and (3.10). Let $\Delta t_k = 2\pi/\sqrt{(\omega+\omega_{\mathrm{d}})^2+c^2}$, and let $\omega+\omega_{\mathrm{d}} > 0$. Then,

$$R_{k+1} = \tilde{R}_{k+1} = R_k S \exp\left(\left(\sqrt{(\omega+\omega_{\mathrm{d}})^2+c^2}-\omega\right)\Delta t_k E_3\right)S^{\mathrm{T}}, \tag{3.11}$$

and

$$\sup_{t\in\mathcal{I}_k} d(R(t),\tilde{R}(t)) = \arccos\frac{(\omega+\omega_{\mathrm{d}})^2-c^2}{(\omega+\omega_{\mathrm{d}})^2+c^2}. \tag{3.12}$$

Proof. It follows from (3.8) and (3.10) that

$$\begin{aligned}\text{tr } R^{\mathrm{T}}(t)\tilde{R}(t) &= \text{tr } \Phi^{\mathrm{T}}(t)\exp\left(\left(\sqrt{(\omega+\omega_{\mathrm{d}})^2+c^2}-\omega\right)tE_3\right)\\ &= \frac{\left(\omega_{\mathrm{n}}-(\omega+\omega_{\mathrm{d}})\right)^2}{\omega_{\mathrm{n}}^2}\cos^2\omega_{\mathrm{n}}t\\ &\quad+\frac{2c^2}{\omega_{\mathrm{n}}^2}\cos\omega_{\mathrm{n}}t+\frac{2(\omega+\omega_{\mathrm{d}})\omega_{\mathrm{n}}+(\omega+\omega_{\mathrm{d}})^2}{\omega_{\mathrm{n}}^2}.\end{aligned}\tag{3.13}$$

Since $\Delta t_k = 2\pi/\omega_{\mathrm{n}}$, it follows that $t_k = 2\pi k/\omega_{\mathrm{n}}$. Therefore, (3.13) implies that tr $R^{\mathrm{T}}(t_k)\tilde{R}(t_k) = 3$, which implies that $d(R_k, \tilde{R}_k) = \arccos 1 = 0$, thus confirming (3.11).

Next, note that

$$\sup_{t\in\mathcal{I}_k} d(R(t),\tilde{R}(t)) = \arccos\frac{\eta_k-1}{2},\tag{3.14}$$

where $\eta_k \triangleq \inf_{t\in\mathcal{I}_k}$ tr $R^{\mathrm{T}}(t)\tilde{R}(t)$. It follows from (3.13) that tr $R^{\mathrm{T}}(t)\tilde{R}(t) = f(\cos\omega_{\mathrm{n}}t)/\omega_{\mathrm{n}}^2$, where $f(x) \triangleq \left(\omega_{\mathrm{n}}-(\omega+\omega_{\mathrm{d}})\right)^2 x^2 + 2c^2x + 2(\omega+\omega_{\mathrm{d}})\omega_{\mathrm{n}} + (\omega+\omega_{\mathrm{d}})^2$ is minimized on the interval $[-1,1]$ by $x=-1$. Thus, tr $R^{\mathrm{T}}(t)\tilde{R}(t)$ is minimized by $\cos\omega_{\mathrm{n}}t = -1$, which implies that

$$\eta_k = \frac{\left(\omega_{\mathrm{n}}-(\omega+\omega_{\mathrm{d}})\right)^2 - 2c^2 + 2(\omega+\omega_{\mathrm{d}})\omega_{\mathrm{n}} + (\omega+\omega_{\mathrm{d}})^2}{\omega_{\mathrm{n}}^2} = \frac{3(\omega+\omega_{\mathrm{d}})^2-c^2}{(\omega+\omega_{\mathrm{d}})^2+c^2}.\tag{3.15}$$

Substituting (3.15) into (3.14) yields (3.12). □

Now define another pure rotation $\bar{R}:[0,\infty)\to\mathrm{SO}(3)$ by

$$\bar{R}(t) \triangleq R_0 S\exp\left(\left(\sqrt{(\omega+\omega_{\mathrm{d}})^2+c^2}-\omega\right)tE_{\mathrm{w}}\right)S^{\mathrm{T}},\tag{3.16}$$

where $E_{\mathrm{w}} \triangleq (cE_1+(\omega+\omega_{\mathrm{d}})E_3)/\sqrt{(\omega+\omega_{\mathrm{d}})^2+c^2}$. Note that (3.16) is the solution of (3.1) with $\Omega(t) = \left(\sqrt{(\omega+\omega_{\mathrm{d}})^2+c^2}-\omega\right)SE_{\mathrm{w}}^{\vee}$, which is a constant control. The

following result compares (3.8) and (3.16). The proof is similar to that of Proposition 3.4 and is omitted.

Proposition 3.3. Consider (3.8) and (3.16). Let $\Delta t_k = 2\pi/\omega$, and let $\omega+\omega_{\mathrm{d}} > 0$. Then,

$$R_{k+1} = \bar{R}_{k+1} = R_k S \exp\left(\left(\sqrt{(\omega+\omega_{\mathrm{d}})^2 + c^2} - \omega\right)\Delta t_k E_{\mathrm{w}}\right) S^{\mathrm{T}},$$

and

$$\sup_{t\in\mathcal{I}_k} d(R(t), \bar{R}(t)) = \arccos\frac{(\omega+\omega_{\mathrm{d}})^2 - c^2}{(\omega+\omega_{\mathrm{d}})^2 + c^2}.$$

Note that the differences between Proposition 3.2 and 3.3 are that

(i) The pure rotations with which (3.8) is compared have different axes of rotation. The axis of rotation for (3.16) depends on c, ω, and ω_{d}; while the axis of rotation for (3.10) doesn't depend on c, ω, or ω_{d}.

(ii) The time instances when the solutions coincide are different. In Proposition 3.2, Δt_k depends on c and ω_{d}; while in Proposition 3.3, Δt_k doesn't depend on c or ω_{d}.

The following propositions are immediate results from Proposition 3.2 and 3.3, for sinusoidal controls where $\omega_{\mathrm{d}} = 0$.

Proposition 3.4. Consider (3.8) and (3.10) where $\omega_{\mathrm{d}} = 0$. Let $\Delta t_k = 2\pi/\sqrt{\omega^2 + c^2}$. Then,

$$R_{k+1} = \tilde{R}_{k+1} = R_k S \exp\left(\left(\sqrt{\omega^2 + c^2} - \omega\right)\Delta t_k E_3\right) S^{\mathrm{T}}, \tag{3.17}$$

and

$$\sup_{t\in\mathcal{I}_k} d(R(t),\tilde{R}(t)) = \arccos\frac{\omega^2-c^2}{\omega^2+c^2}. \tag{3.18}$$

Proposition 3.5. Consider (3.8) and (3.16) where $\omega_{\rm d}=0$. Let $\Delta t_k = 2\pi/\omega$. Then,

$$R_{k+1} = \bar{R}_{k+1} = R_k S \exp\left(\left(\sqrt{\omega^2+c^2}-\omega\right)\Delta t_k E_{\rm w}\right) S^{\rm T},$$

and

$$\sup_{t\in\mathcal{I}_k} d(R(t),\bar{R}(t)) = \arccos\frac{\omega^2-c^2}{\omega^2+c^2}.$$

Example 3.6. *Consider* (3.8) *and* (3.10)*, where* $\omega_{\rm d}=0$*,* $\omega = 10\sqrt{2}\pi$ *rad/s and* $c = 10\sqrt{2}\pi$ *rad/s, and let* $\Delta t_k = 2\pi/\sqrt{\omega^2+c^2} = 1/10$ *s. In this case,* $\Delta t_k = 1/10$ *s, and Proposition 3.4 implies that* $R(k/10) = \tilde{R}(k/10)$ *and* $\sup_{t\in\mathcal{I}_k} d(R(t),\tilde{R}(t)) = \pi/2$ *rad, where* $\mathcal{I}_k = [k/10,(k+1)/10)$*.*

Proposition 3.4 also implies that if c/ω *is smaller while* $\Delta t_k = 1/10$ *s is the same, then* $\sup_{t\in\mathcal{I}_k} d(R(t),\tilde{R}(t))$ *is smaller. Thus, we consider* $\omega = 10\sqrt{3}\pi$ *rad/s and* $c = 10\pi$ *rad/s, which implies that* $c/\omega = 1/\sqrt{3}$ *and* $\Delta t_k = 1/10$ *s. Proposition 3.4 implies that* $R(k/10) = \tilde{R}(k/10)$ *and* $\sup_{t\in\mathcal{I}_k} d(R(t),\tilde{R}(t)) = \pi/3$ *rad, which is less than the previous case. Figure 3.1 shows the trajectory* $d(R(t),\tilde{R}(t))$ *for both cases of* c/ω*.* △

Now, we analyze the structure of the solution (3.8) by approximation and by motion decomposition.

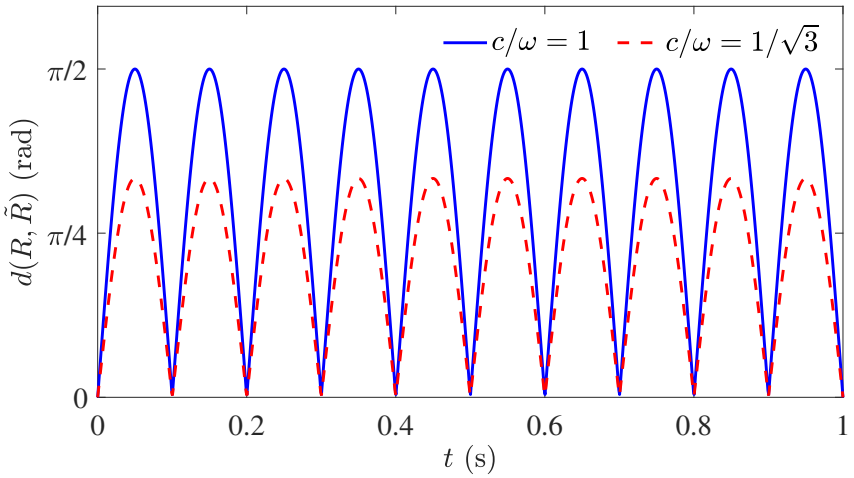

Figure 3.1: The solutions R coincide with the pure rotation $\tilde{R}$ at $t_k = k/10$ s. The maximum distance between R and $\tilde{R}$ is smaller if c/ω is smaller while Δt_k is the same.

To this end, first we consider (3.1) and small control (3.2) with $c_k = O(\epsilon)$ and $\omega_{\rm d} = O(\epsilon)$, where $\epsilon > 0$ is a small scalar. Note that $\omega = O(1)$. Since $\Omega(t)$ is periodic with period $T = 2\pi/\omega$, we define

$$\Omega_{\rm av} \triangleq \frac{1}{T}\int_0^T \Omega(\tau){\rm d}\tau = S\begin{bmatrix}0 & 0 & \omega_{\rm d}\end{bmatrix}^{\rm T}. \tag{3.19}$$

By applying the classic averaging theory [40], we have the following proposition.

Proposition 3.7 (Leonard [71])**.** Consider (3.1) and (3.2), where $\epsilon > 0$ is a small scalar, $c = O(\epsilon)$, and $\omega_{\rm d} = O(\epsilon)$. Let $R(t)$ is the solution to (3.1) and (3.2), with $R(0) = R_0 \in {\rm SO(3)}$. Let $G \triangleq \{R \in {\rm SO(3)} : d(R, R_0) < \pi\}$. Let $R^{(1)}(t)$ be the solution to

$$\dot{R}(t) = R(t)\hat{\Omega}_{\rm av}, \tag{3.20}$$

with $R^{(1)}(0) = R_0^{(1)}$, where $\Omega_{\rm av}$ is defined in (3.19). If there exists $b > 0$, such that

for all $t \in [0, b/\epsilon]$, $R^{(1)}(t) \in G$, and if $d(R_0^{(1)}, R_0) = O(\epsilon)$, then for all $t \in [0, b/\epsilon]$,

$$d(R(t), R^{(1)}(t)) = O(\epsilon).$$

Proposition 3.7 indicates that the solution (3.8) can be approximated with the solution of the average dynamics (3.20) with $O(\epsilon)$ error. That is, if $c = O(\omega_{\rm d})$, the dc component of Ω dominates the system response.

To be more precise, we decompose the motion (3.8) into two parts, an oscillatory motion and a spin. In particular, let $R_{\rm r}(t) = R(t)\exp(-\omega_{\rm d} t S E_3 S^{\rm T})$. By taking derivative of $R_{\rm r}(t)$, It follows that

$$\dot{R}_{\rm r}(t) = \dot{R}_{\rm r}(t)\hat{\Omega}_{\rm r}(t), \quad \Omega_{\rm r}(t) \triangleq S \begin{bmatrix} c\cos((\omega+\omega_{\rm d})t) & c\sin((\omega+\omega_{\rm d})t) & 0 \end{bmatrix}^{\rm T}. \quad (3.21)$$

Therefore, we have the following proposition.

Proposition 3.8. The solution of (3.1) and (3.2) is

$$R(t) = R_{\rm r}(t)\exp(\omega_{\rm d} t S E_3 S^{\rm T}), \quad (3.22)$$

where $R_{\rm r}(t)$ is the solution of (3.21) with $R_{\rm r}(0) = R(0) = R_0$.

Now, assume $c = O(\epsilon)$ and $\omega_{\rm d} = O(\epsilon)$. Then, it follows from Proposition 3.4 that $R_{\rm r}(t)$ is approximated by a spin along Se_3 axis with rotation rate

$$\sqrt{(\omega+\omega_{\rm d})^2 + c^2} - (\omega+\omega_{\rm d}) = \frac{c^2}{\sqrt{(\omega+\omega_{\rm d})^2 + c^2} + (\omega+\omega_{\rm d})} = O(\epsilon^2). \quad (3.23)$$

On the contrary, $\exp(\omega_{\rm d} t S E_3 S^{\rm T})$ is a spin along Se_3 axis with rotation rate $\omega_{\rm d} = O(\epsilon)$, which is much bigger than $R_{\rm r}(t)$. Therefore, $R(t)$ can be approximated by $\exp(\omega_{\rm d} t S E_3 S^{\rm T})$.

Remark. We now assume $\omega > c$ and $\omega + \omega_{\rm d} > 0$. It follows from Proposition 3.2 and Proposition 3.8 that the average rotation is along the positive body z direction if $\omega_{\rm d} > \sqrt{\omega^2 - c^2} - \omega$, and that the average rotation is along the negative body z direction if $\omega_{\rm d} < \sqrt{\omega^2 - c^2} - \omega$.

We note that the kinematic system (3.1) (3.2), in which S, c, $\omega_{\rm d}$ are control variables, is trivially controllable. This is because we can set $c = 0$, and choose S and $\omega_{\rm d}$ properly to drive $R(t)$ to arbitrary state in arbitrary time. Therefore, in the remaining sections of this chapter, we let $\omega_{\rm d} = 0$, and consider controllability, setpoint tracking, and command following problems for (3.1) and sinusoidal control

$$\Omega(t) = cS[(\cos \omega t)e_1 + (\sin \omega t)e_2], \tag{3.24}$$

or piecewise sinusoidal control

$$\Omega(t) = S_k \left[c_k(\cos \omega_k t)e_1 + c_k(\sin \omega_k t)e_2\right], \quad t \in \mathcal{I}_k. \tag{3.25}$$

3.2 Controllability of the attitude kinematic system

The following result provides a relationship between two elements of SO(3) that have equal geodesic distance from I. This preliminary result is used in the controllability analysis of this section and is required for the controller constructions provided later.

Lemma 3.9. Let $A, B \in \mathrm{SO}(3)$, and assume that $d(A, I) = d(B, I)$. Then there exists $S \in \mathrm{SO}(3)$ such that $A = SBS^{\rm T}$.

Proof. Since the exponential map from so(3) to SO(3) is surjective and $d(A, I) = d(B, I)$, there exist unit vectors $a, b \in \mathbb{R}^3$, such that

$$A = \exp(\phi \hat{a}), \quad B = \exp(\phi \hat{b}), \tag{3.26}$$

where $\phi \triangleq d(R_1, I) = d(R_2, I)$. See [67, Proposition 2.5] for a construction of a and b. Define $\alpha \triangleq \arccos a^{\mathrm{T}} b$. For the case that $\sin\alpha \neq 0$, define $w \triangleq \hat{b}a/\sin\alpha$. For the case that $\sin\alpha = 0$, let w be a unit vector in $\mathbb{R}^3$ such that $w^{\mathrm{T}}a = 0$. Define $S \triangleq \exp(\alpha\hat{w})$. It can be shown that $a = Sb$, which implies that

$$\phi\hat{a} = (\phi Sb)^{\wedge} = \phi S\hat{b}S^{\mathrm{T}}. \tag{3.27}$$

It follows from (3.26) and (3.27) that $A = \exp(\phi\hat{a}) = \exp(S\phi\hat{b}S^{\mathrm{T}}) = S\exp(\phi\hat{b})S^{\mathrm{T}} = SBS^{\mathrm{T}}$. □

Remark. Note that S satisfying $A = SBS^{\mathrm{T}}$ is not unique. Specifically, let $\gamma \in \mathbb{R}$, let $a \in \mathbb{R}^3$ be the unit vector that satisfies (3.26), and assume $S \in \mathrm{SO}(3)$ satisfies $A = SBS^{\mathrm{T}}$. Define $S_1 \triangleq \exp(\gamma\hat{a})S$. Then, $A = S_1 B S_1^{\mathrm{T}}$.

The following result implies that (3.1) and (3.24) is completely controllable in time $t_{\mathrm{f}} > 0$. See [72, Definition 3.1.6] for the definition of controllability.

Theorem 3.10. Let $t_{\mathrm{f}} > 0$, $R_0 \in \mathrm{SO}(3)$ and $R_{\mathrm{f}} \in \mathrm{SO}(3)$, and define $\phi \triangleq d(R_{\mathrm{f}}, R_0)$. Assume that $\omega_{\max} > (2\pi - \phi)/t_{\mathrm{f}}$, and let $\ell < (\omega_{\max} t_{\mathrm{f}} + \phi)/(2\pi)$ be a positive integer. Consider (3.1) and (3.24), where $S \in \mathrm{SO}(3)$ satisfies

$$R_{\mathrm{f}}^{\mathrm{T}} R_0 = S\exp(-\phi E_3)S^{\mathrm{T}}, \tag{3.28}$$

and

$$\omega = \frac{2\pi\ell - \phi}{t_{\mathrm{f}}}, \quad c = \frac{\sqrt{4\pi\ell\phi - \phi^2}}{t_{\mathrm{f}}}. \tag{3.29}$$

Then, $R(t_{\mathrm{f}}) = R_{\mathrm{f}}$.

Proof. It follows from (3.9) and (3.29) that

$$t_{\mathrm{f}} = \frac{2\pi\ell}{\omega_{\mathrm{n}}}, \quad \phi = \frac{2\pi\ell(\omega_{\mathrm{n}} - \omega)}{\omega_{\mathrm{n}}}. \tag{3.30}$$

Since (3.8) is the solution of (3.1) and (3.24), it follows from (3.17) of Proposition 3.4 and (3.28)–(3.30) that

$$\begin{aligned} R(t_{\mathrm{f}}) &= \tilde{R}\left(\frac{2\pi\ell}{\omega_{\mathrm{n}}}\right) \\ &= R_0 S \exp\left(\frac{2\pi\ell(\omega_{\mathrm{n}} - \omega)}{\omega_{\mathrm{n}}} E_3\right) S^{\mathrm{T}} \\ &= R_0 S \exp(\phi E_3) S^{\mathrm{T}} \\ &= R_{\mathrm{f}}. \end{aligned}$$

This completes the proof. □

Note that Lemma 3.9 with $A = R_{\mathrm{f}}^{\mathrm{T}} R_0$ and $B = \exp(-\phi E_3)$ confirms the existence of $S \in \mathrm{SO}(3)$ that satisfies (3.28).

Example 3.11. *Consider* (3.1)*, where* $R_0 = \exp(E_2)$*. Let* $R_{\mathrm{f}} = I$ *and* $t_{\mathrm{f}} = 1$ *s, and note that* $d(R_0, R_{\mathrm{f}}) = 1$ *rad. We use Theorem 3.10 to choose the control parameters of* (3.24) *such that the solution of* (3.1) *and* (3.24) *satisfies* $R(t_{\mathrm{f}}) = R_{\mathrm{f}}$*. Let* Ω *be given by* (3.24)*, where* $S = \exp\left(\frac{\pi}{2} E_1\right)$*,* $\omega = 10\pi - 1$ *rad/s, and* $c = \sqrt{20\pi - 1}$ *rad/s. Since* S*,* ω*, and* c *satisfy* (3.28) *and* (3.29) *with* $\ell = 5$*, Theorem 3.10 implies that the solution of* (3.1) *and* (3.24) *satisfies* $R(t_{\mathrm{f}}) = R_{\mathrm{f}}$*. Figure 3.2 shows the trajectory* $d(R(t), R_{\mathrm{f}})$*.* △

Next, we consider (3.1) and (3.24) for the case that the frequency ω is not a control parameter. The motivation for this case is an actuation system that generates constant-frequency piecewise sinusoids. The following result shows that if ω is constant, then (3.1) and (3.24) is completely controllable, but not completely control-

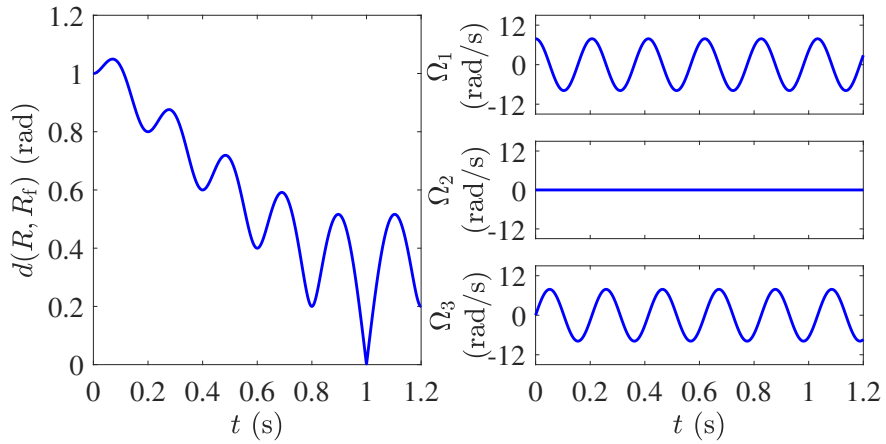

Figure 3.2: Open-loop sinusoidal control (3.24) yields $R(1) = R_{\mathrm{f}}$.

lable in time $t_{\mathrm{f}} > 0$. Completely controllable is a weaker condition than completely controllable in time $t_{\mathrm{f}} > 0$. See [72, Definition 3.1.6] for controllability definitions. The proof of Theorems 3.12 is similar to that of Theorem 3.10 and is thus omitted.

Theorem 3.12. Let $\omega \in (0, \omega_{\max}]$, $R_0 \in \mathrm{SO}(3)$, and $R_{\mathrm{f}} \in \mathrm{SO}(3)$, and define $\phi \triangleq d(R_{\mathrm{f}}, R_0)$. Let ℓ be a positive integer, and define $t_{\mathrm{f}} \triangleq (2\pi\ell - \phi)/\omega$. Consider (3.1) and (3.24), where $S \in \mathrm{SO}(3)$ satisfies

$$R_{\mathrm{f}}^{\mathrm{T}} R_0 = S \exp(-\phi E_3) S^{\mathrm{T}}, \tag{3.31}$$

and

$$c = \frac{\sqrt{4\pi\ell\phi - \phi^2}}{t_{\mathrm{f}}}. \tag{3.32}$$

Then, $R(t_{\mathrm{f}}) = R_{\mathrm{f}}$.

Example 3.13. *Consider* (3.1)*, where* $R_0 = \exp(E_2)$*. Let* $R_{\mathrm{f}} = I$ *and* $\omega = (50\pi - 5)/4$ *rad/s. We use Theorem 3.12 to choose the control parameters of* (3.24)

such that the solution of (3.1) *and* (3.24) *satisfies* $R(t_\mathrm{f}) = R_\mathrm{f}$. *Let* Ω *be given by* (3.24), *where* $S = \exp\left(\frac{\pi}{2}E_1\right)$ *and* $c = 5\sqrt{20\pi - 1}/4$ *rad/s. Since* S *and* c *satisfy* (3.31) *and* (3.32) *with* $\ell = 5$, *Theorem 3.12 implies that the solution of* (3.1) *and* (3.24) *satisfies* $R(t_\mathrm{f}) = R_\mathrm{f}$, *where* $t_\mathrm{f} = 0.8$ *s. Figure 3.3 shows the trajectory* $d(R(t), R_\mathrm{f})$. △

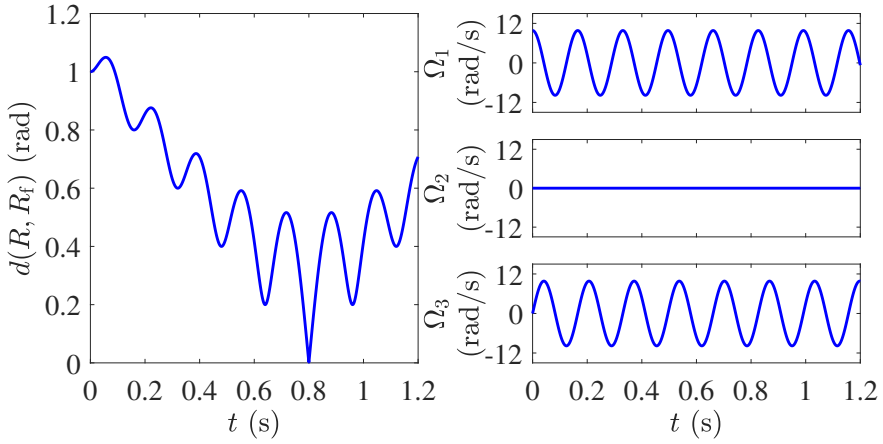

Figure 3.3: Open-loop sinusoidal control (3.24) yields $R(0.8) = R_\mathrm{f}$.

3.3 Setpoint tracking

In this section, we consider setpoint tracking, where $\Omega_\mathrm{d}(t) \equiv 0$, that is, R_d is constant. In this case, Z satisfies

$$\dot{Z}(t) = Z(t)\hat{\Omega}(t), \tag{3.33}$$

where $Z(0) = R_{\mathrm{d}0}^{\mathrm{T}} R_0$. The objective is to design a Z-feedback admissible control such that for all $Z_0 \in \mathrm{SO}(3)$, $\lim_{t\to\infty} z(t) = 0$. We present three control algorithms that achieve this objective. The first algorithm uses nonconstant update rate, while the other two use constant update rate. The motivation for using constant update rate is that it may simplify the digital implementation of the control algorithms.

Algorithm 3.14. Let n be a positive integer, and consider the control (3.25), where S_k, ω_k, c_k, and Δt_k satisfy

$$S_k \exp(-z_k E_3) S_k^{\mathrm{T}} = Z_k, \tag{3.34}$$

$$\frac{c_k}{\omega_k} = \sqrt{\left(\frac{2\pi n}{2\pi n - z_k}\right)^2 - 1}, \tag{3.35}$$

$$\Delta t_k = \frac{2\pi}{\sqrt{\omega_k^2 + c_k^2}}. \tag{3.36}$$

Note that Lemma 3.9 confirms the existence of $S_k \in \mathrm{SO}(3)$ that satisfies (3.34).

Theorem 3.15. Consider (3.25) and (3.33), where S_k, ω_k, c_k, and Δt_k are given by Algorithm 3.14. Then, for all $Z_0 \in \mathrm{SO}(3)$, $\lim_{t\to\infty} z(t) = 0$.

Proof. The right-hand side of the differential equation obtained by substituting (3.25) into (3.33) contains discontinuities at t_k. However, the solution to (3.25) and (3.33) is continuous on $[0, \infty)$. Thus, it follows from (3.17) of Proposition 3.4 that

$$Z_{k+1} = Z_k S_k \exp\left(\left(\sqrt{\omega_k^2 + c_k^2} - \omega_k\right) \Delta t_k E_3\right) S_k^{\mathrm{T}},$$

and using (3.36) yields

$$Z_{k+1} = Z_k S_k \exp(-\omega_k \Delta t_k E_3) S_k^{\mathrm{T}}. \tag{3.37}$$

Substituting (3.34)–(3.36) into (3.37) yields

$$Z_{k+1} = S_k \exp\left(\frac{1-n}{n} z_k E_3\right) S_k^{\mathrm{T}},$$

which implies that

$$z_{k+1} = d(Z_{k+1}, I) = \arccos \frac{\operatorname{tr} \exp(\frac{1-n}{n} z_k E_3) - 1}{2}. \tag{3.38}$$

Since

$$\exp\left(\frac{1-n}{n} z_k E_3\right) = \begin{bmatrix} \cos\frac{1-n}{n} z_k & -\sin\frac{1-n}{n} z_k & 0 \\ \sin\frac{1-n}{n} z_k & \cos\frac{1-n}{n} z_k & 0 \\ 0 & 0 & 1 \end{bmatrix},$$

it follows from (3.38) that

$$z_{k+1} = \arccos\left(\cos\frac{1-n}{n} z_k\right) = \frac{n-1}{n} z_k, \tag{3.39}$$

which implies that $\lim_{k\to\infty} z_k = 0$.

Next, (3.39) implies that $z_k \leq z_0$. Since, in addition, $\omega_k \leq \omega_{\max}$, it follows from (3.35) that

$$c_k = \omega_k \sqrt{\left(\frac{2\pi n}{2\pi n - z_k}\right)^2 - 1} \leq \omega_{\max} \sqrt{\left(\frac{2\pi n}{2\pi n - z_0}\right)^2 - 1}.$$

Thus, (3.36) implies that

$$\Delta t_k \geq \frac{2\pi n - z_0}{n\omega_{\max}} > 0. \tag{3.40}$$

Next, for all $t \in \mathcal{I}_k$, define

$$\tilde{Z}(t) \triangleq Z_k S_k \exp\left(\left(\sqrt{\omega_k^2 + c_k^2} - \omega_k\right)(t - t_k) E_3\right) S_k^{\mathrm{T}}, \tag{3.41}$$

and note that for all $t \in \mathcal{I}_k$,

$$d(\tilde{Z}(t), I) \leq d(\tilde{Z}_k, I) = d(Z_k, I) = z_k. \tag{3.42}$$

In addition, it follows from (3.18) of Proposition 3.4 that

$$\sup_{t \in \mathcal{I}_k} d(Z(t), \tilde{Z}(t)) = \arccos \frac{\omega_k^2 - c_k^2}{\omega_k^2 + c_k^2} = \arccos \frac{1 - \frac{c_k^2}{\omega_k^2}}{1 + \frac{c_k^2}{\omega_k^2}}. \tag{3.43}$$

Thus, using (3.42) and (3.43) implies that for all $t \in \mathcal{I}_k$,

$$\begin{aligned} z(t) &= d(Z(t), I) \\ &\leq d(Z(t), \tilde{Z}(t)) + d(\tilde{Z}(t), I) \\ &\leq \arccos \frac{1 - \frac{c_k^2}{\omega_k^2}}{1 + \frac{c_k^2}{\omega_k^2}} + z_k. \end{aligned} \tag{3.44}$$

Since $\lim_{k \to \infty} z_k = 0$, it follows from (3.35) that $\lim_{k \to \infty} c_k / \omega_k = 0$. Thus, (3.40) and (3.44) imply that $\lim_{t \to \infty} z(t) = 0$. □

It can be shown that (3.34) is satisfied by $S_k = S_0$, where $S_0 \in \mathrm{SO}(3)$ satisfies $S_0 \exp(-z_0 E_3) S_0^{\mathrm{T}} = Z_0$. In this case, S_k does not depend on feedback except the initial condition Z_0. However, if Z_k is corrupted by sensor noise, then $S_k = S_0$ does not generally satisfy (3.34).

Algorithm 3.14 can be implemented by fixing one of the three control parameters ω_k, c_k, and Δt_k. In this case, (3.35) and (3.36) provide a unique solution for the two remaining control parameters. In the following example, Algorithm 3.14 is implemented with constant frequency ω_k but nonconstant amplitude c_k and time step Δt_k.

Example 3.16. *Consider* (3.25) *and* (3.33)*, where*

$$Z_0 = \exp\left(\frac{3\sqrt{14}}{35}\begin{bmatrix} 0 & -3 & 2 \\ 3 & 0 & -1 \\ -2 & 1 & 0 \end{bmatrix}\right).$$

The control parameters S_k*,* c_k*, and* Δt_k *satisfy Algorithm 3.14 with* $n = 5$ *and* $\omega_k = 10\sqrt{2}\pi$ *rad/s. Figure 3.4 shows the performance* z*.* △

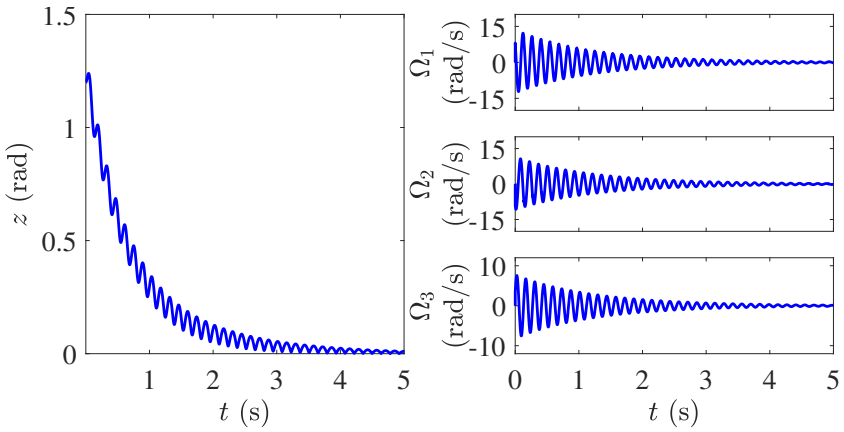

Figure 3.4: Setpoint tracking using Algorithm 3.14 with constant ω_k.

In the next example, Algorithm 3.14 is implemented with constant time step Δt_k but nonconstant frequency ω_k and amplitude c_k.

Example 3.17. *Consider* (3.25) *and* (3.33)*, where* Z_0 *is the same as in Example 3.16. The control parameters* S_k*,* ω_k*, and* c_k *satisfy Algorithm 3.14 with* $n = 5$ *and* $\Delta t_k = 0.1$ *s. Figure 3.5 shows the performance* z*.* △

Algorithm 3.14 cannot generally be implemented with more than one of the control parameters ω_k, c_k, and Δt_k constant. Next, we present two setpoint tracking controllers that can be implemented with constant frequency ω_k and constant time step Δt_k.

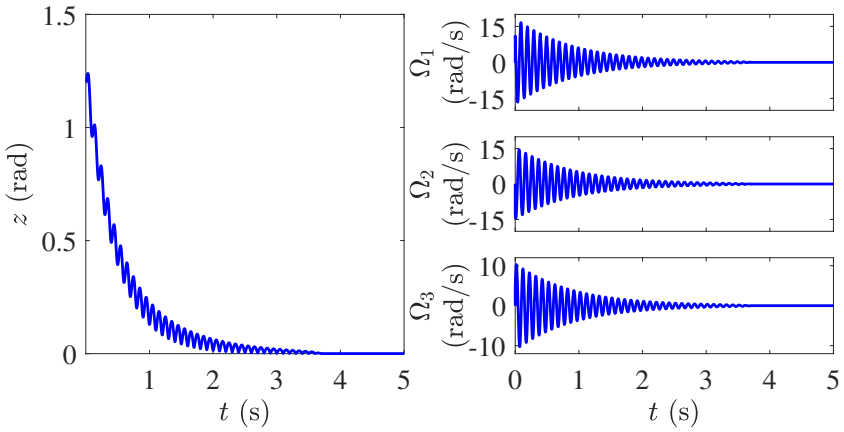

Figure 3.5: Setpoint tracking using Algorithm 3.14 with constant Δt_k.

Algorithm 3.18. Let n be a positive integer and let $\omega \in (0, \omega_{\max}]$. Consider the control (3.25), where

$$\omega_k = \omega, \quad c_k = \omega\sqrt{\left(\frac{z_k + 2\pi n}{2\pi n}\right)^2 - 1}, \quad \Delta t_k = \frac{2\pi}{\omega}, \tag{3.45}$$

and S_k satisfies

$$S_k \exp\left(\frac{-z_k(c_k E_1 + \omega E_3)}{\sqrt{\omega^2 + c_k^2}}\right) S_k^{\mathrm{T}} = Z_k. \tag{3.46}$$

Theorem 3.19. Consider (3.25) and (3.33), where S_k, ω_k, c_k, and Δt_k are given by Algorithm 3.18. Then, for all $Z_0 \in \mathrm{SO}(3)$, $\lim_{t\to\infty} z(t) = 0$.

Proof of Theorem 3.19 relies on Proposition 3.5, and is similar with the proof of Theorem 3.15. Thus, it is omitted for brevity.

Algorithm 3.20. Let $\omega \in (0, \omega_{\max}]$. Consider the control (3.25), where S_k satisfies (3.34) and

$$\omega_k = \omega, \quad c_k = \omega\sqrt{\frac{z_k}{\pi}}, \quad \Delta t_k = \frac{2\pi}{\omega}. \tag{3.47}$$

Theorem 3.21. Consider (3.25) and (3.33), where S_k, ω_k, c_k, and Δt_k are given by Algorithm 3.20. Then, for all $Z_0 \in \mathrm{SO}(3)$, $\lim_{t\to\infty} z(t) = 0$.

Proof. Let $V(t) \triangleq \mathrm{tr}(I - Z(t))$, and thus

$$V_k = \mathrm{tr}(I - Z_k). \tag{3.48}$$

It follows from (3.34) that

$$\begin{aligned} \mathrm{tr}\ Z_k &= \mathrm{tr} \exp\left(-z_k E_3\right) \\ &= \mathrm{tr} \begin{bmatrix} \cos z_k & \sin z_k & 0 \\ -\sin z_k & \cos z_k & 0 \\ 0 & 0 & 1 \end{bmatrix} \\ &= 1 + 2\cos z_k. \end{aligned} \tag{3.49}$$

Combining (3.48) and (3.49) yields

$$V_k = 3 - \mathrm{tr}\ Z_k = 2 - 2\cos z_k,$$

which implies that V_k is nonnegative.

Next, for all $t \in \mathcal{I}_k$, the solution to (3.25) and (3.33) is given by (3.8), with R, S, ω, c, R_0, and t replaced with Z, S_k, ω_k, c_k, $Z(t_k)$, and $t - t_k$. Thus, (3.8), (3.34), (3.47), and (3.48) imply that

$$V_{k+1} - V_k = \Psi(z_k), \tag{3.50}$$

where

$$\begin{aligned}\Psi(z_k) \triangleq \cos z_k & \left(\frac{2+\frac{z_k}{\pi}}{1+\frac{z_k}{\pi}} - \frac{2+\frac{z_k}{\pi}}{1+\frac{z_k}{\pi}} \cos 2\pi \sqrt{1+\frac{z_k}{\pi}} \right) \\ & - \left(\sin z_k \, \frac{2}{\sqrt{1+\frac{z_k}{\pi}}} \right) \sin 2\pi \sqrt{1+\frac{z_k}{\pi}} \\ & - \frac{z_k}{\pi} \frac{\cos 2\pi \sqrt{1+\frac{z_k}{\pi}} - 1}{1+\frac{z_k}{\pi}}. \end{aligned} \tag{3.51}$$

It can be shown that $\Psi(0) = 0$, and for all $\xi \in (0, \pi]$, $\Psi(\xi) < 0$. Thus, (3.50) and (3.51) imply that $V_{k+1} \leq V_k$. Since V_k is nonnegative and nonincreasing, it follows that $\lim_{k\to\infty} V_k$ exists, and thus (3.50) implies that

$$\lim_{k\to\infty} \Psi(z_k) = \lim_{k\to\infty} V_{k+1} - \lim_{k\to\infty} V_k = 0.$$

Since Ψ is nonpositive on $[0, \pi]$, $\lim_{k\to\infty} \Psi(z_k) = 0$, and $z_k \in [0, \pi]$, it follows that $\lim_{k\to\infty} z_k = 0$. Thus, (3.47) implies that $\lim_{k\to\infty} c_k = 0$. Using the same arguments as those used from (3.41) to the end of the proof of Theorem 3.15, it can be shown that $\lim_{t\to\infty} z(t) = 0$. □

Example 3.22. *Consider* (3.25) *and* (3.33)*, where* Z_0 *is the same as in Example 3.16. The control parameters* S_k*,* ω_k*,* c_k*, and* Δt_k *are given by Algorithm 3.20 with* $\omega = 10\sqrt{2}\pi$ *rad/s. Figure 3.6 shows the performance* z*.* △

3.4 Command following

In this section, we consider the general command following problem, where $\Omega_{\rm d} \not\equiv 0$. It follows from (3.1), (2.79), and (2.80) that Z satisfies

$$\dot{Z}(t) = \hat{\Omega}_{\rm d}^{\rm T}(t) Z(t) + Z(t) \hat{\Omega}(t), \tag{3.52}$$

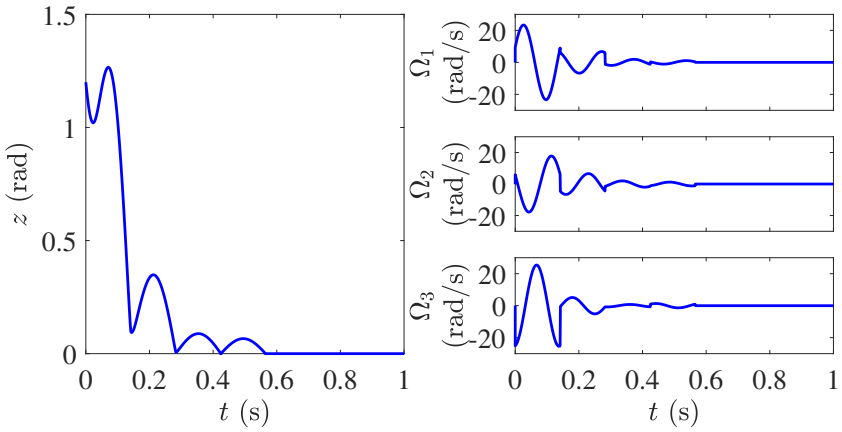

Figure 3.6: Setpoint tracking using Algorithm 3.20 with constant ω_k and Δt_k.

where $Z(0) = R_{\mathrm{d}0}^{\mathrm{T}} R_0$.

Let $\Omega_* : \mathrm{SO}(3) \to \mathbb{R}^3$ be an ideal Z-feedback control such that letting $\Omega = \Omega_*$ in (3.52) yields a desired closed-loop response. Possible choices of Ω_* are given in [4, 10, 19], which present Z-feedback controls such that the identity equilibrium is almost globally asymptotically stable. We provide an example of Ω_* later in this section. Note that Ω_* need not be an admissible control. In fact, the controllers in [4, 10, 19] are not admissible controls.

For all $t \in \mathcal{I}_k$, the *ideal command-following error* $Z_* : [0, \infty) \to \mathrm{SO}(3)$ is defined to be the solution of

$$\dot{Z}_*(t) = \hat{\Omega}_{\mathrm{d}}^{\mathrm{T}}(t) Z_*(t) + Z_*(t) \hat{\Omega}_*(Z_{*k}), \tag{3.53}$$

where $Z_*(0) = Z_0$. Define the *ideal performance* $z_*(t) \triangleq d(Z_*(t), I)$. Our objective is to design an admissible control (3.25) such that the closed-loop response of (3.25) and (3.52) approximates the ideal command-following error Z_*. We present two control algorithms that achieve this objective. Similar to last section, the first algorithm uses nonconstant update rate, while the second uses constant update rate. The motivation for using constant update rate is that it may simplify the digital implementation of

the control algorithms.

Algorithm 3.23. Define

$$\Gamma_k \triangleq \begin{cases} \frac{\sqrt{2}}{\|\hat{\Omega}_*(Z_k)\|_{\mathrm{F}}}\hat{\Omega}_*(Z_k), & \text{if } \|\hat{\Omega}_*(Z_k)\|_{\mathrm{F}} \neq 0, \\ E_3, & \text{if } \|\hat{\Omega}_*(Z_k)\|_{\mathrm{F}} = 0, \end{cases} \tag{3.54}$$

and consider the control (3.25), where S_k, ω_k, c_k, and Δt_k satisfy

$$S_k \exp(E_3) S_k^{\mathrm{T}} = \exp(\Gamma_k), \tag{3.55}$$

$$c_k = \sqrt{\left(\frac{\|\hat{\Omega}_*(Z_k)\|_{\mathrm{F}}}{\sqrt{2}} + \omega_k\right)^2 - \omega_k^2}, \tag{3.56}$$

$$\Delta t_k = \frac{2\pi}{\sqrt{\omega_k^2 + c_k^2}}. \tag{3.57}$$

Note that Lemma 3.9 confirms the existence of $S_k \in \mathrm{SO}(3)$ that satisfies (3.55).

Theorem 3.24. Consider (3.25) and (3.52), where S_k, ω_k, c_k, and Δt_k are given by Algorithm 3.23. Then,

$$Z_k = Z_{*k}, \tag{3.58}$$

and

$$\sup_{t \in \mathcal{J}_k} d(Z(t), Z_*(t)) = \arccos\left(\frac{2\omega_k^2}{\left(\frac{\|\hat{\Omega}_*(Z_k)\|_{\mathrm{F}}}{\sqrt{2}} + \omega_k\right)^2} - 1\right). \tag{3.59}$$

Furthermore, let $\epsilon \in (0, \pi)$, and assume that $\omega_k \in [\omega_{\min}, \omega_{\max}]$, where

$$\omega_{\min} \triangleq \frac{\sup_{k\in\mathbb{N}} \|\hat{\Omega}_*(Z_k)\|_{\mathrm{F}}}{2\sqrt{\frac{1}{1+\cos\epsilon}} - \sqrt{2}}. \tag{3.60}$$

Then, $\sup_{t\in\mathcal{I}_k} d(Z(t), Z_*(t)) \leq \epsilon$.

Proof. For all $t \in \mathcal{I}_k$, let $R_*(t) \triangleq R_{\mathrm{d}}(t)Z_*(t)$, and note that

$$d(Z(t), Z_*(t)) = d(R_{\mathrm{d}}(t)Z(t), R_{\mathrm{d}}(t)Z_*(t)) = d(R(t), R_*(t)). \tag{3.61}$$

To show (3.58), we use induction on $k \in \mathbb{N}$. First, note that $Z_0 = Z_*(0) = Z_{*0}$, which implies that (3.58) holds for $k = 0$.

Next, assume that (3.58) holds for $k = \ell \in \mathbb{N}$, and it follows from (3.61) that $R_\ell = R_{*\ell}$. We then show that (3.58) holds for $k = \ell + 1$.

It follows from (2.79) and (3.53) that for all $t \in \mathcal{I}_\ell$,

$$\dot{R}_*(t) = R_*(t)\hat{\Omega}_*(Z_{*\ell}),$$

which has the solution

$$R_*(t) = R_{*\ell} \exp\left((t - t_\ell)\hat{\Omega}_*(Z_{*\ell})\right). \tag{3.62}$$

Since $Z_\ell = Z_{*\ell}$, substituting (3.54) into (3.62) yields that for all $t \in \mathcal{I}_\ell$,

$$R_*(t) = R_{*\ell} \exp\left(\frac{\|\hat{\Omega}_*(Z_\ell)\|_{\mathrm{F}}}{\sqrt{2}}(t - t_\ell)\Gamma_\ell\right). \tag{3.63}$$

It follows from (3.56) that

$$\frac{\|\hat{\Omega}_*(Z_\ell)\|_{\mathrm{F}}}{\sqrt{2}} = \sqrt{\omega_\ell^2 + c_\ell^2} - \omega_\ell. \tag{3.64}$$

Substituting (3.64) into (3.63) yields for all $t \in \mathcal{I}_\ell$,

$$R_*(t) = R_{*\ell} \exp\left(\sqrt{\omega_\ell^2 + c_\ell^2} - \omega_\ell\right)(t - t_\ell)\Gamma_\ell. \tag{3.65}$$

Since $\exp\left(S_\ell E_3 S_\ell^{\mathrm{T}}\right) = S_\ell \exp\left(E_3\right) S_\ell^{\mathrm{T}}$, it follows from (3.55) that

$$\exp\left(S_\ell E_3 S_\ell^{\mathrm{T}}\right) = \exp\left(\Gamma_\ell\right).$$

The eigenvalues of $S_\ell E_3 S_\ell^{\mathrm{T}}$ and Γ_ℓ are 0 and $\pm\jmath$. Therefore, [68, Fact 11.14.5] implies that

$$S_\ell E_3 S_\ell^{\mathrm{T}} = \Gamma_\ell. \tag{3.66}$$

Substituting (3.66) into (3.65) yields for all $t \in \mathcal{I}_\ell$,

$$R_*(t) = R_{*\ell} S_\ell \exp\left(\left(\sqrt{\omega_\ell^2 + c_\ell^2} - \omega_\ell\right)(t - t_\ell)E_3\right) S_\ell^{\mathrm{T}}.$$

Next, it follows from (3.1) and (3.25) that for all $t \in \mathcal{I}_\ell$,

$$\dot{R}(t) = R(t) c_\ell S_\ell \left[(\cos \omega_\ell t)E_1 + (\sin \omega_\ell t)E_2\right] S_\ell^{\mathrm{T}}. \tag{3.67}$$

Note that the solution R to (3.67) is continuous on $[0, \infty)$. Since $R_\ell = R_{*\ell}$, it follows from (3.17) of Proposition 3.4 with $S, \omega, c, R_0, \Delta t_k$, and $\tilde{R}$ replaced by $S_\ell, \omega_\ell, c_\ell, R_\ell, \Delta t_\ell$, and R_* that $R_{\ell+1} = R_{*(\ell+1)}$. Thus, (3.61) implies that $Z_{\ell+1} = Z_{*(\ell+1)}$, which confirms (3.58).

To show (3.59), it follows from (3.61) and (3.18) of Proposition 3.4 with S, ω, c,

R_0, t, and $\tilde{R}$ replaced by S_k, ω_k, c_k, R_k, $t - t_k$, and R_* that

$$\sup_{t\in\mathcal{J}_k} d(Z(t), Z_*(t)) = \sup_{t\in\mathcal{J}_k} d(R(t), R_*(t)) = \arccos \frac{\omega_k^2 - c_k^2}{\omega_k^2 + c_k^2}, \tag{3.68}$$

and substituting (3.56) into (3.68) yields (3.59).

To show the last statement of the theorem, let $\epsilon \in (0, \pi)$, and assume that $\omega_k \in [\omega_{\min}, \omega_{\max}]$. Therefore, (3.60) implies that

$$\omega_k \geq \frac{\|\hat{\Omega}_*(Z_k)\|_{\mathrm{F}}}{2\sqrt{\frac{1}{1+\cos\epsilon}} - \sqrt{2}},$$

which implies that

$$\cos\epsilon \leq \frac{2\omega_k^2}{\left(\frac{\|\hat{\Omega}_*(Z_k)\|_{\mathrm{F}}}{\sqrt{2}} + \omega_k\right)^2} - 1. \tag{3.69}$$

Since $\epsilon \in (0, \pi)$, substituting (3.69) into (3.59) yields $\sup_{t\in\mathcal{J}_k} d(Z(t), Z_*(t)) \leq \epsilon$. □

The final statement of Theorem 3.24 implies that $d(Z(t), Z_*(t))$ is arbitrarily small if ω_k is sufficiently large. Note that (3.56) implies that c_k is large if ω_k is large.

One possible choice for $\hat{\Omega}_*$ is given in [17, 19], specifically,

$$\hat{\Omega}_*(Z) = -k_c \log(Z) - Z^{\mathrm{T}} \hat{\Omega}_{\mathrm{d}}^{\mathrm{T}} Z, \tag{3.70}$$

where $k_c > 0$. It follows from [19, Theorem 2.A] that the identity is an almost globally asymptotically stable equilibrium of (3.52) and (3.70), where $\Omega = \Omega_*$.

Example 3.25. *Consider* (3.25) *and* (3.52)*, and the ideal command-following error* (3.53)*, where* Ω_* *is given by* (3.70)*, where* $k_{\mathrm{c}} = 1$*. Let*

$$\Omega_{\mathrm{d}}(t) = \begin{bmatrix} \frac{t^2+20t-20}{100} & \frac{\sin 2t}{5} & \frac{1}{10} \end{bmatrix}^{\mathrm{T}}.$$

The control parameters of (3.25) *are given by Algorithm 3.23 with* $\omega_k = 1000$ *rad/s. Figure 3.7 shows the performance* z *and the ideal performance* z_**. Note that for all* $t \geq 0$*,* $d(Z(t), Z_*(t)) < 0.12$ *rad.* △

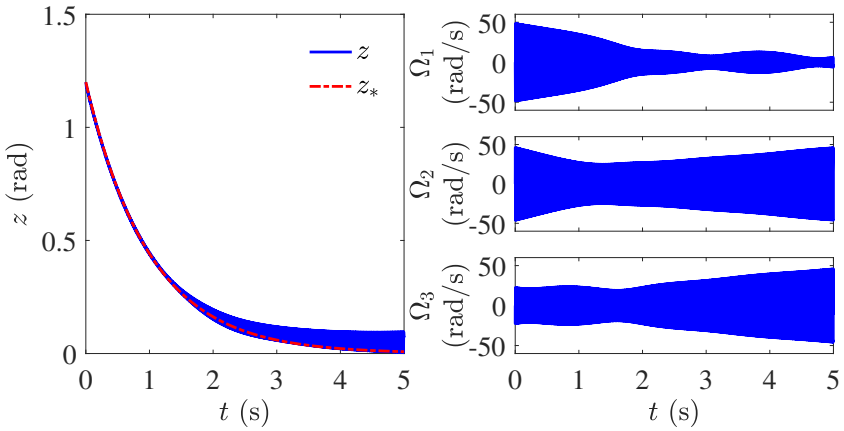

Figure 3.7: Closed-loop command following example using Algorithm 3.23 with constant ω_k but nonconstant Δt_k.

Algorithm 3.23 can be used for setpoint tracking, provided that the ideal control Ω_* is such that $\lim_{t\to\infty} Z_*(t) = I$. The following result shows that Algorithm 3.23 and (3.70) with $\Omega_\mathrm{d} = 0$ achieve setpoint tracking.

Proposition 3.26. Consider (3.52) and the ideal control (3.70), where $\Omega_\mathrm{d}(t) = 0$ and $k_c \in (0, \omega_{\max}/(2\pi))$. Consider the control (3.25), where S_k, ω_k, c_k, and Δt_k are given by Algorithm 3.23, and let $\omega_k > 2\pi k_c$. Then, $\lim_{t\to\infty} Z(t) = I$.

The proof of Proposition 3.26 relies on [19, Proposition 4] and uses arguments similar to those in the proof of Theorem 3.15. This proof is omitted for brevity.

Algorithm 3.23 cannot generally be implemented with constant ω_k and Δt_k. Next, we present a command-following controller that is implemented with constant frequency ω_k and constant time step Δt_k but nonconstant amplitude c_k.

Algorithm 3.27. Define

$$\Lambda_k \triangleq \begin{cases} \frac{\sqrt{2}}{\|\hat{\Omega}_*(Z_k)\|_{\mathrm{F}}}\hat{\Omega}_*(Z_k), & \text{if } \|\hat{\Omega}_*(Z_k)\|_{\mathrm{F}} \neq 0, \\ E_3, & \text{if } \|\hat{\Omega}_*(Z_k)\|_{\mathrm{F}} = 0, \end{cases}$$

and let $\omega \in (0, \omega_{\max}]$. Consider the control (3.25), where S_k satisfies

$$S_k \exp\left(\frac{c_k E_1 + \omega E_3}{\sqrt{\omega^2 + c_k^2}}\right) S_k^{\mathrm{T}} = \exp(\Lambda_k), \tag{3.71}$$

and

$$\begin{aligned} \omega_k &= \omega, \\ c_k &= \sqrt{\left(\frac{\|\hat{\Omega}_*(Z_k)\|_{\mathrm{F}}}{\sqrt{2}} + \omega\right)^2 - \omega^2}, \\ \Delta t_k &= \frac{2\pi}{\omega}. \end{aligned}$$

The following result compares the closed-loop response of (3.25) and (3.52), where S_k, ω_k, c_k, and Δt_k are given by Algorithm 3.27, with the ideal command-following error Z_*. The proof, which uses Proposition 3.5, is similar to that of Theorem 3.24.

Theorem 3.28. Consider (3.25) and (3.52), where S_k, ω_k, c_k, and Δt_k are given by Algorithm 3.27. Then,

$$Z_k = Z_{*k},$$

and

$$\sup_{t\in\mathcal{J}_k} d(Z(t), Z_*(t)) = \arccos\left(\frac{2\omega^2}{\left(\frac{\|\hat{\Omega}_*(Z_k)\|_{\mathrm{F}}}{\sqrt{2}}+\omega\right)^2} - 1\right).$$

Example 3.29. *Consider* (3.25) *and* (3.52)*, and the ideal command-following error* (3.53)*, where* Ω_* *and* Ω_{d} *are the same as in Example 3.25. The control parameters of* (3.25) *are given by Algorithm 3.27 with* $\omega = 1000$ *rad/s. Figure 3.29 shows the performance* z *and the ideal performance* z_**.*

We note that Figure 3.29 is similar to Figure 3.7 because the control parameters ω *is the same as* ω_k *in Example 3.25, and* $c_k \ll \omega$*. In this case,* Δt_k *of Algorithm 3.23 is approximately equal to* Δt_k *of Algorithm 3.27, and* E_{w} *of Algorithm 3.27 is approximately equal to* E_3*. Thus, Algorithm 3.23 and Algorithm 3.27 generate similar controls.* △

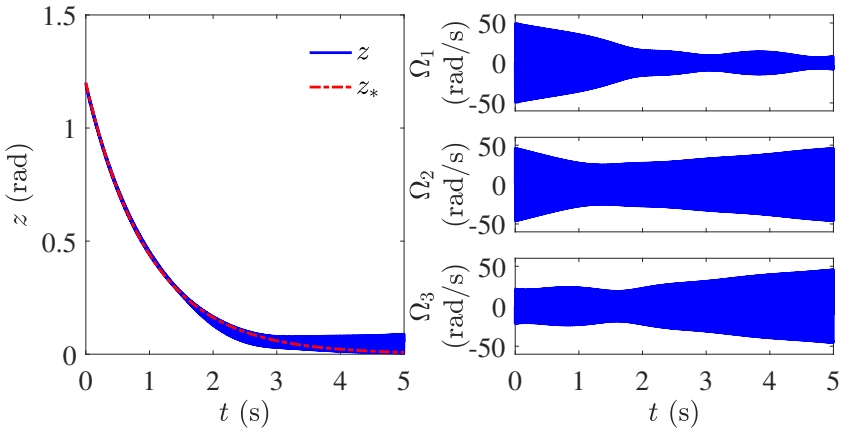

Figure 3.8: Closed-loop command following example using Algorithm 3.27 with constant ω_k and Δt_k.

Algorithm 3.27 can be used for setpoint tracking, provided that the ideal control Ω_* is such that $\lim_{t\to\infty} Z_*(t) = I$. The following result shows that Algorithm 3.23

and (3.70) with $\Omega_{\mathrm{d}} = 0$ achieve setpoint tracking.

Proposition 3.30. Consider (3.52) and the ideal control (3.70), where $\Omega_{\mathrm{d}} = 0$ and $k_c \in (0, \omega_{\max}/(2\pi))$. Consider the control (3.25), where S_k, ω_k, c_k, and Δt_k are given by Algorithm 3.27, and let $\omega > 2\pi k_c$. Then, $\lim_{t\to\infty} Z(t) = I$.

Chapter 4 Dynamic-Level Attitude Control

In this chapter, we extend the kinematic-level attitude control analysis of the previous chapter to account for dynamic effects. The previous chapter considers kinematic-level attitude control in which angular velocity is treated as a control input to the attitude kinematics. Piecewise sinusoidal kinematic-level controls are given that address setpoint tracking and command following. In practice, angular velocity cannot be controlled directly, but rather the angular velocity is driven by the kinetic equations of motion. Moreover, piecewise sinusoidal controls at the dynamic level do not in general induce purely piecewise sinusoidal angular velocity.

This chapter considers piecewise sinusoidal controls at the dynamic level. We consider a representative dynamic system model, which is the CubeSat system discussed in Chapter 2. The CubeSat system consists of a rigid body with vibrational momentum-wheel actuators. Small amplitude piecewise sinusoidal internal torques are designed to achieve setpoint tracking. Numerical examples are also provided to illustrate the control technique. In addition, we study the external damping effect on the CubeSat kinetics through numerical simulation.

4.1 Dynamic-level attitude control using steady-state approximation

As derived in Section 2.4, in the absence of external damping and gravitational force, the kinetic equations of motion for the CubeSat system are

$$\kappa\Omega(t) + \dot{\beta}(t) = 0, \tag{2.75}$$

$$\ddot{\beta}(t) + 2\zeta\dot{\beta}(t) + \beta(t) = -\kappa u(t). \tag{2.76}$$

Since $u(t)$ is piecewise smooth, its right derivative exists. Taking the right derivative

of (2.76) and using (2.75) yields

$$\ddot{\Omega}(t) + 2\zeta\dot{\Omega}(t) + \Omega(t) = \dot{u}(t). \tag{4.1}$$

This is a second order linear system, and thus $\Omega(t)$ can be solved analytically. Note that $\dot{\Omega}(t)$ is only piecewise continuous, and the initial conditions for (4.1) need to be solved using β.

Consider the case of sinusoidal controls. Specifically, if all of the components of $u(t)$ are sinusoids of frequency $\omega > 0$, then each component of the response $\Omega(t)$ consists of a transient response, which decays exponentially to zero, and a steady-state response, which is a sinusoid of frequency ω. If the transient response is regarded as negligible, then the approximate response to sinusoidal controls is purely sinusoidal.

In this section, we consider a steady-state control approach, which treats the transient response as negligible. In this case, it is possible to apply the kinematic-level control approaches from the previous chapter. The following algorithm is a steady-state implementation of Algorithm 3.14.

Algorithm 4.1. Let n be a positive integer, and consider the control

$$u(t) = \alpha S_k \left[c_k(\cos\omega t)e_1 + c_k(\sin\omega t)e_2\right], \quad t \in \mathcal{I}_k,$$

where $\alpha > 0$ is a scaling factor, and S_k, c_k, and Δt_k satisfy

$$\begin{aligned} &S_k \exp(-z_k E_3) S_k^{\mathrm{T}} = Z_k, \\ &\frac{c_k}{\omega} = \sqrt{\left(\frac{2\pi n}{2\pi n - z_k}\right)^2 - 1}, \\ &\Delta t_k = \frac{2\pi}{\sqrt{\omega^2 + c_k^2}}. \end{aligned}$$

Example 4.2. *Consider* (3.33), (2.75), *and* (2.76), *where* $\zeta = 0.05$, $\kappa = 6$, *and*

$$Z_0 = \exp\left(\frac{3\sqrt{14}}{35}\begin{bmatrix} 0 & -3 & 2 \\ 3 & 0 & -1 \\ -2 & 1 & 0 \end{bmatrix}\right).$$

The control parameters $\alpha = 0.15$, $\omega = 1.2$, *and* S_k, c_k, *and* Δt_k *satisfy Algorithm 4.1 with* $n = 5$. *Figure 4.1 shows the performance* z *and the control* u. △

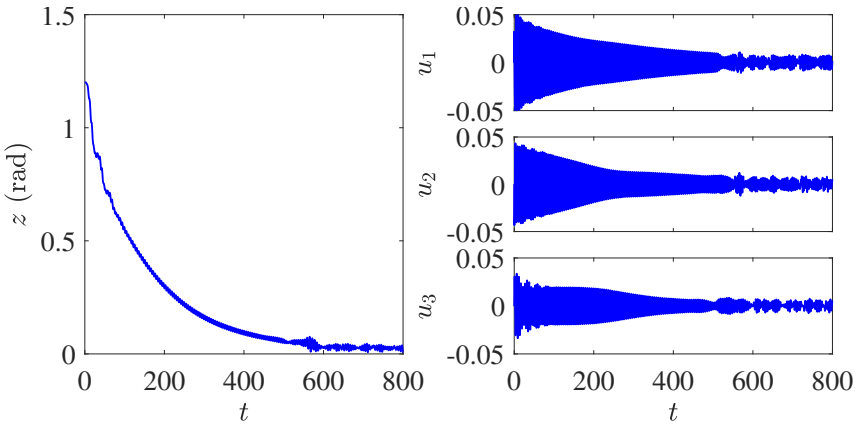

Figure 4.1: Setpoint tracking using Algorithm 4.1.

In Fig. 4.1, the setpoint tracking performance only converges to a neighborhood of zero. Recall that the equivalent kinematic-level controller in Algorithm 3.14 yields $z \to 0$. Thus, the transient response has a negative impact on the performance, at least when the performance is close to zero.

To minimize the adverse effect caused by the transient response of $\Omega(t)$, we apply small amplitude torques, which yield small angular velocity $\Omega = O(\epsilon) \in \mathbb{R}^3$, where $\epsilon > 0$ is a small quantity. It follows from (3.23) that if $\Omega = O(\epsilon)$, then the net rotation rate of the CubeSat, ignoring the transient response of Ω, will be in the order of $O(\epsilon^2)$. This is smaller than the transient response of Ω, which is in the order of $O(\epsilon)$. Although the transient response of Ω decays exponentially, it is not

clear how $R(t)$ will evolve since the effect of the small transient part of Ω may grow dramatically over a long period of time for the average rotation to be significant.

Concretely, consider the quaternion kinematics (2.26) together with (2.75) and (2.76). Note that the unit quaternions can be embedded in $\mathbb{R}^4$, and thus many classical nonlinear analysis techniques are applicable to analyze the motion of the system. Let $u(t) = [\epsilon \cos \omega t \quad \epsilon \sin \omega t \quad 0]^{\mathrm{T}}$, $\beta(0) = 0$, and $\dot{\beta}(0) = 0$. It follows from (4.1) that

$$\begin{aligned}
\Omega_1(t) &= \epsilon K_{11} \cos(\omega t + \phi_{11}) + \epsilon K_{12} e^{-\zeta t} \cos(\omega_{\mathrm{d}} t + \phi_{12}),\\
\Omega_2(t) &= \epsilon K_{11} \sin(\omega t + \phi_{11}) + \epsilon K_{22} e^{-\zeta t} \sin(\omega_{\mathrm{d}} t + \phi_{22}),\\
\Omega_3(t) &= 0,
\end{aligned}$$

where $\omega_{\mathrm{d}} \triangleq \sqrt{1 - \zeta^2} = O(1)$ and $K_{11}, K_{12}, K_{22} = O(1)$. Define

$$\begin{aligned}
\Omega_{11}(t) &\triangleq \epsilon K_{11} \cos(\omega t + \phi_{11}),\\
\Omega_{12}(t) &\triangleq \epsilon K_{12} e^{-\zeta t} \cos(\omega_{\mathrm{d}} t + \phi_{12}),\\
\Omega_{21}(t) &\triangleq \epsilon K_{11} \sin(\omega t + \phi_{11}),\\
\Omega_{22}(t) &\triangleq \epsilon K_{22} e^{-\zeta t} \sin(\omega_{\mathrm{d}} t + \phi_{22}),\\
M_1(t) &\triangleq \begin{bmatrix} 0 & -\Omega_{11}(t) & -\Omega_{12}(t) & -\Omega_{13}(t) \\ \Omega_{11}(t) & 0 & \Omega_{13}(t) & -\Omega_{12}(t) \\ \Omega_{12}(t) & -\Omega_{13}(t) & 0 & \Omega_{11}(t) \\ \Omega_{13}(t) & \Omega_{12}(t) & -\Omega_{11}(t) & 0 \end{bmatrix},\\
M_2(t) &\triangleq \begin{bmatrix} 0 & -\Omega_{21}(t) & -\Omega_{22}(t) & -\Omega_{23}(t) \\ \Omega_{21}(t) & 0 & \Omega_{23}(t) & -\Omega_{22}(t) \\ \Omega_{22}(t) & -\Omega_{23}(t) & 0 & \Omega_{21}(t) \\ \Omega_{23}(t) & \Omega_{22}(t) & -\Omega_{21}(t) & 0 \end{bmatrix},
\end{aligned}$$

$$f(t,q) \triangleq \frac{1}{2}M_1(t)q,$$
$$g(t,q) \triangleq \frac{1}{2}M_2(t)q.$$

Then the quaternion kinematics can be written as

$$\dot{q}(t) = f(t,q) + g(t,q).$$

Let $\bar{q}(t)$ be the solution of

$$\dot{\bar{q}}(t) = f(t,\bar{q}), \quad \bar{q}(0) = q(0). \tag{4.2}$$

We compare the trajectories of $q(t)$ and $\bar{q}(t)$ using [40, Theorem 3.4], where $q(t)$ corresponds to the original system response and $\bar{q}(t)$ corresponds to the system response with the steady state sinusoidal angular velocity input.

Note that $f(t,q)$ is piecewise continuous in t and is Lipschitz in q on S^3, with Lipschitz constant $L = \epsilon K_{11}/2$. Specifically, for all $t \geq 0$ and $q_1, q_2 \in S^3$,

$$\begin{aligned}
\|f(t,q_1) - f(t,q_2)\|_2 &= \|\frac{1}{2}M_1(t)(q_1 - q_2)\|_2 \\
&\leq \frac{1}{2}\|M_1(t)\|_2\|q_1 - q_2\|_2 \\
&= \frac{1}{2}\sqrt{\lambda_{\max}(M_1(t)^{\mathrm{T}}M_1(t))}\|q_1 - q_2\|_2 \\
&= \frac{1}{2}\epsilon K_{11}\|q_1 - q_2\|_2,
\end{aligned}$$

where $\lambda_{\max}(M_1(t)^{\mathrm{T}}M_1(t))$ denotes the largest eigenvalue of $M_1(t)^{\mathrm{T}}M_1(t)$, which is a diagonal matrix with all the diagonal elements being $\Omega_{11}^2 + \Omega_{21}^2$. In addition, for all $(t,q) \in [0,\infty) \times S^3$, $\|g(t,q)\|_2$ is bounded, since

$$\|g(t,q)\|_2 \leq \frac{1}{2}\|M_2(t)\|_2\|q\|_2 = \frac{1}{2}\|M_2(t)\|_2,$$

and

$$\|M_2(t)\|_2 = \sqrt{\lambda(M_2(t)^{\mathrm{T}} M_2(t)} = \sqrt{\Omega_{12}^2 + \Omega_{22}^2} \leq \epsilon \sqrt{K_{12}^2 + K_{22}^2} \triangleq \mu.$$

Now it follows from [40, Theorem 3.4] that

$$\|q(t) - \bar{q}(t)\|_2 \leq \frac{\mu}{L}(e^{Lt} - 1) = \frac{2\sqrt{K_{12}^2 + K_{22}^2}}{K_{11}}(e^{\frac{K_{11}}{2}\epsilon t} - 1). \tag{4.3}$$

Therefore, if $t = O(1)$, then $\|q(t) - \bar{q}(t)\|_2 = O(\epsilon)$. However, it follows from Proposition 3.4 that the average rotation rate for (4.2) is

$$\sqrt{\omega^2 + \epsilon^2 K_{11}^2} - \omega = \frac{\epsilon^2 K_{11}^2}{\sqrt{\omega^2 + \epsilon^2 K_{11}^2} + \omega} = O(\epsilon^2).$$

Thus, even though small amplitude internal torques are applied, the exponential term in (4.3) makes the difference between $q(t)$ and $\bar{q}(t)$ too large to yield a meaningful comparison.

4.2 Related work

In this section, we review some related results on the rotation kinematics with small angular velocity controls. For $i \in \{1, 2, 3\}$, let $v_i : [0, \infty) \to \mathbb{R}$ be piecewise-continuous and define

$$\tilde{v}_i(t) \triangleq \int_0^t v_i(\tau) \mathrm{d}\tau.$$

Furthermore, define

$$v(t) \triangleq [v_1(t)\ v_2(t)\ v_3(t)]^{\mathrm{T}}, \quad V(t) \triangleq \hat{v}(t), \tag{4.4}$$

$$\tilde{v}(t) \triangleq [\tilde{v}_1(t)\ \tilde{v}_2(t)\ \tilde{v}_3(t)]^{\mathrm{T}}, \quad \tilde{V}(t) \triangleq \hat{\tilde{v}}(t), \tag{4.5}$$

and

$$a_{ij}(t) \triangleq \frac{1}{2}\int_0^t \left(\tilde{v}_i(\tau)\dot{\tilde{v}}_j(\tau) - \tilde{v}_j(\tau)\dot{\tilde{v}}_i(\tau)\right) \mathrm{d}\tau. \tag{4.6}$$

Lemma 4.3 (Leonard [47])**.** Consider system

$$\dot{R} = \epsilon R\hat{v}(t), \quad v(t) = \sum_{i=1}^{m} v_i(t)e_i, \tag{4.7}$$

where $0 < \epsilon < 1$ and $m \in \{2, 3\}$. Assume that $v(t)$ is periodic with period T and has continuous derivatives up to the third order for $t \in [0, \infty)$. Assume $\tilde{v}(T) = 0$. Let $D \triangleq \{\xi \in \mathbb{R}^3 : \ \|\xi\|_2 < \pi\}$. Let $R(t)$ be the solution to (4.7) with $R(0) = \exp(\hat{\xi}_0)$ and $\xi_0 = \begin{bmatrix}\xi_{10} & \xi_{20} & \xi_{30}\end{bmatrix}^{\mathrm{T}} \in D = O(\epsilon)$. Let $\xi_0^{(2)} = \begin{bmatrix}\xi_{10}^{(2)} & \xi_{20}^{(2)} & \xi_{30}^{(2)}\end{bmatrix}^{\mathrm{T}} \in \mathbb{R}^3$ and define

$$\xi_k^{(2)}(t) \triangleq \epsilon\tilde{v}_k(t) + \epsilon^2\frac{t}{T}\sum_{i,j=1;i<j}^{m} a_{ij}(T)\Gamma_{ij}^k + \xi_{k0}^{(2)}, \quad k{=}1, 2, 3,$$

$$R^{(2)}(t) \triangleq \exp(\hat{\xi}^{(2)}(t)), \quad \xi^{(2)}(t) \triangleq [\xi_1^{(2)}(t)\ \xi_2^{(2)}(t)\ \xi_3^{(2)}(t)]^{\mathrm{T}},$$

where for $i, j, k \in \{1, 2, 3\}$, a_{ij} is defined by (4.6) and Γ_{ij}^k is defined such that $[E_{\mathrm{i}}, E_j] = \sum_{k=1}^{3}\Gamma_{ij}^k E_k$. If $\|\xi_0 - \xi_0^{(2)}\| = O(\epsilon^2)$ and there exists $b > 0$ such that for all $t \in [0, b/\epsilon]$, $\xi^{(2)}(t) \in D$, then

$$d(R(t), R^{(2)}(t)) = O(\epsilon^2), \quad \forall t \in [0, b/\epsilon].$$

If the inputs $v_i(t)$ to system (4.7) are sinusoids, we have the following proposition, which follows directly from Lemma 4.3.

Proposition 4.4. Consider system

$$\dot{R} = \epsilon R\hat{v}(t), \quad v = \begin{bmatrix} a_1 \sin(\omega t) \\ a_2 \sin(\omega t + \theta_2) \\ a_3 \sin(\omega t + \theta_3) \end{bmatrix},$$

with $R(0) = I$, where $a_1, a_2, a_3 > 0$ and $\theta_2, \theta_3 \in \mathbb{R}$. Define

$$\xi^{(2)}(t) \triangleq \frac{\epsilon}{\omega} \begin{bmatrix} a_1(1 - \cos(\omega t)) \\ a_2(\cos\theta_2 - \cos(\omega t + \theta_2)) \\ a_3(\cos\theta_3 - \cos(\omega t + \theta_3) \end{bmatrix} + \frac{\epsilon^2}{2\omega} t \begin{bmatrix} a_2 a_3 \sin(\theta_2 - \theta_3) \\ a_1 a_3 \sin\theta_3 \\ a_1 a_2 \sin(-\theta_2) \end{bmatrix}, \tag{4.8}$$

$R^{(2)}(t) \triangleq \exp(\hat{\xi}^{(2)}(t))$.

Let $D \triangleq \{\xi \in \mathbb{R}^3 : \ \|\xi\|_2 < \pi\}$. If there exists $b > 0$ such that for all $t \in [0, b/\epsilon]$, $\xi^{(2)}(t) \in D$, then

$$d(R(t), R^{(2)}(t)) = O(\epsilon^2), \quad \forall t \in [0, b/\epsilon]. \tag{4.9}$$

Proof. It follows from (4.5) and (4.6) that

$$\tilde{v}(t) = \frac{\epsilon}{\omega} \begin{bmatrix} a_1(1 - \cos(\omega t)) \\ a_2(\cos\theta_2 - \cos(\omega t + \theta_2)) \\ a_3(\cos\theta_3 - \cos(\omega t + \theta_3)) \end{bmatrix}$$

and

$$\begin{aligned} a_{23}(T) &= \frac{1}{2} \int_0^{\frac{2\pi}{\omega}} (\tilde{v}_2(t) v_3(t) - \tilde{v}_3(t) v_2(t)) \, \mathrm{d}t = \int_0^{\frac{2\pi}{\omega}} \tilde{v}_2 v_3 \mathrm{d}t \\ &= \int_0^{\frac{2\pi}{\omega}} \frac{a_2}{\omega} (\cos\theta_2 - \cos(\omega t + \theta_2)) a_3 \sin(\omega t + \theta_3) \mathrm{d}t = \frac{\pi a_2 a_3}{\omega^2} \sin(\theta_2 - \theta_3). \end{aligned}$$

It can also be shown that

$$a_{12}(T) = \frac{\pi a_1 a_2}{\omega^2} \sin(-\theta_2),$$
$$a_{13}(T) = \frac{\pi a_1 a_3}{\omega^2} \sin(-\theta_3),$$

By noticing the nonzero structural constants are $\Gamma^3_{12} = \Gamma^1_{23} = \Gamma^2_{31} = 1$ and $a_{ij}(T) = -a_{ji}(T)$, it follows from Lemma 4.3 that (4.9) holds. □

Note that the first term of (4.8) is periodic, and for $t = 2k\pi/\omega$, $k = 0, 1, 2, \cdots$, the first term vanishes. The second term is a secular term, which causes a net rotation, and the average velocity of the rotation vector is

$$r = \frac{\epsilon^2}{2\omega} \begin{bmatrix} a_2 a_3 \sin(\theta_2 - \theta_3) \\ a_1 a_3 \sin\theta_3 \\ a_1 a_2 \sin(-\theta_2) \end{bmatrix}. \tag{4.10}$$

This agrees with the Conjecture (C) in [59]. Note that if the dynamics considered in the conjecture is negligible, then the equations in the conjecture hold approximately. In addition, if $a_3 = 0$, then the average velocity r of the rotation vector equals $[0,\ 0,\ \epsilon^2 a_1 a_2/(2\omega)\sin(\theta_2 - \theta_3)]^{\mathrm{T}}$, i.e., sinusoidal angular velocities of a rigid body on its body x- and y-axis will induce a net rotation about its body z-axis. In this case, $\|r\|_2$ is sinusoidal function of θ_2.

Note that the approximation in Lemma 4.3 and Proposition 4.4 only hold locally, i.e., for $t \in [0, b/\epsilon]$, $b > 0$; whereas in the previous chapter, generality of the periodic signal is sacrificed for a global exact closed form solution of the rotation kinematics.

4.3 Small angular velocity controls

In this section, we consider (2.74) with small angular velocity input, that is, $\Omega(t) = \epsilon v(t)$, where $\epsilon > 0$ is a small number. The following lemma provides a solution to (2.74) in the form of infinite series.

Lemma 4.5. [Magnus [73], Karasev [74], Leonard [47]] Consider system

$$\dot{R}(t) = \epsilon R(t)\hat{v}(t), \quad R(0) = I. \tag{4.11}$$

If $v(t)$ satisfies

$$\int_0^t \|\epsilon\hat{v}(\tau)\|_2 \mathrm{d}\tau < \ln 2, \tag{4.12}$$

then the solution to (4.11) is

$$R(t) = \exp\left(\hat{\xi}(t)\right), \tag{4.13}$$

where

$$\begin{aligned}\hat{\xi}(t) = \epsilon \int_0^t V(\tau)\mathrm{d}\tau + \frac{\epsilon^2}{2}\int_0^t [\tilde{V}(\tau), V(\tau)]\mathrm{d}\tau \\ + \frac{\epsilon^3}{4}\int_0^t [\int_0^\tau [\tilde{V}(\sigma), V(\sigma)]\mathrm{d}\sigma, V(\tau)]\mathrm{d}\tau \\ + \frac{\epsilon^3}{12}\int_0^t [\tilde{V}(\tau), [\tilde{V}(\tau), V(\tau)]]\mathrm{d}\tau + \cdots,\end{aligned} \tag{4.14}$$

where $V(t)$ and $\tilde{V}(t)$ are defined in (4.4) and (4.5).

Next, we let $t_{\mathrm{a}} > 0$ and consider (4.14) for the case that

$$v(t) = \begin{cases} \begin{bmatrix} \cos(\omega t+\theta_0)+m_{11}e^{-\zeta t}\sin(\omega_{\mathrm{d}} t+\theta_{11}) \\ \sin(\omega t+\theta_0)+m_{21}e^{-\zeta t}\sin(\omega_{\mathrm{d}} t+\theta_{21}) \\ m_{31}e^{-\zeta t}\sin(\omega_{\mathrm{d}} t+\theta_{31}) \end{bmatrix}, & t\in[0,t_{\mathrm{a}}], \\ \begin{bmatrix} m_{12}e^{-\zeta t}\sin(\omega_{\mathrm{d}} t+\theta_{12}) \\ m_{22}e^{-\zeta t}\sin(\omega_{\mathrm{d}} t+\theta_{22}) \\ m_{32}e^{-\zeta t}\sin(\omega_{\mathrm{d}} t+\theta_{32}) \end{bmatrix}, & t\in(t_{\mathrm{a}},\infty), \end{cases} \tag{4.15}$$

where $\omega > 0$, $\theta_0 \in \mathbb{R}$, $\omega_{\mathrm{d}} \triangleq \sqrt{1-\zeta^2}$, and for all $i = 1,2,3$, $j = 1,2$, $m_{ij} > 0$ and $\theta_{ij} \in \mathbb{R}$.

Lemma 4.6. Consider (4.14), where v is given by (4.15). Then, there exists $t_{\mathrm{a}} = O(1/\epsilon)$ such that (4.14) converges for all $t > 0$.

Proof. Define $m \triangleq \max\left\{m_{ij} : i \in \{1,2,3\}, j \in \{1,2\}\right\}$. For all $t > 0$,

$$\begin{aligned} \int_0^t \|\epsilon\hat{v}(\tau)\|_2 \mathrm{d}\tau &\leq \int_0^\infty \|\epsilon\hat{v}(\tau)\|_2 \mathrm{d}\tau \\ &\leq \int_0^{t_{\mathrm{a}}} \epsilon \left\| \begin{bmatrix} \cos(\omega\tau+\theta_0) \\ \sin(\omega\tau+\theta_0) \\ 0 \end{bmatrix} \right\|_2 \mathrm{d}\tau + \int_0^{t_{\mathrm{a}}} \epsilon m \left\| \begin{bmatrix} e^{-\zeta\tau}\sin(\omega_{\mathrm{d}}\tau+\theta_{11}) \\ e^{-\zeta\tau}\sin(\omega_{\mathrm{d}}\tau+\theta_{21}) \\ e^{-\zeta\tau}\sin(\omega_{\mathrm{d}}\tau+\theta_{31}) \end{bmatrix} \right\|_2 \mathrm{d}\tau \\ &\quad + \int_{t_{\mathrm{a}}}^\infty \epsilon m \left\| \begin{bmatrix} e^{-\zeta\tau}\sin(\omega_{\mathrm{d}}\tau+\theta_{12}) \\ e^{-\zeta\tau}\sin(\omega_{\mathrm{d}}\tau+\theta_{22}) \\ e^{-\zeta\tau}\sin(\omega_{\mathrm{d}}\tau+\theta_{32}) \end{bmatrix} \right\|_2 \mathrm{d}\tau \\ &\leq \epsilon t_{\mathrm{a}} + \sqrt{3}\epsilon m \int_0^\infty e^{-\zeta\tau}\mathrm{d}\tau = \epsilon\left(t_{\mathrm{a}} + \frac{\sqrt{3}m}{\zeta}\right). \end{aligned} \tag{4.16}$$

Therefore, if

$$t_{\mathrm{a}} < \frac{1}{\epsilon}\ln 2 - \frac{\sqrt{3}m}{\zeta}, \tag{4.17}$$

then condition (4.12) is met for all t. Thus, by Lemma 4.5, there exists $t_{\mathrm{a}} = O(1/\epsilon)$ such that (4.14) converges for all $t > 0$. □

The following result gives a second order approximation of (4.14) if $v(t)$ is in the form of (4.15) and further satisfies an integral condition.

Theorem 4.7. Consider (4.11) and (4.13). Assume $v(t)$ is in the form of (4.15). In (4.15), let $t_{\mathrm{a}} = O(1/\epsilon)$ be such that (4.14) converges for all $t > 0$. Let $t_{\mathrm{b}} = O(1/\epsilon) > t_{\mathrm{a}}$ and $t_{\mathrm{s}} \in \{t_{\mathrm{b}}, \infty\}$. Further, assume $\int_0^{t_{\mathrm{s}}} v(t)\mathrm{d}t = O(\epsilon)$. Then,

$$\xi(t_{\mathrm{s}}) - \xi_{\mathrm{f}} = O(\epsilon^2), \tag{4.18}$$

where $\xi_{\mathrm{f}} \triangleq \begin{bmatrix} 0 & 0 & \epsilon^2 \frac{t_{\mathrm{a}}}{2\omega} \end{bmatrix}^{\mathrm{T}} = O(\epsilon)$.

Proof. It follows from (4.14) and (4.15) that

$$\hat{\xi}(t_{\mathrm{s}}) = \epsilon \int_0^{t_{\mathrm{s}}} \hat{v}(\tau)\mathrm{d}\tau + \frac{\epsilon^2}{2}\int_0^{t_{\mathrm{s}}} [\hat{\tilde{v}}(\tau), \hat{v}(\tau)]\mathrm{d}\tau + O(\epsilon^2).$$

Since $\int_0^{t_{\mathrm{s}}} v(t)\mathrm{d}t = O(\epsilon)$, it follows that

$$\begin{aligned}
\xi(t_{\mathrm{s}}) &= \epsilon \int_0^{t_{\mathrm{s}}} v(\tau)\mathrm{d}\tau + \frac{\epsilon^2}{2}\int_0^{t_{\mathrm{s}}} \tilde{v}(\tau) \times v(\tau)\mathrm{d}\tau + O(\epsilon^2) \\
&= \frac{\epsilon^2}{2}\int_0^{t_{\mathrm{s}}} \tilde{v}(\tau) \times v(\tau)\mathrm{d}\tau + O(\epsilon^2) \\
&= \frac{\epsilon^2}{2}\int_0^{t_{\mathrm{s}}} \begin{bmatrix} \tilde{v}_2(\tau)v_3(\tau) - \tilde{v}_3(\tau)v_2(\tau) \\ \tilde{v}_3(\tau)v_1(\tau) - \tilde{v}_1(\tau)v_3(\tau) \\ \tilde{v}_1(\tau)v_2(\tau) - \tilde{v}_2(\tau)v_1(\tau) \end{bmatrix} \mathrm{d}\tau + O(\epsilon^2).
\end{aligned} \tag{4.19}$$

Since $\tilde{v}(t_{\rm s}) = O(\epsilon)$, and $\tilde{v}(0) = 0$, integrating (4.19) by parts yields

$$\xi(t_{\rm s}) = \epsilon^2 \begin{bmatrix} \int_0^{t_{\rm s}} \tilde{v}_2(\tau) v_3(\tau) {\rm d}\tau \\ \int_0^{t_{\rm s}} \tilde{v}_3(\tau) v_1(\tau) {\rm d}\tau \\ \int_0^{t_{\rm s}} \tilde{v}_1(\tau) v_2(\tau) {\rm d}\tau \end{bmatrix} + O(\epsilon^2). \tag{4.20}$$

Note that for any $\alpha \in \mathbb{R}$,

$$\int e^{-\zeta t} \sin(\omega_{\rm d} t + \alpha) {\rm d}t = -\frac{e^{-\zeta t}}{\omega_{\rm d}^2 + \zeta^2} \left(\omega_{\rm d} \cos(\omega_{\rm d} t + \alpha) \, + \zeta \sin(\omega_{\rm d} t + \alpha) \right),$$

and $\int_0^\infty e^{-\zeta t} f(t) {\rm d}t = O(1)$ for any bounded function $f : \mathbb{R} \to [-f_{\rm m}, f_{\rm m}]$, where $f_{\rm m} > 0$. It follows that

$$\int_0^{t_{\rm s}} \tilde{v}_2(\tau) v_3(\tau) {\rm d}\tau = O(1), \tag{4.21}$$

$$\int_0^{t_{\rm s}} \tilde{v}_3(\tau) v_1(\tau) {\rm d}\tau = O(1), \tag{4.22}$$

$$\int_0^{t_{\rm s}} \tilde{v}_1(\tau) v_2(\tau) {\rm d}\tau = \int_0^{t_{\rm a}} \frac{1}{\omega} \sin^2 \omega\tau {\rm d}\tau + O(1) = \frac{t_{\rm a}}{2\omega} + O(1). \tag{4.23}$$

Thus, it follows from (4.20)–(4.23) that

$$\xi(t_{\rm s}) = \begin{bmatrix} O(\epsilon^2) & O(\epsilon^2) & \epsilon^2 \frac{t_{\rm a}}{2\omega} + O(\epsilon^2) \end{bmatrix}^{\rm T},$$

which confirms (4.18). □

4.4 Dynamic level control

Now, consider the rotation kinematics (2.74) together with the dynamics (2.75), (2.76). In this section, we analyze the motion of $R(t)$ with piecewise sinusoidal internal torque inputs.

Lemma 4.8. Consider (2.74), (2.75), and (2.76), where u is given by

$$u(t) = \begin{cases} \frac{\epsilon}{\omega a} \begin{bmatrix} \cos \omega t & \sin \omega t & 0 \end{bmatrix}^{\mathrm{T}}, & 0 \leq t \leq t_{\mathrm{a}}, \\ 0, & t > t_{\mathrm{a}}, \end{cases} \tag{4.24}$$

where $t_{\mathrm{a}} > 0$, and

$$a \triangleq \frac{1}{\sqrt{(1-\omega^2)^2 + 4\zeta^2\omega^2}}. \tag{4.25}$$

Assume for $i \in \{1, 2, 3\}$,

$$\beta_i(0) = O(\epsilon^2), \quad \dot{\beta}_i(0) = O(\epsilon^2). \tag{4.26}$$

Let $\Omega(t) = \epsilon v(t)$. Then $v(t)$ is in the form of (4.15).

Proof. It follows from (4.24) that the components of $u(t)$ satisfy

$$\dot{u}_i = \frac{\epsilon}{a} \cos(\omega t + \phi_i), \quad \text{for } t \leq t_a, \tag{4.27}$$

where $\phi_i \in \mathbb{R}$, for $i = 1, 2, 3$. Furthermore, it follows from (4.26), (2.75), and (2.76) that $\Omega_i(0) = O(\epsilon)$ and $\dot{\Omega}_i(0) = O(\epsilon)$. Therefore, it is the direct result of the linear system theory that $v(t)$ is in the form of (4.15). □

Remark. For $i \in \{1, 2\}$, and for $t \leq t_a$, $v_i(t)$ is in the form of

$$v_i(t) = \cos(\omega t + \theta_i) + m_{i1} e^{-\zeta t} \sin(\omega_{\mathrm{d}} t + \theta_{i1}),$$

where $\theta_i, \theta_{i1} \in \mathbb{R}$. Note that $m_{i1} = O(1)$ poses some difficulties for analyzing the motion of $R(t)$ using the standard perturbation techniques, because classic perturbation techniques usually require that the perturbation term is smaller than the nominal

input by an order of magnitude.

Lemma 4.9. Consider the same system and the same assumption as in Lemma 4.8. In (4.24), let $t_{\mathrm{a}} = O(1/\epsilon)$ be such that (4.14) converges for all $t > 0$. Let $t_{\mathrm{b}} = O(1/\epsilon) > t_{\mathrm{a}}$ and $t_{\mathrm{s}} \in \{t_{\mathrm{b}}, \infty\}$. Then,

$$\int_0^{t_{\mathrm{s}}} v(t)\mathrm{d}t = O(\epsilon). \tag{4.28}$$

Proof. We prove (4.28) for both cases of t_{s}. First, consider the case where $t_{\mathrm{s}} = \infty$. Because of the existence of damping in (2.76), (4.24) implies that $\lim_{t\to\infty} \beta(t) = \lim_{t\to\infty} \dot{\beta}(t) = 0$. Thus, it follows from (2.75) that $\lim_{t\to\infty} \Omega(t) = 0$ and

$$\kappa \int_0^{\infty} \Omega(t)\mathrm{d}t + \int_0^{\infty} \dot{\beta}(t)\mathrm{d}t = 0. \tag{4.29}$$

Since $\beta(0) = O(\epsilon^2)$ by (4.26), it follows that $\int_0^{\infty} \dot{\beta}(t)\mathrm{d}t = \beta(\infty) - \beta(0) = O(\epsilon^2)$. Therefore, (4.29) implies that

$$\int_0^{\infty} \Omega(t)\mathrm{d}t = O(\epsilon^2),$$

Thus, $\int_0^{\infty} v(t)\mathrm{d}t = O(\epsilon)$.

Next, consider the case where $t_{\mathrm{s}} = t_{\mathrm{b}}$. Since $t_{\mathrm{b}} = O(1/\epsilon) > t_{\mathrm{a}}$, we write $t_{\mathrm{b}} = t_{\mathrm{a}} + b_1/\epsilon$, where $b_1 = O(1)$. It follows from (2.76) and (4.24) that

$$\beta(t_{\mathrm{b}}) = O(\epsilon) \exp\left(-\zeta \frac{b_1}{\epsilon}\right),$$

and $\beta(t_{\mathrm{a}}) = O(\epsilon)$. Note that $\exp\left(-\zeta b_1/\epsilon\right) = O(\epsilon)$, for

$$\frac{\exp\left(-\frac{\zeta b_1}{\epsilon}\right)}{\epsilon} \leq \frac{1}{\zeta b_1 e}, \quad \forall \epsilon > 0.$$

Therefore, $\beta(t_{\mathrm{b}}) = O(\epsilon^2)$. Thus, it follows from (2.75) that

$$\begin{aligned}\int_0^{t_{\mathrm{b}}} \Omega(t)\mathrm{d}t &= -\frac{1}{\kappa}\int_0^{t_{\mathrm{b}}} \dot{\beta}(t)\mathrm{d}t \\ &= -\frac{1}{\kappa}(\beta(t_{\mathrm{b}}) - \beta(0)) \\ &= -\frac{1}{\kappa}(O(\epsilon^2) - O(\epsilon^2)) \\ &= O(\epsilon^2).\end{aligned}$$

Therefore, $\int_0^{t_{\mathrm{b}}} v(t)\mathrm{d}t = O(\epsilon)$. □

The following theorem is a direct result of Lemma 4.6, 4.8, 4.9 and Theorem 4.7. Note that the rotation matrix S affects the average rotation direction.

Theorem 4.10. Consider (2.74), (2.75), and (2.76), where u is given by

$$u(t) = \begin{cases} \frac{\epsilon}{\omega a} S \begin{bmatrix} \cos(\omega t) & \sin(\omega t) & 0 \end{bmatrix}^{\mathrm{T}}, & 0 \le t \le t_{\mathrm{a}}, \\ 0, & t > t_{\mathrm{a}}, \end{cases} \tag{4.30}$$

where $S \in \mathrm{SO}(3)$, $t_{\mathrm{a}} > 0$, and a is defined by (4.25). Assume (4.26) holds. Then, there exists $t_{\mathrm{a}} = O(1/\epsilon)$ such that (4.14) converges for all $t > 0$. Furthermore, let $t_{\mathrm{b}} = O(1/\epsilon) > t_{\mathrm{a}}$ and $t_{\mathrm{s}} \in \{t_{\mathrm{b}}, \infty\}$. Then,

$$d(R(t_{\mathrm{s}}), R_{\mathrm{f}}) = O(\epsilon^2), \tag{4.31}$$

where

$$R_{\mathrm{f}} = S \exp\left(\epsilon^2 \frac{t_{\mathrm{a}}}{2\omega} E_3\right) S^{\mathrm{T}}.$$

Example 4.11. *Consider* (2.74), (2.75), *and* (2.76), *where the control is given by* (4.30), *where* $\omega = 1.2$, $\zeta = 0.05$, $\kappa = 6$, $\epsilon = 0.01$, *and* $S = I$. *It follows from* (4.17)

that $t_a < 34.67$*, where we have used* $m = 1$*. Let* $t_a = 30$*. The simulation results are shown in Figure 4.2–4.4. Figure 4.2 shows the exponential coordinates* $\xi = [\xi_1\ \xi_2\ \xi_3]^T$ *of* R *which satisfies* $R = \exp\left(\hat{\xi}\right)$*, and note that* $\xi(100) = 10^{-3} \times [-0.2\ 0.1\ 1.8]^T$*. Theorem 4.10 implies that the second order approximation of* $R(\infty)$ *is* $\exp(0.0013E_3)$*. Since* $d(\exp(\hat{\xi}(100)), \exp(0.0013E_3)) = 5.5 \times 10^{-4}$*, (4.31) is confirmed.*

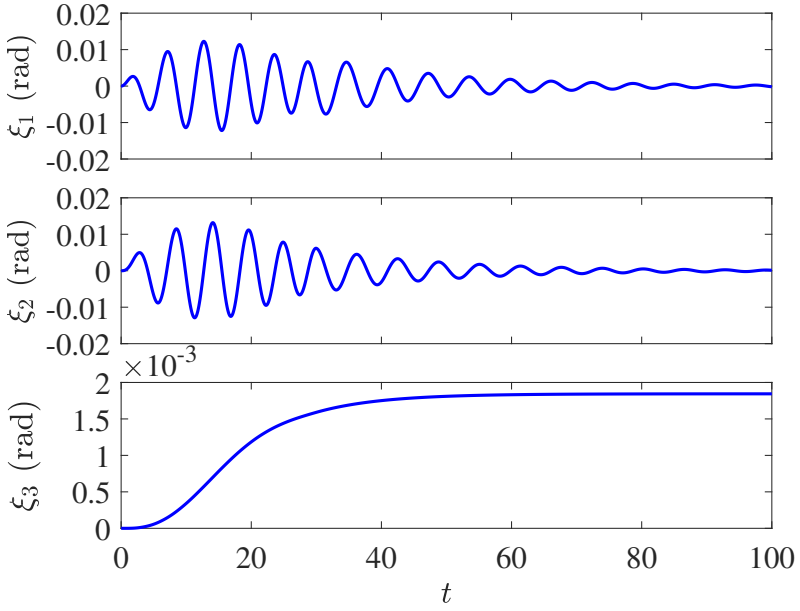

Figure 4.2: The rotation vector ξ of $R(\infty)$ is $10^{-3} \times [-0.2\ 0.1\ 1.8]^T$, and its second order approximation is $10^{-3} \times [0\ 0\ 1.3]^T$.

Theorem 4.10 implies sinusoidal control (4.24) steers R from I to R_f with $O(\epsilon^2)$ error. Therefore, for the setpoint tracking problem, we can generate a list of attitude points, R_0, R_1, R_2, $\cdots$, R_ℓ, where $R_0 = I$, $R_\ell = R_d$, and $d(R_k, R_{k+1}) = O(\epsilon)$ for $k = 0, 1, \cdots, \ell - 1$; then Theorem 4.10 can be used to steer R from R_k to R_{k+1} with

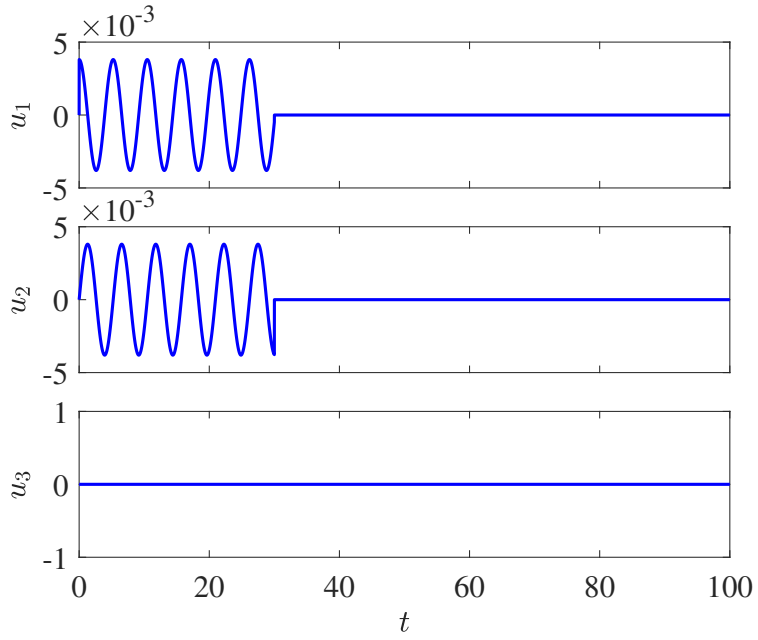

Figure 4.3: The sinusoidal control u (torque) induces a net rotation about body z axis.

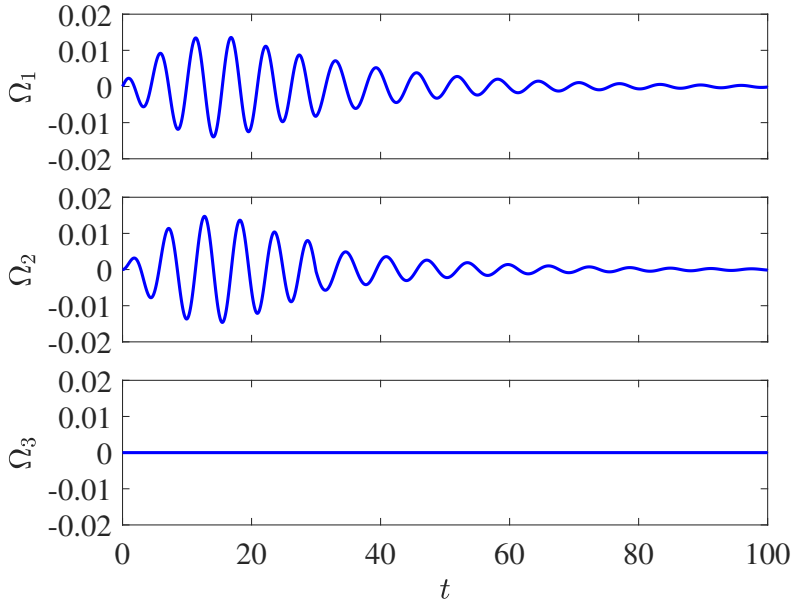

Figure 4.4: The angular velocity Ω of the rigid body is not periodic because of the transient response of the actuator dynamics.

$O(\epsilon^2)$ error. Specifically, consider admissible control

$$u(t) = \begin{cases} \frac{\epsilon}{\omega a} S_k \begin{bmatrix} \cos(\omega(t-t_k)) \\ \sin(\omega(t-t_k)) \\ 0 \end{bmatrix}, & t_k \le t \le t_k + t_{\mathrm{a}k}, \\ 0, & t_k + t_{\mathrm{a}k} < t < t_{k+1}, \end{cases} \tag{4.32}$$

where $t_0 = 0$, and for $k = 1, 2, \cdots$, $t_{k+1} = t_k + t_{\mathrm{s}k}$, $t_{\mathrm{a}k}$ and $t_{\mathrm{s}k}$ are specified in the same manner as t_{a} and t_{b} are in Theorem 4.10, and S_k satisfies

$$S_k \exp(\eta E_3) S_k^{\mathrm{T}} = R(t_k)^{\mathrm{T}} R_{\mathrm{d}}, \tag{4.33}$$

where $0 < \eta \le \pi$. Then, we have the following theorem for setpoint tracking.

Theorem 4.12. Consider (2.74), (2.75), and (2.76), where $u(t)$ is given by (4.32). Let $R(0) = I$ and $R_{\mathrm{d}} \in \mathrm{SO}(3)$. Then, for any $\delta > 0$, there exists $t_{\mathrm{f}} > 0$ and admissible control $u(t)$ such that

$$d(R(t), R_{\mathrm{d}}) < \delta, \quad \forall t \ge t_{\mathrm{f}}. \tag{4.34}$$

Example 4.13. *Consider* (2.74), (2.75), *and* (2.76), *where the control is given by* (4.32), *where the system and control design parameters* ω, ζ, κ, *and* ϵ *are the same as in Example 4.11,* $t_{\mathrm{a}k} \equiv 30$, $t_k = 50k$, *for* $k = 0, 1, 2, \cdots$. *Control parameter* S_k *is calculated from* (4.33). *In this example, the desired attitude is* $R = \exp(\hat{\xi}_{\mathrm{d}})$, *where* $\xi_{\mathrm{d}} = [0.1\ 0.3\ 0.2]^{\mathrm{T}}$. *Figure 4.5 shows the distance* $d(R(t), R_{\mathrm{d}})$, *and Figure 4.6 shows* $\Omega(t)$ *for* $2000 \le t \le 2100$. *Note that* $d(R(12000), R_{\mathrm{d}}) = 0.0027$ *rad.*

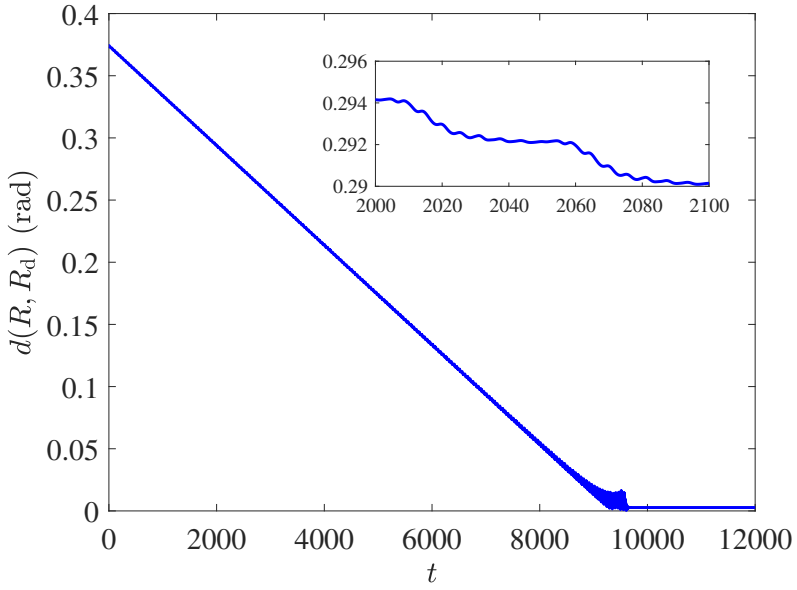

Figure 4.5: Dynamic level control $u(t)$ is designed to steer $R(t)$ to R_d with $O(\epsilon^2)$ error.

4.5 The effect of external damping

In this section, we investigate the nonlinear CubeSat kinetics (2.66) (2.67) using numerical simulations. The system parameters used in the simulation is summarized in Table 4.1. Note that here we use the original equations with dimension.

Table 4.1: System parameters used in numerical simulations

Parameters	Value	Unit
$I_1,\ I_2,\ I_3$	0.003	kg·m^2
I_a	0.001	kg·m^2
I_t	0.0015	kg·m^2
m	0.5	kg
C	0.05	N·m·s/rad
K	100	N·m/rad
μ	0.01	N·m·s/rad
g	9.81	m/s^2
h	0	m

We set $h = 0$ to enable the CubeSat to rotate in an arbitrary direction. Let $u = [A_1 \cos(\omega t)\ A_2 \sin(\omega t)\ 0]^\mathrm{T}$, where $A_1 = A_2 = 10$ N·m, and $\omega = 40\pi$ rad/s. The

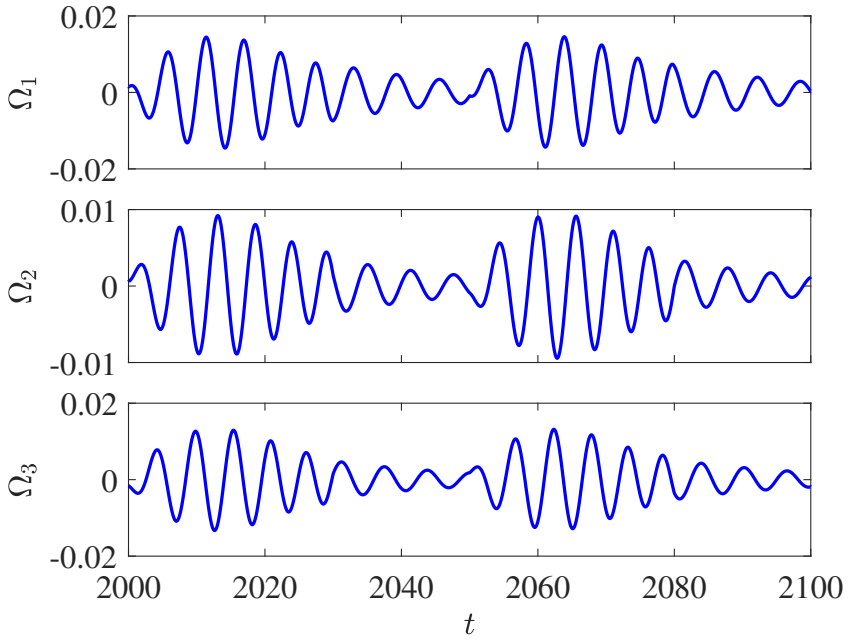

Figure 4.6: Angular velocity $\Omega(t)$ of the rigid body induced by the dynamic level control $u(t)$.

simulation results are shown in Fig. 4.7 – 4.9. As shown in Fig. 4.7, the CubeSat oscillates about its body x and y axis, but there is a net rotation about the body z axis. The yaw angle ψ increases first and then starts to decrease. As shown in Fig. 4.8, Ω_1 and Ω_2 are sinusoidal signals with the phase of Ω_1 leading that of Ω_2 by $\pi/2$ (the phase difference is better shown in Fig. 4.9); Ω_3 decreases before reaching a steady state value. Figure 4.9 shows $\Omega_1(t)$, $\Omega_2(t)$, $\dot{\beta}_1(t)$, and $\dot{\beta}_2(t)$, which are the angular velocity components of the cube and the momentum wheels.

Since Ω_3 varies slowly with respect to sinusoidal Ω_1 and Ω_2, we can treat Ω_3 as a constant within a short period of time. In the case where $\Omega_3 = 0$, it follows from Proposition 3.4 that the net rotation is along the positive body z direction, since the phase of sinusoidal Ω_1 leads that of Ω_2 by $\pi/2$. In the case where $\Omega_3 < 0$, as pointed out in Chapter 3, the net rotation direction depends on the relative magnitude of Ω_3 with respect to the amplitude of Ω_1 and Ω_2. In particular, assume the amplitude of

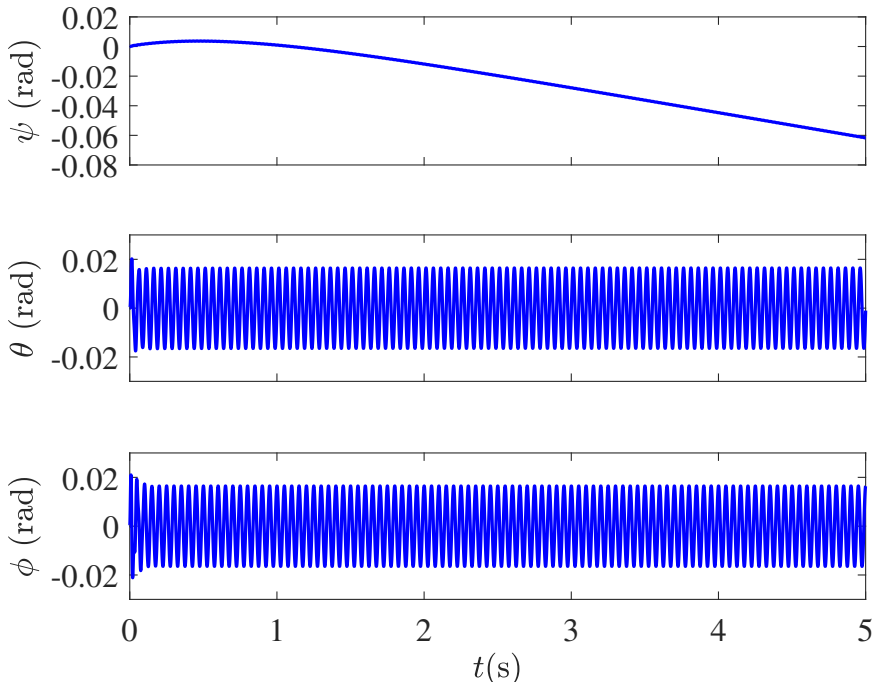

Figure 4.7: Euler angles of the CubeSat system with sinusoidal internal torque inputs.

Ω_1 and Ω_2 are both c and $c < \omega$. As discussed in Section 3.1, if $\Omega_3 < \sqrt{\omega^2 - c^2} - \omega$, then the net rotation is in the negative body z direction. This explains the motion of the yaw angle.

However, it is interesting that the CubeSat generates an angular velocity in the body z direction in the first place, even though no internal torques are applied in the body z direction ($u_3 = 0$).

Following the derivation of the equations of motion in Section 2.4, we note that the sum of the torques and moments acting on the cube about its rotational center is $\mathbf{M}_p + \mathbf{T}_o + \mathbf{T}_\mathrm{d}$ (See Eq. (2.33)). It can be shown that the z-component M_3 is

$$M_3 = -2I_\mathrm{t}\dot{\Omega}_3 - \mu\Omega_3 + I_\mathrm{a}(\Omega_2\dot{\beta}_1 - \Omega_1\dot{\beta}_2). \tag{4.35}$$

We note that external damping affects the phases of sinusoidal signals $\Omega_1(t)$, $\Omega_2(t)$, $\dot{\beta}_1(t)$, and $\dot{\beta}_2(t)$. For linear systems, a pole induces 90° phase lag while a damped pole

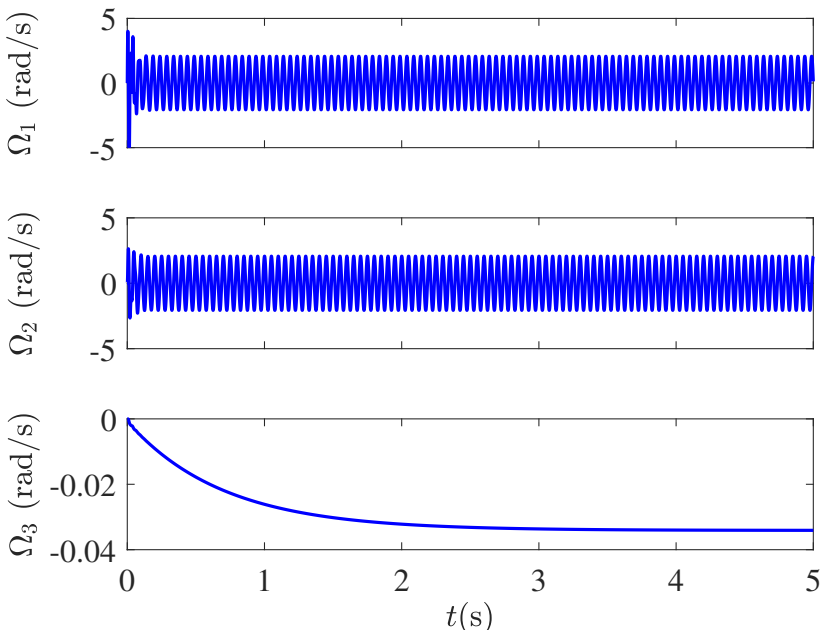

Figure 4.8: Angular velocity $\Omega(t)$ of the rigid body induced by the dynamic level control $u(t)$.

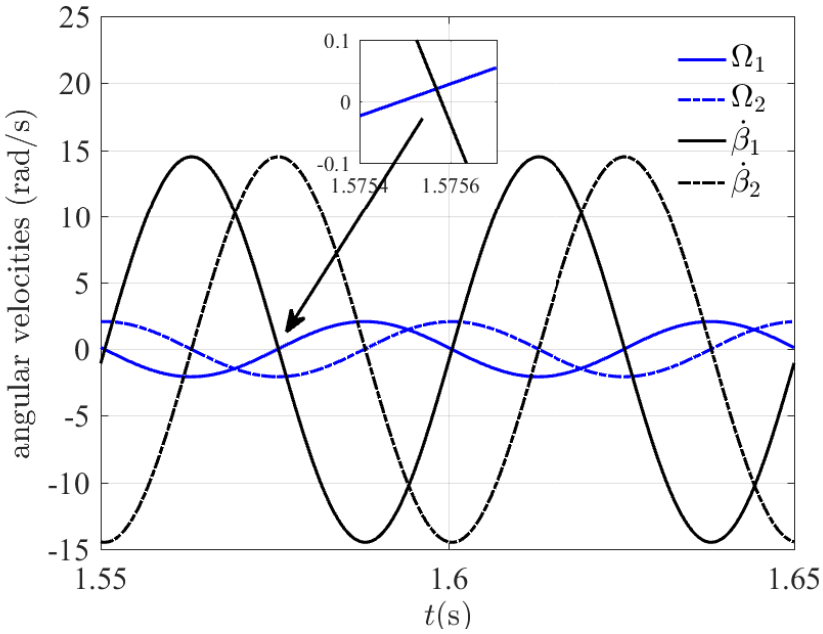

Figure 4.9: Angular velocities of the CubeSat and the momentum wheels.

induces a phase lag between 0° and 90°. Based on the waveforms shown in Fig. 4.9, we assume for $i = 1, 2$, $\beta_i(t)$ and $\Omega_i(t)$ are single tone sinusoidal signals, and $\dot{\beta}_i(t)$

leads $\Omega_i(t)$ by $\pi - \alpha$, where $\alpha \in (0, \pi/2)$. In particular, we assume $\dot{\beta}_i(t)$ and $\Omega_i(t)$ are of the following form

$$\Omega_1(t) = k_1 A_1 \cos(\omega t + \beta), \quad \dot{\beta}_1(t) = k_2 A_1 \cos(\omega t + \beta + \pi - \alpha), \tag{4.36}$$

$$\Omega_2(t) = k_1 A_2 \sin(\omega t + \beta), \quad \dot{\beta}_2(t) = k_2 A_2 \sin(\omega t + \beta + \pi - \alpha), \tag{4.37}$$

where $k_1 > 0$, $k_2 > 0$, $\beta \in \mathbb{R}$, and $\alpha \in (0, \pi)$. It follows from (4.36) and (4.37) that

$$\Omega_2 \dot{\beta}_1 - \Omega_1 \dot{\beta}_2 = -k_1 k_2 A_1 A_2 \sin \alpha < 0.$$

Therefore, the terms $\Omega_2 \dot{\beta}_1 - \Omega_1 \dot{\beta}_2$ in (4.35) create a nonzero torque M_3, which in turn yields a nonzero Ω_3.

Next, we propose a heuristic setpoint tracking control algorithm for the case where the CubeSat system is subject to external damping. Note that if the external damping is significant, the direction of the net rotation of the CubeSat is the opposite direction relative to the case where there is no external damping. This motivates using the inverse of the error rotation matrix Z as feedback. In particular, consider the following setpoint tracking algorithm.

Algorithm 4.14. Let n be a positive integer, and consider the dynamic level control

$$u(t) = \alpha S_k \left[c_k(\cos \omega t) e_1 + c_k(\sin \omega t) e_2 \right], \quad t \in \mathcal{I}_k \tag{4.38}$$

where $\alpha > 0$ is a scaling factor, and S_k, ω, c_k, and Δt_k satisfy

$$S_k \exp(-z_k E_3) S_k^{\mathrm{T}} = Z_k^{\mathrm{T}}, \tag{4.39}$$

$$\frac{c_k}{\omega} = \sqrt{\left(\frac{2\pi n}{2\pi n - z_k}\right)^2 - 1}, \tag{4.40}$$

$$\Delta t_k = \frac{2\pi}{\sqrt{\omega^2 + c_k^2}}. \tag{4.41}$$

Similar to Algorithm 4.1, Algorithm 4.14 is only able to yield a setpoint tracking error that is bounded in a neighborhood of zero. In order to achieve zero setpoint tracking error, small amplitude control techniques discussed in Section 4.4 should be used.

Example 4.15. *Consider* (2.66), (2.67) *with* (2.27) *and* (2.25)*, where the system parameters are given in Table 4.1, and the initial orientation*

$$R(0) = \exp\left(\frac{1}{10}\begin{bmatrix} 0 & -3 & 2 \\ 3 & 0 & -1 \\ -2 & 1 & 0 \end{bmatrix}\right).$$

The desired orientation $R_{\mathrm{d}} = I$*. The scaling factor* $\alpha = 1$*, and the control parameters* S_k*,* c_k*, and* Δt_k *satisfy Algorithm 4.14 with* $n = 5$ *and* $\omega = 40\pi$ *rad/s. Figure 4.10 shows the performance* z*.*

△

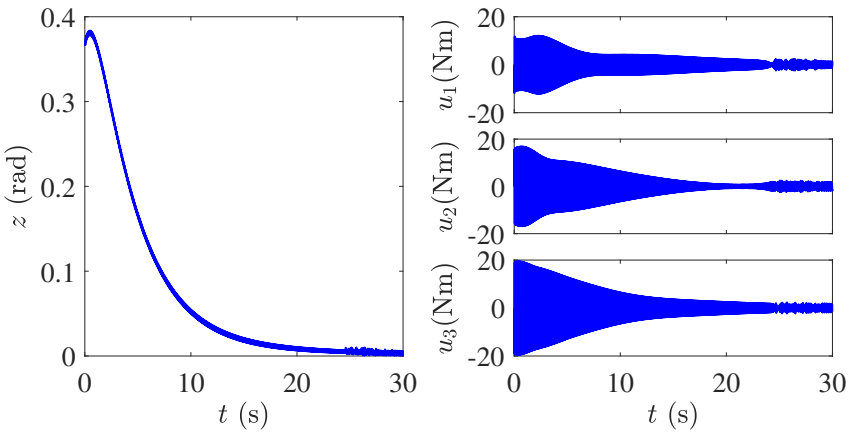

Figure 4.10: Setpoint tracking using Algorithm 4.14.

Chapter 5 CubeSat Experiments

In this chapter, we present experimental results related to the theoretical and simulation results presented in Chapter 3 and 4. The mechanical system that is used for these experiments consists of a CubeSat frame that is equipped with a vibrational attitude-actuation system. The actuation system is composed of piezoelectric beam actuator arrays that are used to vibrate the CubeSat frame about each body-fixed axis. The CubeSat is mounted to a spherical air bearing, which allows for three rotational degrees of freedom. We investigate the feasibility of the sinusoidal actuation approach through open-loop and closed-loop experiments. Additionally, we demonstrate the effect of the external damping on the CubeSat kinetics with experimental results.

5.1 CubeSat mechanical system

The experimental CubeSat system, shown in Fig. 5.1(a), is constructed around a $10\times10\times10$ cm cubic frame made of 6061 aluminum alloy. There are three trays inside the cubic frame to hold the control circuit board, battery, and other electronics. A 3D model of the cubic frame is shown in Fig. 5.1(b).

There is one set of actuators on each face of the cubic frame. Each actuator consists of a piezoelectric beam and tip masses (square nuts) that are glued at the end of the beam. The piezoelectric beam is manufactured by STEMiNC (Part number: SMBA4510T05M) and its dimensions are $40 \times 10 \times 0.5$ mm. Four actuators are installed in an equally spaced manner on a 3D printed hub. Polylactic acid (PLA) is used for printing the beam hubs. A pair of piezoelectric beams are shown in Fig. 5.2(a) and a set of actuators is shown in Fig. 5.2(b).

The piezoelectric beams are capacitive load with 60$\sim$70 nF capacitance. The

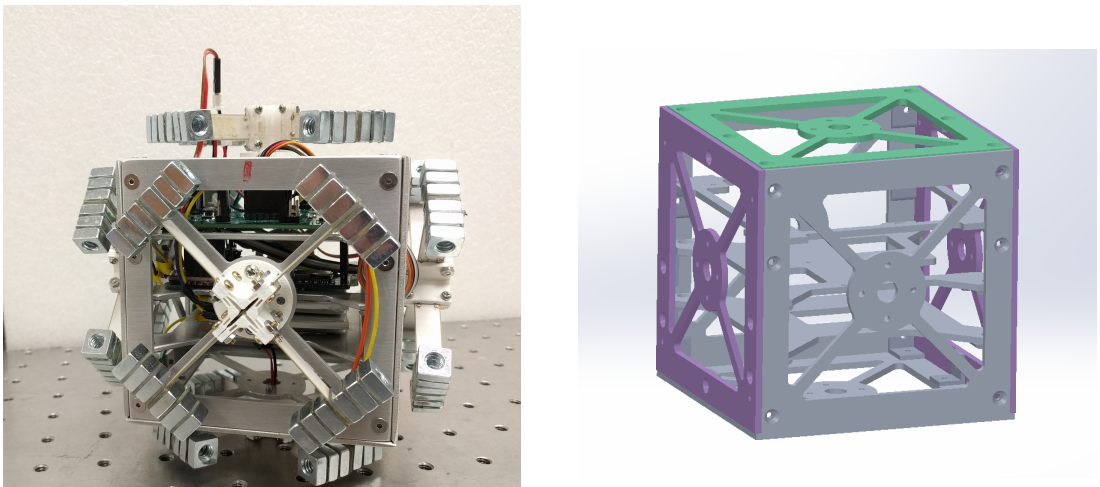

(a) (b)

Figure 5.1: The experimental CubeSat system is constructed around a cubic frame.

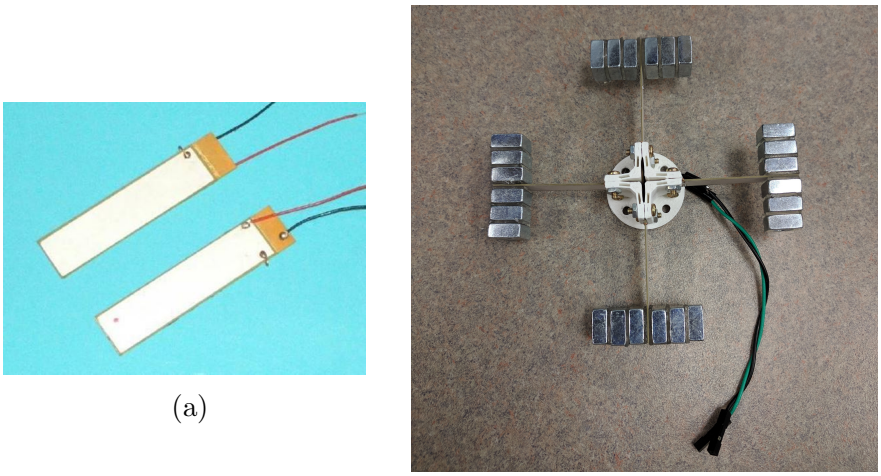

(a) (b)

Figure 5.2: (a) Piezoelectric bimorph actuators (Image courtesy of https://www.steminc.com/); (b) Four actuators are installed on a 3D printed hub.

beams vibrate if sinusoidal voltage is applied.

5.2 CubeSat attitude control system hardware

In this section, we describe the control system hardware in detail. The CubeSat attitude control system consists of a microcontroller, three piezo drivers to drive the

piezoelectric beams, an inertia measurement unit (IMU) sensor to measure Euler angles and angular velocities of the CubeSat, a data logger to log the sensor data, and a Bluetooth Low Energy (BLE) module to communicate with external devices. The schematic of the CubeSat attitude control system is shown in Fig. 5.3.

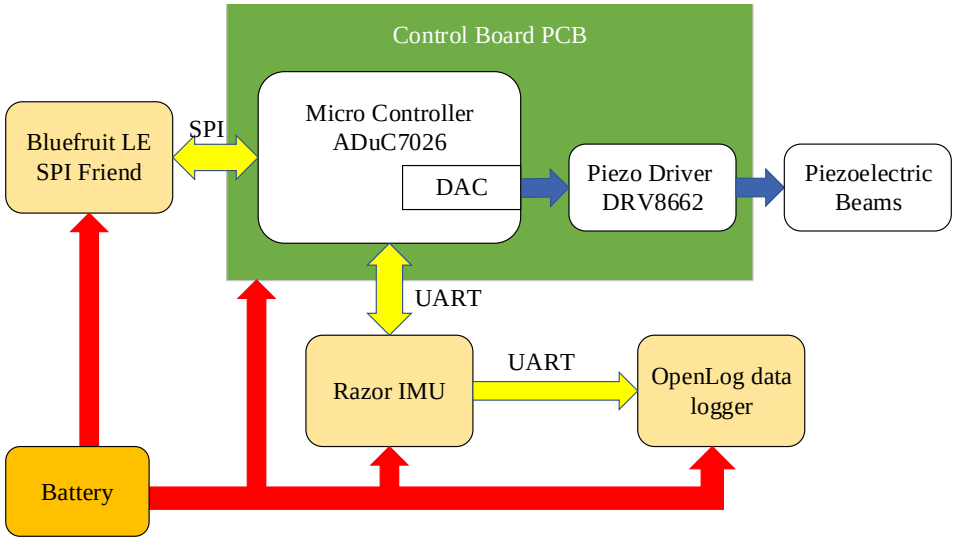

Figure 5.3: CubeSat attitude control system.

The control system is designed to drive each piezoelectric actuator with a sinusoidal voltage signal. The most common approaches to generate sinusoidal control signals on embedded platforms use digital-to-analog conversion (DAC) or pulse-width modulation (PWM). The signals generated by DAC or PWM are piecewise constant signals, which are passed through a low-pass filter to generate the desired sinusoids. The low-pass filter is not always necessary for a high precision DAC module when the sampling frequency of the DAC is much larger than the bandwidth of the system that is driven by the sinusoids. In the CubeSat system, we utilize the DAC modules to generate sinusoidal signals.

The piezoelectric beams are driven by piezo haptic driver DRV8662, which is manufactured by Texas Instruments. The single-chip piezo haptic driver DRV8662 is integrated with a 105 V boost switch and a fully-differential amplifier. There are

four amplification gains available: 28.8 dB, 34.8 dB, 38.4 dB, and 40.7 dB. The gains are optimized to get approximately 50 V_{pp}, 100 V_{pp}, 150 V_{pp}, or 200 V_{pp} at the output without clipping from a 1.8 V_{pp} single-ended input source. A typical application circuit of the piezo haptic driver is shown in Fig. 5.4. Note that the single-ended output signal from the DAC is nonnegative; if the DAC output signal is sinusoidal, the AC coupling capacitors C4, C5 in Fig. 5.4 shift the average of the sinusoidal signal to zero.

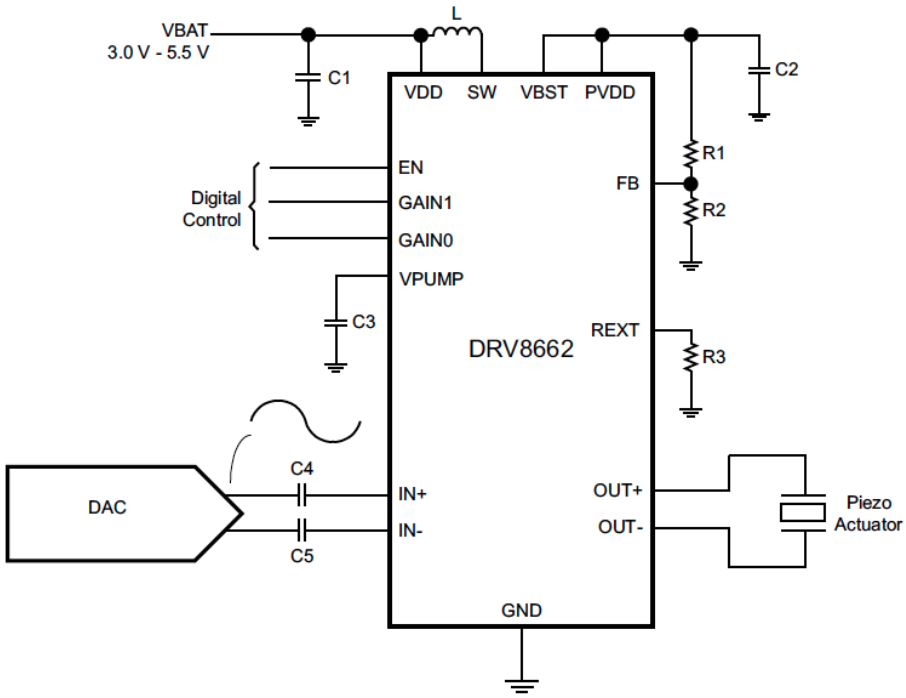

Figure 5.4: DRV8662 application circuit with DAC input (this design is from the DRV8662 manual).

The microcontroller used in the control system is ADuC7026 from Analog Devices. This microcontroller features an ARM7TDMI core, four 12-bit voltage output DAC channels, four general-purpose timers, and various serial I/O ports, including one universal asynchronous receiver-transmitter (UART), one serial peripheral interface (SPI), and two inter-integrated circuit (I^2C) ports. We use the DACs to generate sinusoids as inputs to the piezo haptic driver.

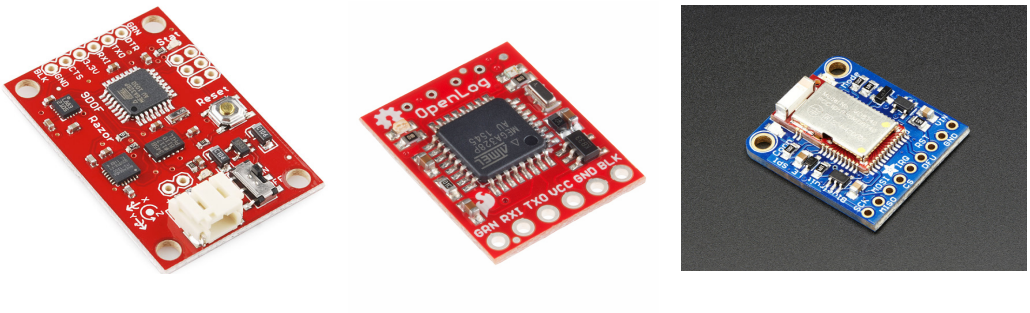

(a) (b) (c)

Figure 5.5: (a) Nine degree-of-freedom Razor IMU (Image courtesy of https://www.sparkfun.com/); (b) OpenLog data logger (Image courtesy of https://www.sparkfun.com/); (c) Adafruit Bluefruit LE SPI Friend (Image courtesy of https://learn.adafruit.com/).

The IMU used in this system is the Razor IMU (SparkFun part number: SEN-10736). This stand-alone IMU incorporates an ATmega328 microcontroller and three sensors, i.e., an ITG-3200 (MEMS triple-axis gyro), ADXL345 (triple-axis accelerometer), and HMC5883L (triple-axis magnetometer). The ATmega328 controller fuses the outputs of these three on-board sensors and provides triple-axis angular velocities and (3-2-1) Euler angles over a UART port. A picture of the IMU is shown in Fig. 5.5 (a). SparkFun OpenLog is a stand-alone open source data logger that records the angular velocities and Euler angle data to a microSD card. An image of the data logger is shown in Fig. 5.5 (b).

Adafruit Bluefruit LE SPI Friend is a stand-alone Bluetooth Low Energy (BLE) module added to the CubeSat system to enable wireless communication between the CubeSat system and external devices, e.g., a smartphone. The Bluetooth Low Energy module communicates with the ADuC7026 microcontroller through Serial Peripheral Interface (SPI), and acts as a data tube between the user interface on a smartphone and the ADuC7026 microcontroller. An image of the Adafruit Bluefruit LE module is shown in Fig. 5.5 (c).

A customized printed circuit board (PCB) is the main control board, housing the ADuC7026 microcontroller and three DRV8662 drivers, as well as connecting the

IMU, the data logger, and the Bluetooth Low Energy module as the mother board. The main control board contains four layers (two routing layers, a ground plane, and a power plane) and is designed with Altium Designer. The PCB is fabricated and populated by PCBWay[1]. The schematics of the PCB is shown in Fig. 5.6 and the finished PCB is shown in Fig. 5.7.

The CubeSat system is powered by a Lithium-ion polymer battery. Its output ranges from 4.2 V when fully charged to 3.7V and it has a capacity of 2500 mAh.

5.3 CubeSat attitude control software

Embedded software can be designed using various architectures. Four that are commonly used are round-robin, round-robin with interrupts, function-queue-scheduling, and real-time operating system [75]. These architectures vary with increasing complexity, but generally offer increasingly better performance. Response requirements often drive the choice of software architecture; when response requirements are satisfied, a simpler architecture usually provides a simpler but more reliable solution.

The main software routines/processes of the CubeSat system are:

A. System initialization (including DACs, Timers, SPI/UART ports, etc.);

B. Taking user inputs and reporting status to user;

C. Retrieving sensor data from IMU;

D. Computing feedback control (in the case of closed-loop control);

E. Generating sinusoidal signals.

Routines C, D, E have a more stringent response requirement. Because there are a limited number of routines, we choose the round-robin with interrupts as the architecture for the embedded control system. The microcontroller ADuC7026 can

[1]https://www.pcbway.com.

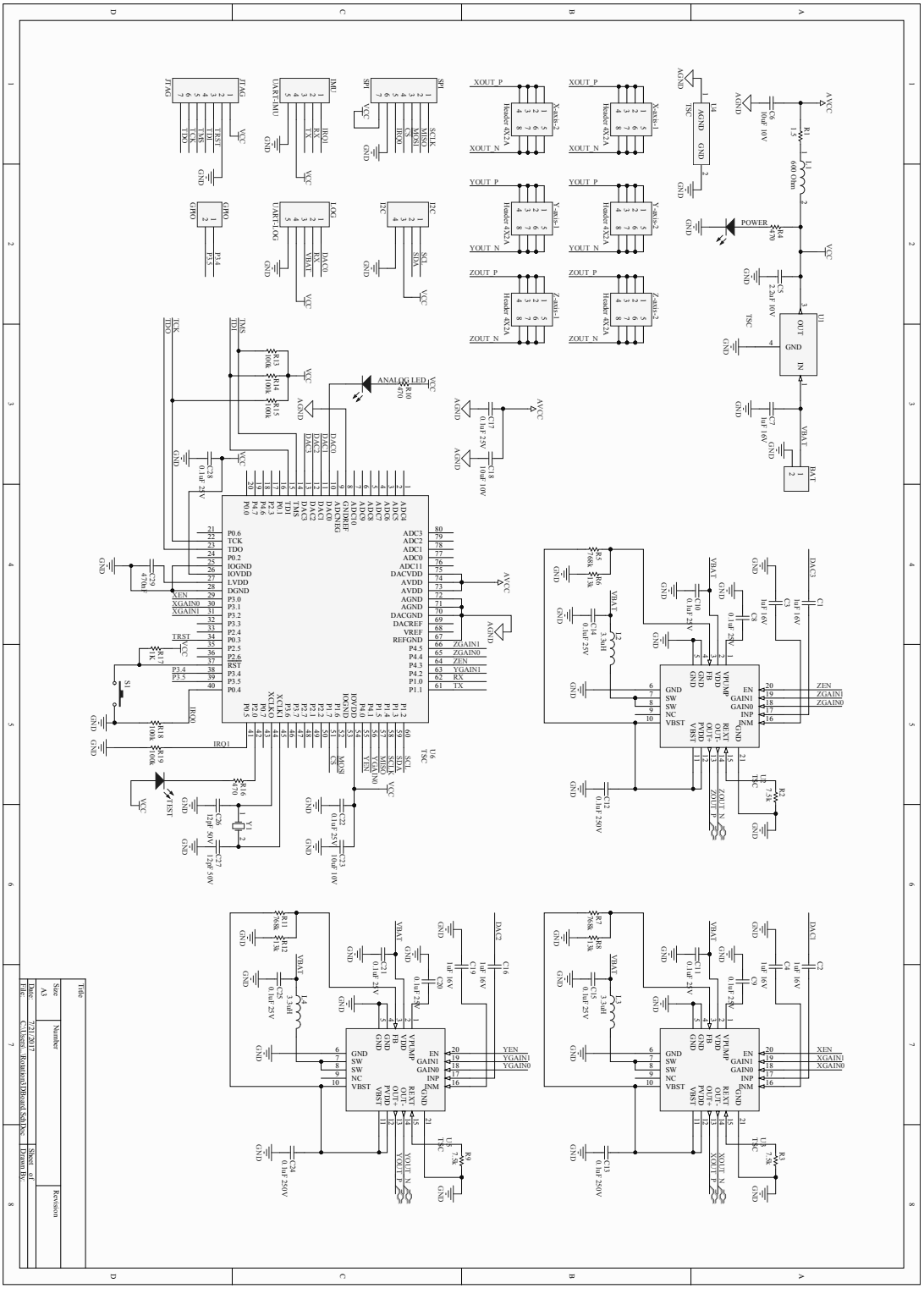

Figure 5.6: Control board schematics.

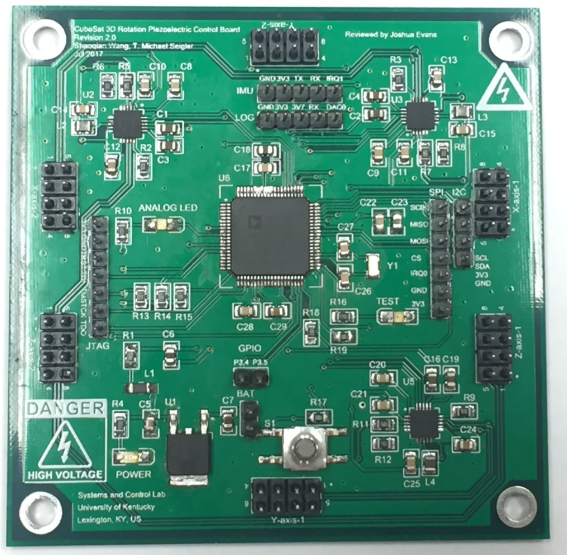

Figure 5.7: The main control board houses the microcontroller and three piezo haptic drivers, as well as connecting multiple modules as the mother board.

effectively implement this software architecture. In particular, ADuC7026 operates at the frequency of 41.78 MHz, and supports interrupts at two priority levels.

In the case of closed-loop control, the piecewise sinusoidal control signal is calculated at the beginning of each time interval $\mathcal{I}_k$, and the system operates in an open-loop manner within each time interval. A timer is set to determine the end of an interval. At the beginning of a new time interval, the microcontroller first retrieves the current attitude data from the IMU, then computes the amplitude and phase of the control signal on this interval. Next, the microcontroller ADuC7026 generates the sinusoidal signal with a lookup table, since indexing into the sine table and scaling the values are much more efficient than computing trigonometric functions. A lookup table with 256 points is used.

The sampling frequency of sinusoids (how often the DAC output voltage is updated) is 6400 Hz (every 156 μs). The time consumption for routine E (indexing into the sine table, scaling the values, and updating the DAC input) is approximately 36 μs. The time consumption of feedback control calculation is approximately 1700 μs.

5.4 Experiment setup

The CubeSat is mounted on a spherical air bearing, which allows for three rotational degrees of freedom. The air bearing (model number: A-656C010) is manufactured by Physik Instrumente (PI), and it is shown in Fig. 5.8. An air preparation kit feeds the compressed air to the air bearing. It filters the air and regulates the air pressure. The compressed air enters the bearing base though six tiny holes arranged in a circle and is vented at the edge of the base. The nominal air pressure is 80 psi. Disturbance torque caused by the compressed air has been observed. In particular, if the air pressure is above 10 psi, then the air bearing hemisphere would rotate about the vertical axis. In order to minimize the disturbance torque, the air pressure is adjusted to 2-3 psi.

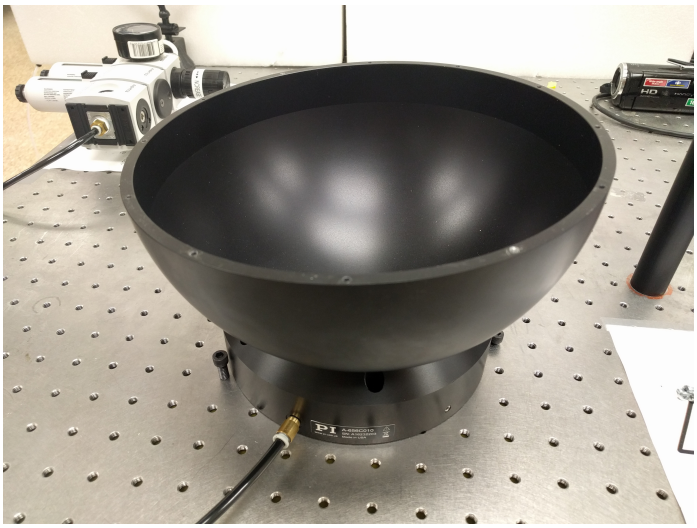

Figure 5.8: The spherical air bearing allows for three rotational degrees of freedom.

The mounting fixture can be seen in Fig. 5.9 and Fig. 5.10. Fig. 5.9 shows a 3D model of the whole mechanical system and Fig. 5.10 shows the actual CubeSat. The orientation of a body-fixed frame that is used to describe the orientation and the motion of the CubeSat is also shown in Fig. 5.9.

As shown in Fig. 5.9, a ring is mounted on the air bearing. On top of the ring,

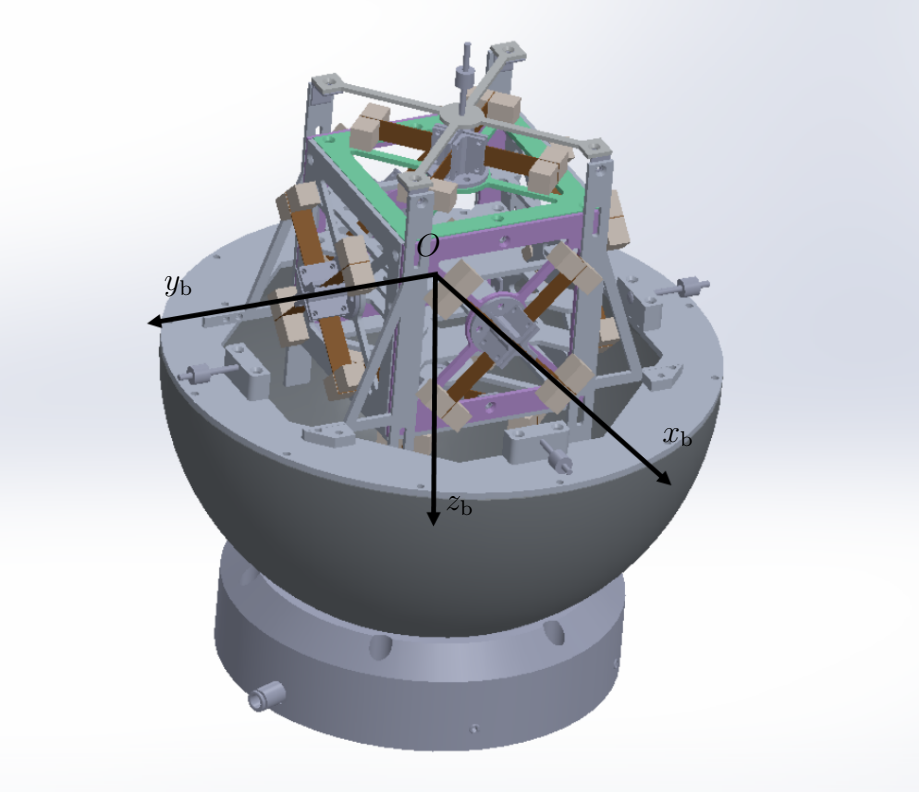

Figure 5.9: 3D model of the CubeSat mechanical system and the body-fixed frame (x_b, y_b, and z_b axes point in forward, right, and down direction).

there are four moving mass blocks which can move along threaded rods. These masses are used to adjust the center of gravity (CG) of the whole system in a plane parallel to the ring. The CubeSat itself can slide vertically along the slots of the connecting bars to coarsely adjust the CG in the vertical direction. An additional moving mass above the CubeSat is used to adjust the CG more accurately.

Before experiments are conducted, the height of the CubeSat as well as the position of the moving masses are manually adjusted in a recursive manner to move the center of gravity (CG) of the whole system close to the rotational center. Ideally, we would like to adjust the CG of the system to coincide with the rotational center, so that the CubeSat could freely rotate in an arbitrary direction. However, with the current setup, this is very difficult. Nevertheless, the CubeSat is able to freely rotate about the vertical axis.

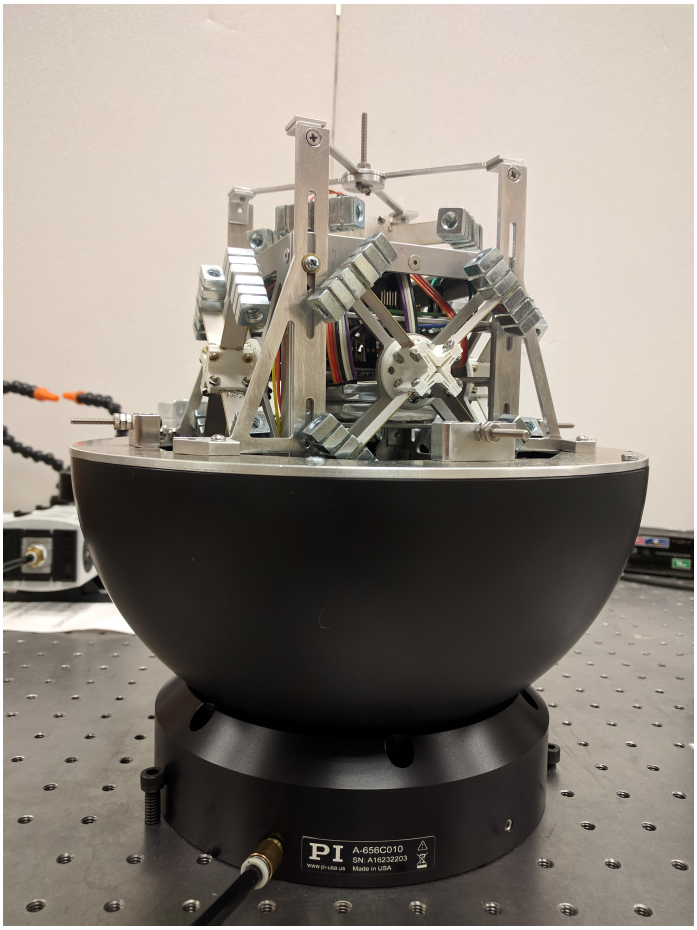

Figure 5.10: The experimental CubeSat system.

Before each experiment, we use microfiber cloth to clean the air bearing contact surfaces. Cleaning the air bearing contact surfaces greatly affect the experiment results regarding the open-loop yaw rate, closed-loop overshoot, etc. One possible reason is that wiping the air bearing contact surfaces removes dust particles that might otherwise stay on the air bearing contact surface and affect the air flow. Attempt to carry out experiments in a clean room has been made, but the ventilation rate is too high, defeating the purpose of minimizing disturbance.

Next, we estimate the actuation frequency that provides the highest control authority by frequency sweep. If the actuation frequency is close to the system's natural frequency, then the cube would get bigger angular velocities, thus yielding a higher

control authority. By applying sinusoidal voltages from 10 Hz to 30 Hz, we have found that the best actuation frequency is about 19 Hz. Note that this actuation frequency depends on a lot of factors, for example, the mass of the tip masses that are glued to the beams, the length of the beams, the stiffness of the actuator hub, etc.

We apply the same sinusoidal voltage signals to the four piezoelectric beams on each hub, and apply voltage signals with opposite polarities to the beams on opposite sides of the cube. This ensures that the two set of actuators on the opposite sides of the cube rotate in the same direction.

We note that in the kinetics model of the CubeSat system (2.75) (2.76), the controls are internal torques. For simplicity, we assume that the internal torques generated by the oscillatory actuators are proportional to the voltages applied to the actuators.

5.5 Experiment results and discussion

The CubeSat system, with the current design, could not perform roll and pitch motion, for two reasons. First, we could not perfectly balance the system, that is, making the CG of the whole system coincide with the air bearing rotational center. Second, the piezoelectric actuators are not powerful enough to counter the moment due to gravity. Therefore, in this section, we focus on the CubeSat yaw motion control, present and discuss the experimental results. We use $V_1(t)$, $V_2(t)$, and $V_3(t)$ to denote the sinusoidal voltages applied to the actuators about the body x, y, and z axes.

Open-loop control. We implement the kinematic-level open loop control on the dynamic level, and we show two open-loop experimental results. First, let $V_3(t) = 0$

for $t > 0$, and let

$$V_1(t) = \begin{cases} 54\cos(38\pi(t-10)), & \text{if } 10 \le t \le 40, \\ 0, & \text{otherwise,} \end{cases} \tag{5.1}$$

$$V_2(t) = \begin{cases} 54\sin(38\pi(t-10)), & \text{if } 10 \le t \le 40, \\ 0, & \text{otherwise.} \end{cases} \tag{5.2}$$

The Euler angles of the CubeSat are shown in the first subfigure of Fig. 5.11. Second, let $V_3(t) = 0$ for $t > 0$, and let

$$V_1(t) = \begin{cases} 54\sin(38\pi(t-10)), & \text{if } 10 \le t \le 40, \\ 0, & \text{otherwise,} \end{cases} \tag{5.3}$$

$$V_2(t) = \begin{cases} 54\cos(38\pi(t-10)), & \text{if } 10 \le t \le 40, \\ 0, & \text{otherwise.} \end{cases} \tag{5.4}$$

The Euler angles of the CubeSat are shown in the second subfigure of Fig. 5.11. In both experiments, the rotation rate is approximately 1°/sec. The angular velocities of the CubeSat for the two experiments are shown in Fig. 5.12 and Fig. 5.13. A zoom-in view of Ω_1 and Ω_2 is shown in Fig. 5.14 (we have connected the data points for a better view). We discuss the angular velocities later.

Closed-loop control. We now present two setpoint tracking experimental results. The two desired attitudes represented with 3-2-1 Euler angles, are $\psi = -50^\circ$, $\phi = \theta = 0$, and $\psi = -110^\circ$, $\phi = \theta = 0$. We apply sinusoidal voltages that are proportional to the control torques from Algorithm 4.1. The results are shown in Fig. 5.15.

IMU measurement error. There is a sensor measurement error for the yaw angle measurement, which can be seen from both Fig. 5.11 and Fig. 5.15. The yaw

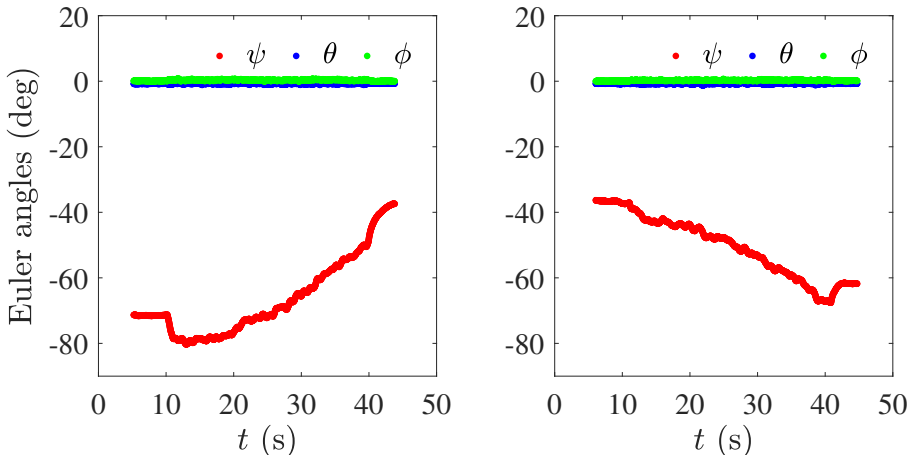

Figure 5.11: Open-loop control yields pure rotations about body-z axis.

angle shifts at the beginning and at the end of the actuation. This is likely caused by the magnetic field induced by the AC current used by the actuation system. Note that the IMU makes use of a magnetometer, whose readings may be corrupted by this magnetic field.

Six sessions of open-loop experiments have been carried out to qualitatively investigate the the yaw angle measurement error with respect to different actuation voltage levels. Each session is 30 sec long and the same actuation voltage frequency of 19Hz is used for all six sessions. The first two sessions use 53 V_{rms} sinusoidal voltage to yield a positive and a negative yaw change; the third and the fourth session use 38 V_{rms} sinusoidal voltage to yield a positive and a negative yaw change; and the last two sessions use zero actuation voltage.

As shown in Fig. 5.16, the yaw angle measurement error is smaller if smaller voltage is applied to the actuation system. This has an important implication, that is, in closed-loop experiments if the attitude of the CubeSat is close to the desired attitude, then the actuation voltage is approximately zero, yielding a small measurement error.

CubeSat kinetic model error. In the open-loop experiments, the angular velocity along the body z axis is nonzero (see Fig. 5.12 and Fig. 5.13). The nonzero

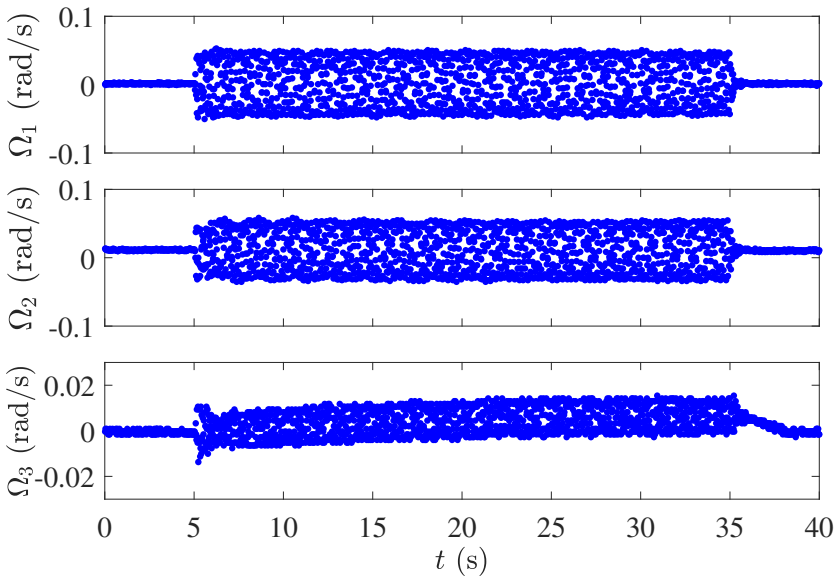

Figure 5.12: Sinusoidal actuation voltage yields sinusoidal angular velocity along body x and y axes. A small positive angular velocity along body z axis is induced (likely by the unmodeled air dynamics of the air bearing).

Ω_3 is likely due to the unmodeled air dynamics of the air bearing. It turns out that the nonzero Ω_3 contributes most to the yaw motion. Recall that sinusoidal Ω_1 and Ω_2 induce a average yaw motion, and if the phase difference between Ω_1 and Ω_2 is 90°, then the average yaw rate is

$$s = \sqrt{\omega^2 + c^2} - \omega, \tag{5.5}$$

where ω and c are the angular frequency and amplitude of Ω_1 and Ω_2. We take $\omega = 38\pi$ rad/s, and $c = 0.1$ rad. It follows from (5.5) that the average yaw rate is 4.2×10^{-5} rad/s (0.0024 deg/s), which is much smaller than Ω_3. Nevertheless, the dynamic level control presented in the previous chapter yields the correct rotation direction, and it is able to achieve setpoint tracking.

The effect of external damping. We study the effect of the external damping by conducting experiment using the CubeSat designed in [76]. This CubeSat is de-

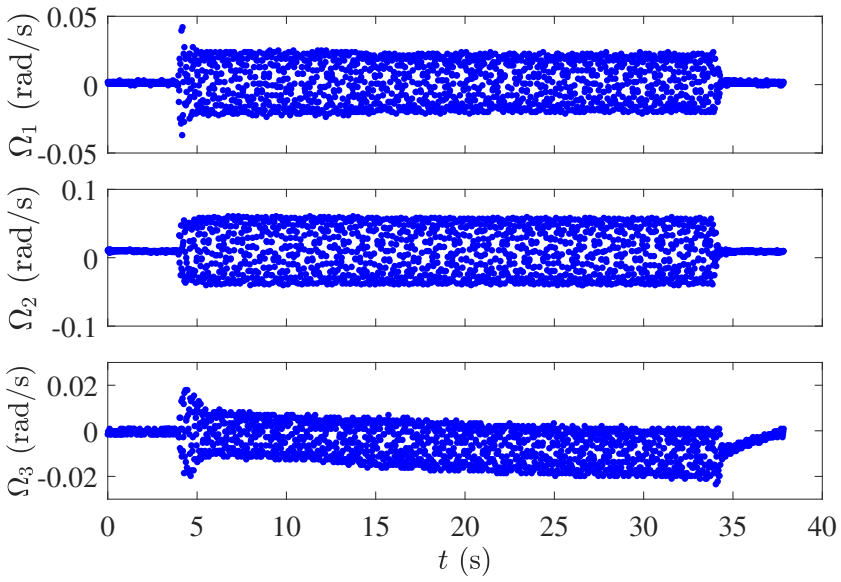

Figure 5.13: Sinusoidal actuation voltage yields sinusoidal angular velocities along body x and y axes. A small negative angular velocity along z axis is induced (likely by the unmodeled air dynamics of the air bearing).

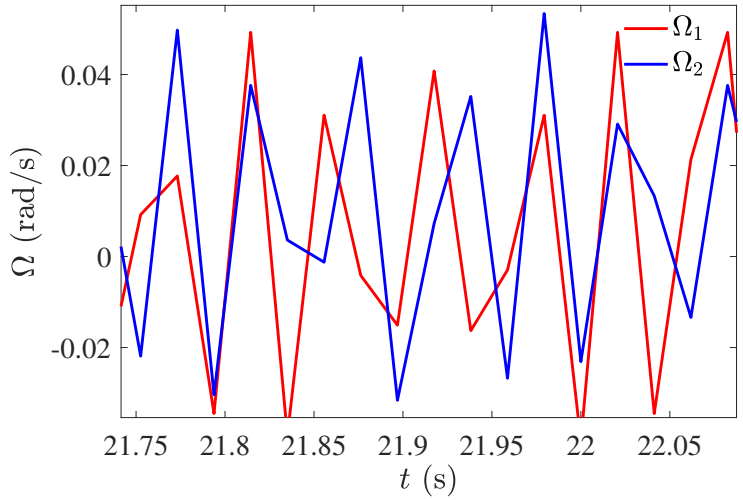

Figure 5.14: A zoom in view shows that Ω_1 leads Ω_2 by 90°.

signed to rotate on top of a pole through a ball joint, and thus it is subject to much bigger external damping than the CubeSat that is mounted on an air bearing. Two sessions of open-loop experiments are carried out using the same voltage (5.1)–(5.4),

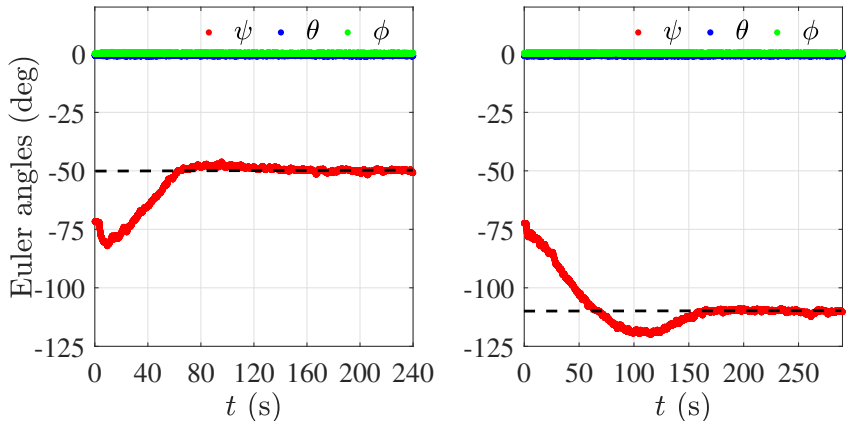

Figure 5.15: CubeSat tracks the yaw angle of -50 deg and -110 deg, which are marked with dashed lines.

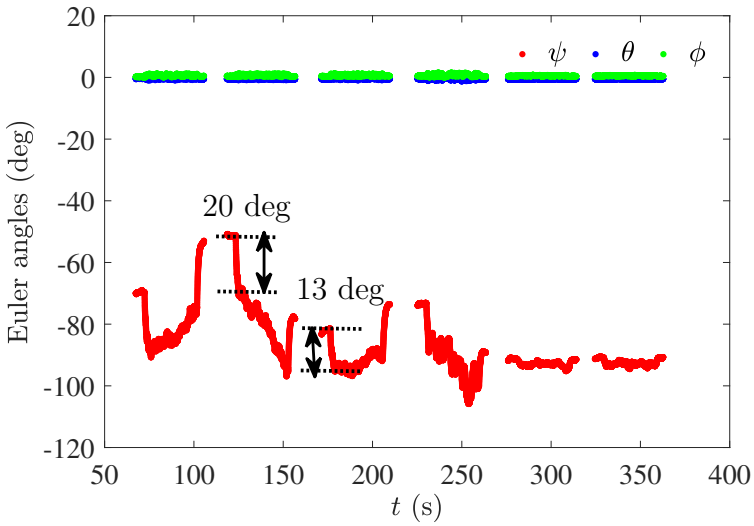

Figure 5.16: The yaw angle measurement error is smaller if smaller actuation voltage is applied to the actuation system.

with the difference that each session lasts 20 seconds. The angular velocity of the CubeSat is shown in Fig. 5.17. A zoom-in view of Ω_1 and Ω_2 is shown in Fig. 5.18 (we have connected the data points for a better view). In the first session, $V_1(t)$ leads $V_2(t)$ by 90°, and thus $\Omega_1(t)$ leads $\Omega_2(t)$ by 90°. Note that in contrast to Fig. 5.12, the CubeSat generates a negative Ω_3. In the second session, $V_2(t)$ leads $V_1(t)$ by 90°, and thus $\Omega_2(t)$ leads $\Omega_1(t)$ by 90°. Note that in contrast to Fig. 5.13, the CubeSat

generates a positive Ω_3. This agrees with the analysis of the external damping effect presented in the previous chapter.

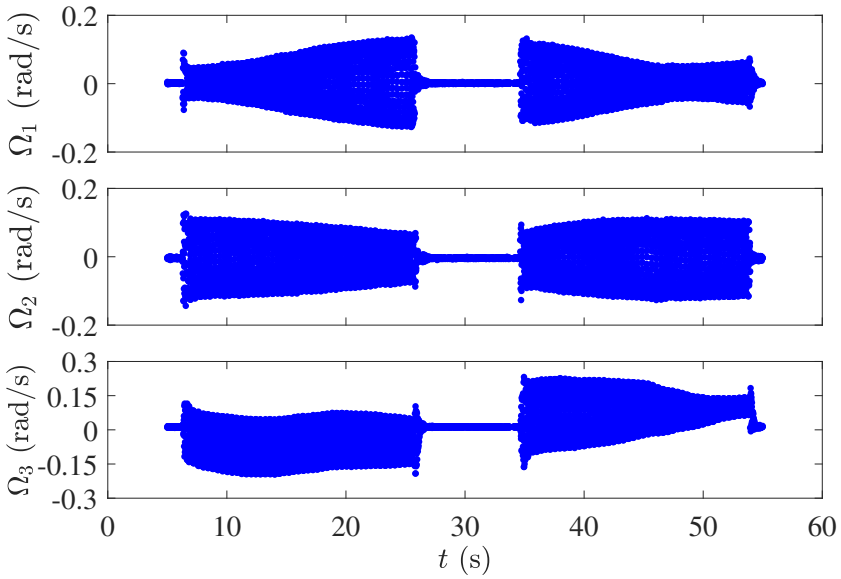

Figure 5.17: Sinusoidal actuation voltage yields sinusoidal angular velocities along body x and y axes. Nonzero Ω_3 is induced because of the external damping.

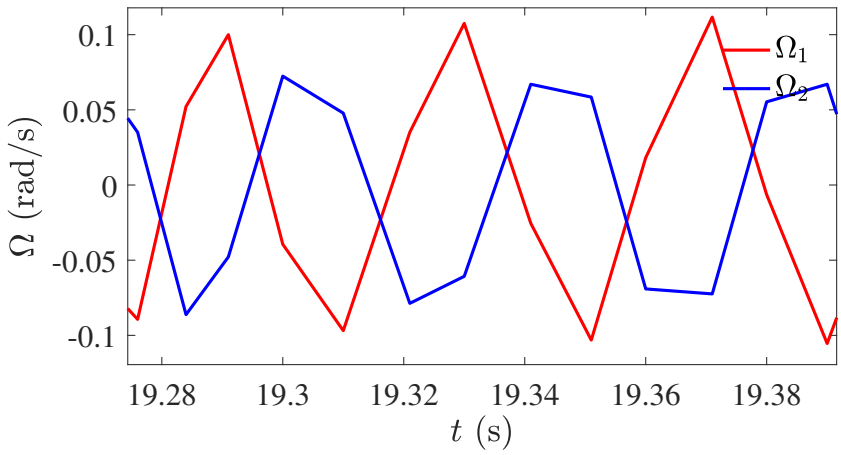

Figure 5.18: A zoom in view shows that Ω_1 leads Ω_2 by 90°.

Chapter 6 Conclusion and Future Work

6.1 Conclusion

This dissertation addresses rigid-body attitude control using piecewise sinusoidal controls. The contributions of this dissertation are summarized as follows.

First, we consider the SO(3) rigid-body attitude kinematics

$$\dot{R}(t) = R(t)\hat{\Omega}(t) \tag{6.1}$$

for the case that the elements of Ω consists of sinusoidal signals of the form

$$\Omega(t) = S\left[c\cos\omega t \quad c\sin\omega t \quad \omega_{\mathrm{d}}\right]^{\mathrm{T}}. \tag{6.2}$$

A new closed-form solution of (6.1) and (6.2) is derived, and we provide a key result that the solution of (6.1) and (6.2) approximates the trajectory of a pure rotation. Next, we consider the kinematic-level control problem in which $R(t)$ is available for feedback, $\omega_{\mathrm{d}} = 0$, and $c(t)$, $S(t)$, and $\omega(t)$ are treated as piecewise-constant controls. Kinematic-level controllers can be used as inner-loop steering controls and are also applicable for dynamic systems with high-bandwidth actuation and negligible transient response. It is shown that the SO(3) kinematic system with admissible controls is controllable in the sense that it is possible to steer R to any desired attitude by an appropriate choice of c, S, and ω. Next, we present kinematic-level controllers that use piecewise sinusoidal controls for $c(t)$, $S(t)$, and $\omega(t)$ to yield attitude stabilization and command following.

Second, we consider a dynamic-level problem consisting of (6.1) and a kinetic

system

$$\dot{\Omega}(t) = f(\Omega, u), \tag{6.3}$$

with piecewise-sinusoidal controls of the form

$$u(t) = S\left[c\cos\omega t \quad c\sin\omega t \quad 0\right]^{\mathrm{T}}. \tag{6.4}$$

where $S(t)$ and $c(t)$ are piecewise constant. Setpoint tracking controls are presented for a representative dynamic system of the form (6.3) and (6.4). Specifically, we consider a CubeSat that is equipped with a vibrational actuation system driven by piecewise sinusoidal torques. We assume there is no external forcing and the initial angular velocity is zero. In this case, the system conserves zero total angular momentum and the kinetic equations are linear. We use a steady-state approximation, which disregards the transient response of the attitude kinetics and thus allows for the application of kinematic-level control techniques. However, numerical simulations demonstrate that the control performance is significantly influenced by the transient response of (6.3) and (6.4). By taking advantage of an integral property of the angular velocity response of (6.3) and (6.4), we derive a second order approximation of the attitude matrix of the system. We then present a feedback control approach that accounts for the transient response of (6.3) and (6.4) and yields setpoint tracking.

In addition, we consider the case where the CubeSat is subject to external damping. In this case, the system doesn't conserve total angular momentum, and the kinetic equations of the system are nonlinear. This nonlinear CubeSat system exhibits interesting dynamics with internal sinusoidal torque inputs. We showed that if the system is subject to external damping, then sinusoidal torque inputs about two orthogonal axes can generate angular velocity about the remaining orthogonal axis to which there is no applied torque. For example, if sinusoidal torques are applied

to the body x and y directions, the existence of external damping can cause nonzero angular velocity in the body z direction. We study the nonlinear CubeSat dynamics with numerical simulation and design empirical piecewise sinusoidal controls to drive the attitude of the CubeSat to a small neighborhood of the desired attitude.

Finally, we designed and built an experimental CubeSat system. We present the design details of the CubeSat mechanical system, the control system hardware, and the attitude control software, which can be adapted for future use. We have found that the CubeSat is not able to perform rotations about an arbitrary axis. This is because with the current design the system cannot be perfectly mass-balanced; furthermore, the piezoelectric actuators are not powerful enough to counter the moment due to gravity. Nevertheless, open-loop and closed-loop yaw angle control experiments were performed. In addition, we have experimentally demonstrated the external damping effect on the CubeSat kinetics.

6.2 Future work

The controls considered in this dissertation are in piecewise sinusoidal form because the rotation kinematics are more amenable with this class of the angular velocity inputs. However, it would be interesting to consider sinusoidal control inputs with varying amplitude. Angular velocity controls of this form are smooth, which may lead to smooth dynamic-level control. Additionally, dynamic-level sinusoidal control with varying amplitude would induce a much smoother response, improving system performance.

The air dynamics of the air bearing is also left for further investigation. In this dissertation, we apply piecewise sinusoidal controls to the CubeSat system and achieve open-loop and closed-loop yaw angle control. However, the CubeSat yaw motion is mainly attributed to the nonzero angular velocity in the body z axis, which is likely due to the unmodeled air dynamics of the air bearing. Similarly, the effect of external

damping on the CubeSat kinetics needs to be studied further. In the future, it is interesting to design optimal sinusoidal controls by exploiting this external damping effect.

Regarding the experimental CubeSat system, a stronger oscillatory actuator is required to perform rotations about an arbitrary axis. A smaller air bearing also helps by decreasing moment of inertia of the system and external moment due to gravity. With the current design, the 850g air bearing with its mass distributed around the CubeSat, is largely responsible for the moment of inertia of the whole system; the piezoelectric bimorph actuators are not able to induce a significant oscillatory motion for the CubeSat. Hopefully, a more powerful actuator, e.g., a DC motor, may be able to generate large internal torques and induce a larger angular velocity for the system. Concerning the balancing mechanism of the CubeSat system, a more precise auto-balancing system is in demand if rotation about an arbitrary axis is to be achieved. We didn't design such an auto-balancing system since this extra system would further increase the moment of inertia that the piezoelectric actuators have to deal with. However, it may be allowable if a more powerful actuator is in place.

Bibliography

[1] J. R. Wertz, *Spacecraft attitude determination and control*. Springer Science & Business Media, 2012, vol. 73.

[2] F. L. Markley and J. L. Crassidis, *Fundamentals of spacecraft attitude determination and control*. Springer, 2014, vol. 33.

[3] P. Crouch, "Spacecraft attitude control and stabilization: Applications of geometric control theory to rigid body models," *IEEE Transactions on Automatic Control*, vol. 29, no. 4, pp. 321–331, 1984.

[4] J. T. Wen and K. Kreutz-Delgado, "The attitude control problem," *IEEE Transactions on Automatic Control*, vol. 36, no. 10, pp. 1148–1162, 1991.

[5] J. M. Coron and E. Y. Keraï, "Explicit feedbacks stabilizing the attitude of a rigid spacecraft with two control torques," *Automatica*, vol. 32, no. 5, pp. 669–677, 1996.

[6] S. P. Bhat and D. S. Bernstein, "A topological obstruction to continuous global stabilization of rotational motion and the unwinding phenomenon," *Systems & Control Letters*, vol. 39, no. 1, pp. 63–70, 2000.

[7] P. Tsiotras, H. Shen, and C. Hall, "Satellite attitude control and power tracking with energy/momentum wheels," *Journal of Guidance, Control, and Dynamics*, vol. 24, no. 1, pp. 23–34, 2001.

[8] R. Kristiansen, P. J. Nicklasson, and J. T. Gravdahl, "Satellite attitude control by quaternion-based backstepping," *IEEE Transactions on Control Systems Technology*, vol. 17, no. 1, pp. 227–232, 2009.

[9] W. Ren, "Distributed cooperative attitude synchronization and tracking for multiple rigid bodies," *IEEE Transactions on Control Systems Technology*, vol. 18, no. 2, pp. 383–392, 2010.

[10] N. A. Chaturvedi, A. K. Sanyal, and N. H. McClamroch, "Rigid-body attitude control," *IEEE Control Systems Magazine*, vol. 31, no. 3, pp. 30–51, 2011.

[11] Z. Sun, M.-C. Park, B. D. Anderson, and H.-S. Ahn, "Distributed stabilization control of rigid formations with prescribed orientation," *Automatica*, vol. 78, pp. 250–257, 2017.

[12] S. Bharadwaj, M. Osipchuk, K. Mease, and F. Park, "Geometry and inverse optimality in global attitude stabilization," *Journal of Guidance, Control, and Dynamics*, vol. 21, no. 6, pp. 930–939, 1998.

[13] S. P. Bhat and D. S. Bernstein, "A topological obstruction to continuous global stabilization of rotational motion and the unwinding phenomenon," *System & Control Letters*, vol. 39, no. 1, pp. 63–70, 2000.

[14] M. D. Shuster, "A survey of attitude representations," *Navigation*, vol. 8, no. 9, pp. 439–517, 1993.

[15] S. Sastry, *Nonlinear systems: analysis, stability, and control*. Springer Science & Business Media, 2013, vol. 10.

[16] G. Meyer, "Design and global analysis of spacecraft attitude control systems," 1971.

[17] F. Bullo and R. M. Murray, "Proportional derivative (PD) control on the Euclidean group," in *European Control Conference*, vol. 2, 1995, pp. 1091–1097.

[18] F. Lizarralde and J. T. Wen, "Attitude control without angular velocity measurement: a passivity approach," *IEEE Transactions on Automatic Control*, vol. 41, no. 3, pp. 468–472, 1996.

[19] J. Markdahl and X. Hu, "Exact solutions to a class of feedback systems on SO(n)," *Automatica*, vol. 63, pp. 138–147, 2016.

[20] J.-E. Slotine and M. Di Benedetto, "Hamiltonian adaptive control of spacecraft," *IEEE Transactions on Automatic Control*, vol. 35, no. 7, pp. 848–852, 1990.

[21] H. Yoon and P. Tsiotras, "Adaptive spacecraft attitude tracking control with actuator uncertainties," *The Journal of the Astronautical Sciences*, vol. 56, no. 2, pp. 251–268, 2008.

[22] A. Weiss, I. Kolmanovsky, D. S. Bernstein, and A. Sanyal, "Inertia-free spacecraft attitude control using reaction wheels," *Journal of Guidance, Control, and Dynamics*, vol. 36, no. 5, pp. 1425–1439, 2013.

[23] C. I. Byrnes and A. Isidori, "On the attitude stabilization of rigid spacecraft," *Automatica*, vol. 27, no. 1, pp. 87–95, 1991.

[24] H. Krishnan, M. Reyhanoglu, and H. McClamroch, "Attitude stabilization of a rigid spacecraft using two control torques: A nonlinear control approach based on the spacecraft attitude dynamics," *Automatica*, vol. 30, no. 6, pp. 1023–1027, 1994.

[25] P. Tsiotras and J. M. Longuski, "Spin-axis stabilization of symmetrical spacecraft with two control torques," *Systems & Control Letters*, vol. 23, no. 6, pp. 395–402, 1994.

[26] P. Morin and C. Samson, "Time-varying exponential stabilization of a rigid spacecraft with two control torques," *IEEE Transactions on Automatic Control*, vol. 42, no. 4, pp. 528–534, 1997.

[27] P. Tsiotras and J. Luo, "Control of underactuated spacecraft with bounded inputs," *Automatica*, vol. 36, no. 8, pp. 1153–1169, 2000.

[28] H. Gui, G. Vukovich, and S. Xu, "Attitude tracking of a rigid spacecraft using two internal torques," *IEEE Transactions on Aerospace and Electronic Systems*, vol. 51, no. 4, pp. 2900–2913, 2015.

[29] R. W. Brockett, "Asymptotic stability and feedback stabilization," *Differential geometric control theory*, vol. 27, no. 1, pp. 181–191, 1983.

[30] P. Morin, C. Samson, J.-B. Pomet, and Z.-P. Jiang, "Time-varying feedback stabilization of the attitude of a rigid spacecraft with two controls," *Systems & Control Letters*, vol. 25, no. 5, pp. 375–385, 1995.

[31] R. Chavan, S. Wang, T. M. Seigler, and J. B. Hoagg, "Consensus on SO(3) with piecewise-continuous sinusoids," in *American Control Conference (ACC)*. IEEE, 2018, pp. 1635–1640.

[32] S. N. Singh and T. C. Bossart, "Exact feedback linearization and control of space station using CMG," *IEEE Transactions on Automatic Control*, vol. 38, no. 1, pp. 184–187, 1993.

[33] G. C. Walsh, R. Montgomery, and S. Sastry, "Orientation control of the dynamic satellite," in *American Control Conference, 1994*, vol. 1. IEEE, 1994, pp. 138–142.

[34] D. Lee, H. J. Kim, and S. Sastry, "Feedback linearization vs. adaptive sliding mode control for a quadrotor helicopter," *International Journal of Control, Automation and Systems*, vol. 7, no. 3, pp. 419–428, 2009.

[35] I. Ali, G. Radice, and J. Kim, "Backstepping control design with actuator torque bound for spacecraft attitude maneuver," *Journal of Guidance, Control, and Dynamics*, vol. 33, no. 1, pp. 254–259, 2010.

[36] J. L. Crassidis and F. L. Markley, "Sliding mode control using modified Rodrigues parameters," *Journal of Guidance, Control, and Dynamics*, vol. 19, no. 6, pp. 1381–1383, 1996.

[37] N. Zhou, Y. Xia, M. Wang, and M. Fu, "Finite-time attitude control of multiple rigid spacecraft using terminal sliding mode," *International Journal of Robust and Nonlinear Control*, vol. 25, no. 12, pp. 1862–1876, 2015.

[38] R. Sharma and A. Tewari, "Optimal nonlinear tracking of spacecraft attitude maneuvers," *IEEE Transactions on Control Systems Technology*, vol. 12, no. 5, pp. 677–682, 2004.

[39] W. Luo, Y.-C. Chu, and K.-V. Ling, "H-infinity inverse optimal attitude-tracking control of rigid spacecraft," *Journal of Guidance, Control, and Dynamics*, vol. 28, no. 3, pp. 481–494, 2005.

[40] H. K. Khalil, "Nonlinear systems, 3rd," *New Jewsey, Prentice Hall*, vol. 9, 2002.

[41] S. N. Singh, "Nonlinear adaptive attitude control of spacecraft," *IEEE Transactions on Aerospace and Electronic Systems*, no. 3, pp. 371–379, 1987.

[42] P. Tsiotras and J. Luo, "Reduced effort control laws for underactuated rigid spacecraft," *Journal of Guidance, Control, and Dynamics*, vol. 20, no. 6, pp. 1089–1095, 1997.

[43] J. M. Longuski, "Real solutions for the attitude motion of a self-excited rigid body," *Acta Astronautica*, vol. 25, no. 3, pp. 131–139, 1991.

[44] P. Tsiotras and J. Longuski, "Analytic solutions for a spinning rigid body subject to time-varying body-fixed torques, Part II: Time-varying axial torque," *Journal of applied mechanics*, vol. 60, no. 4, pp. 976–981, 1993.

[45] J. M. Longuski and P. Tsiotras, "Analytic solution of the large angle problem in rigid body attitude dynamics," *Journal of the Astronautical Sciences*, vol. 43, no. 1, pp. 25–46, 1995.

[46] T. Dwyer, "Exact nonlinear control of large angle rotational maneuvers," *IEEE Transactions on Automatic Control*, vol. 29, no. 9, pp. 769–774, 1984.

[47] N. E. Leonard and P. S. Krishnaprasad, "Motion control of drift-free, left-invariant systems on Lie groups," *IEEE Transactions on Automatic Control*, vol. 40, no. 9, pp. 1539–1554, 1995.

[48] J. Shen, N. McClamroch, and D. Bernstein, "Air spindle attitude control via proof mass actuators," in *Decision and Control, 2001. Proceedings of the 40th IEEE Conference on*, vol. 5. IEEE, 2001, pp. 4616–4621.

[49] S. K. Koh, J. P. Ostrowski, and G. Ananthasuresh, "Control of micro-satellite orientation using bounded-input, fully-reversed MEMS actuators," *The International Journal of Robotics Research*, vol. 21, no. 5-6, pp. 591–605, 2002.

[50] C. Rui, I. V. Kolmanovsky, and N. H. McClamroch, "Nonlinear attitude and shape control of spacecraft with articulated appendages and reaction wheels," *IEEE Transactions on Automatic Control*, vol. 45, no. 8, pp. 1455–1469, 2000.

[51] S. Cho, N. H. McClamroch, and M. Reyhanoglu, "Dynamics of multibody vehicles and their formulation as nonlinear control systems," in *American Control Conference, 2000*, vol. 6. IEEE, 2000, pp. 3908–3912.

[52] J. Shen and N. H. McClamroch, "Translational and rotational maneuvers of an underactuated space robot using prismatic actuators," *The International Journal of Robotics Research*, vol. 21, no. 5-6, pp. 607–618, 2002.

[53] D. S. Bernstein, N. H. McClamroch, and J. Shen, "Shape change actuation for precision attitude control," *IEEE Control Systems*, vol. 23, no. 5, pp. 44–56, 2003.

[54] S. K. Koh and G. K. Ananthasuresh, "Inverse kinematics of an untethered rigid body undergoing a sequence of forward and reverse rotations," *Journal of Mechanical Design*, vol. 126, no. 5, pp. 813–821, 2004.

[55] Y. Kuo and T. Wu, "Open-loop and closed-loop attitude dynamics and controls of miniature spacecraft using pseudowheels," *Computers & Mathematics with Applications*, vol. 64, no. 5, pp. 1282–1290, 2012.

[56] G. Jacob, "Motion planning by piecewise constant or polynomial inputs," in *Nonlinear Control Systems Design 1992*. Elsevier, 1993, pp. 239–244.

[57] G. Lafferriere and H. J. Sussmann, "A differential geometric approach to motion planning," in *Nonholonomic motion planning*. Springer, 1993, pp. 235–270.

[58] R. M. Murray and S. Sastry, "Nonholonomic motion planning: Steering using sinusoids," *IEEE Transactions on Automatic Control*, vol. 38, no. 5, pp. 700–716, 1993.

[59] S. Wang, A. H. Ghasemi, J. Evans, and T. M. Seigler, "Orientation control using oscillating momentum wheels," in *ASME 2015 Dynamic Systems and Control Conference*. American Society of Mechanical Engineers, 2015, p. V001T06A007.

[60] I. Kolmanovsky and N. H. McClamroch, "Developments in nonholonomic control problems," *IEEE Control Systems Magazine*, vol. 15, no. 6, pp. 20–36, 1995.

[61] N. E. Leonard, "Control synthesis and adaptation for an underactuated autonomous underwater vehicle," *IEEE Journal of Oceanic Engineering*, vol. 20, no. 3, pp. 211–220, 1995.

[62] R. W. Brockett, "Control theory and singular Riemannian geometry," *New Directions in Applied Mathematics*, pp. 13–27, 1982.

[63] S. Wang, J. B. Hoagg, and T. M. Seigler, "Steering on SO(3) with sinusoidal inputs," in *American Control Conference (ACC), 2017*. IEEE, 2017, pp. 604–609.

[64] N. E. Leonard, "Periodic forcing, dynamics and control of underactuated spacecraft and underwater vehicles," in *Decision and Control, 1995., Proceedings of the 34th IEEE Conference on*, vol. 4. IEEE, 1995, pp. 3980–3985.

[65] I. A. Raptis, K. P. Valavanis, and W. A. Moreno, "A novel nonlinear backstepping controller design for helicopters using the rotation matrix," *IEEE Transactions on Control Systems Technology*, vol. 19, no. 2, pp. 465–473, 2011.

[66] M. L. Curtis, *Matrix groups*. Springer-Verlag New York Inc., 1979.

[67] R. M. Murray, Z. Li, and S. S. Sastry, *A mathematical introduction to robotic manipulation*. CRC press, 1994.

[68] D. S. Bernstein, *Matrix Mathematics: Theory, Facts, and Formulas*, 2nd ed. Princeton University Press, 2009.

[69] J. Ginsberg, *Engineering dynamics*. Cambridge University Press, 2008, vol. 10.

[70] A. H. Nayfeh, *Introduction to perturbation techniques*. John Wiley & Sons, 2011.

[71] N. E. Leonard and P. Krishnaprasad, "Averaging for attitude control and motion planning," in *Decision and Control, 1993., Proceedings of the 32nd IEEE Conference on*. IEEE, 1993, pp. 3098–3104.

[72] E. D. Sontag, *Mathematical Control Theory: Deterministic Finite Dimensional Systems*, 2nd ed. Springer-Verlag New York Inc., 1991.

[73] W. Magnus, "On the exponential solution of differential equations for a linear operator," *Communications on pure and applied mathematics*, vol. 7, no. 4, pp. 649–673, 1954.

[74] M. V. Karasev and M. Mosolova, "Infinite products and T products of exponentials," *Theoretical and Mathematical Physics*, vol. 28, no. 2, pp. 721–729, 1976.

[75] D. E. Simon, *An embedded software primer*. Addison-Wesley Professional, 1999, vol. 1.

[76] J. L. Evans, "Small satellite noncommutative rotation sequence attitude control using piezoelectric actuators," 2016.

Vita

Shaoqian Wang received the B. S. degree in Mechanical Engineering from Harbin Institute of Technology (China) in 2011, and the M. S. degree in Electrical Engineering from the University of Kentucky in 2016. His current research interest is in the control of mechanical systems and robotics.